

# **Generation of Ultra-stable Microbubbles for Industrial Applications**

**Papoole Valadbaigi**

Submitted in accordance with the requirements for the degree of

Doctorate of Philosophy

The University of Leeds

School of Food Science and Nutrition

January 2019

The candidate confirms that the work submitted is his/her own, except where work which has formed part of jointly-authored publications has been included. The contribution of the candidate and the other authors to this work has been explicitly indicated below. The candidate confirms that appropriate credit has been given within the thesis where reference has been made to the work of others.

The work in Chapters 3 of the thesis have appeared in publication as followed:

*Generation of Ultra-stable Pickering Microbubbles via Poly alkyl cyanoacrylates*;  
Submitted: 25 July 2018, Accepted: 3 October 2018, Published 15 February 2019 ;  
Valadbaigi, P., Ettelaie, R., Kulak , A.N. and Murray, B.S.

I was responsible for all experimental work and measurements, data analysis, data interpretation, and made the major contributions to the first draft of the manuscript. Murray, B.S. helped with the final draft and provided supervision and feedback. Kulak , A.N helped with SEM images and Ettelaie, R provided supervision and feedback and edited the manuscript.

This copy has been supplied on the understanding that it is copyright material and that no quotation from the thesis may be published without proper acknowledgement.

© <2018> *The University of Leeds <Papoole Valadbaigi>*

The right of Papoole Valadbaigi to be identified as Author of this work has been asserted by her in accordance with the Copyright, Designs and Patents Act 1988.

## **Acknowledgement**

First and foremost I would like to thank my two supervisors, Professor Brent S. Murray and Dr Rammile Ettelaie, who encouraged me to pursue my PhD in this project. I would like to thank them both for their help, time, care and support throughout the project. Much of my work would not have been completed without their valuable guidance and continuous support.

I would also like to thank the members of staff at the School of Food Science and Nutrition and the members of the Food Colloids group for creating such a friendly and relaxed environment, and especially to Dr Nataricha Phisarnchananan, Dr Linda C. Pravinata and Mr Neil Rigby for helping me numerous times with equipment and experiments. My sincere thanks go to Dr Alexander N. Kulak who helped me with SEM images.

I would also like to acknowledge the financial sponsorship from EPSRC and SOFI CDT. Additional support and guidance from Akzo-Nobel, particularly Daragh McLoughlin is acknowledged.

I would like to express my sincere gratitude to all my friends and family, especially my parents, mother-in-law, brothers and sister for all their support, interest, motivation and belief that have given me throughout my life. I am extremely grateful towards each and every one of you.

Words cannot express how grateful I am to my incredible husband Saeed, for his unconditional love and unlimited support, great patience and encouragement in my stressful and critical times. I am a stronger person with you, and I will always be grateful for this.

## Abstract

Microbubbles (MBs) are fine bubbles with a radius of 1 – 100  $\mu\text{m}$ . Microbubbles has been subject of interest for researchers and industries over the past few decades as they proved to be the most effective contrast agent for ultrasound radiography. More recently microbubbles potential for use in drug delivery, gene therapy and also for non-medical application such as food, thermal insulating material and low weight structure has been investigated. Development in applications of MBs increased the need for more advanced understanding of microbubble formation and stability. The thermodynamically unstable nature of microbubbles remains as an issue in all of their applications. Air bubbles in water stabilized by particles ('Pickering' bubbles) can be indefinitely stable, but the slower mass transport of particles to interfaces compared to molecules means that the final stable bubble size is a fine balance between the rates of bubble formation, particle coverage and shrinkage.

In this project the two types of Pickering nanoparticles (NPs) namely Class II hydrophobin (HFBII) and poly alkyl cyanoacrylate NPs were investigated in terms of their ability to form and stabilize microbubbles. HFBII is an edible protein acts like a very small Janus nanoparticle since it is known not to unfold or denature at air-water interfaces and has a hydrophobic patch on one side. Microbubbles stabilized by HFBII alone are stable for a relatively long time (several days) but it is difficult to obtain a high volume fraction of bubbles due to HFBII aggregation. However, combining HFBII with other surfactants increases the overrun and a strong negative correlation is seen between the surface tension decrease resulting from the added surfactant and the volume fraction of microbubbles after 48 hours.

Different monomers from alkyl cyanoacrylate family (butyl (BCA), octyl (OCA) and Ethyl (ECA)) were polymerized under different conditions (pH, surfactant type and concentration) to form NPs, with the potential to stabilize MBs via Pickering mechanism. Poly butyl cyanoacrylates (PBCA) NPs, polymerized at pH 4 and in presence of 1 wt.% Tyloxapol were the best stabilizing NPs compared to other PACA NPs. MBs stabilized by this NPs were stable for the period of 10 weeks or more. The SEM micrographs indicated that MBs are stabilized via the self-assembly of PBCA NPs around the surface of microbubbles (contact angle  $77 \pm 10$ ) during aeration via high shear mixer. Increasing the aeration steps led to increase the volume fraction of MBs up to 3 vol. %. On the other hand PBCA NPs polymerized in the absence of any surfactant were unable to stabilize any bubbles. Our results shows that roughly 25 wt.% of the Tyloxapol incorporate into the NPs during polymerization. This incorporation of Tyloxapol changes the physicochemical characteristic of the NPs in the way that NPs can adsorb to the air- water interface and protect MBs against shrinkage.

The PBCA + surfactant system was studied in more detail, by controlling the rate of formation and initial size of the bubbles more exactly, so a balance was achieved whereby very efficient microbubble production took place (e.g., > 10 vol.%).

## Abbreviations

HFBII – Hydrophobin HFBII

NaCas – Sodium Caseinate

WPI – Whey Protein Isolate

PBCA – Poly Butyl Cyanoacrylate

NP – Nano Particle

MB – Micro Bubble

PACA – Poly Alkyl Cyanoacrylate

PECA – Poly Ethyl Cyanoacrylate

POCA – Poly Octyl Cyanoacrylate

CLSM – Confocal Laser Microscopy

SEM – Scanning Electron Microscopy

h – hour(s)

min – minute(s)

wt. % – weight percentage

DSL – Dynamic Light Scattering

# Table of contents

<b>Acknowledgement</b> .....	<b>i</b>
<b>Abstract</b> .....	<b>ii</b>
<b>Abbreviations</b> .....	<b>iii</b>
<b>Table of contents</b> .....	<b>iv</b>
<b>List of figures</b> .....	<b>vii</b>
<b>List of tables</b> .....	<b>xi</b>
<b>Chapter 1 :</b> .....	<b>1</b>
1.1 Objectives .....	1
1.2 Colloidal phenomena .....	2
1.3 Interaction forces that influence stability.....	2
1.3.1 Van der Waals interaction .....	4
1.3.2 Electrostatic repulsion .....	6
1.3.3 DLVO theory .....	11
1.3.4 Steric repulsion .....	14
1.4 Foams, bubbles .....	18
1.5 Surface behaviour of surfactants, proteins and nanoparticles.....	19
1.5.1 Surface tension .....	19
1.5.2 Dynamic surface tension .....	21
1.5.3 Surface viscoelasticity .....	23
1.6 Microbubble generation techniques .....	25
1.6.1 Sonication .....	25
1.6.2 High shear mixing .....	26
1.6.3 Membrane processing.....	27
1.6.4 Coaxial electro hydrodynamic atomisation .....	28
1.6.5 Microfluidics .....	29
1.7 Significance of the Laplace pressure .....	31
1.8 Foam/ bubble stability.....	31
1.8.1 Drainage.....	32
1.8.2 Coalescence .....	32
1.8.3 Disproportionation.....	37
1.9 Mechanism to overcome foam/ bubble instability.....	38
1.10 Pickering stabilization.....	40

1.10.1	Particles/ nanoparticles .....	40
1.10.2	Definition and classification of polymer nanoparticles .....	42
1.10.3	PNP preparation techniques.....	43
1.10.4	Food grade nanoparticles.....	50
1.10.5	Contact angle .....	50
1.10.6	Capillary interactions between solid particles at interface .....	53
1.11	Overview.....	53
<b>Chapter 2 :</b> .....		<b>55</b>
2.1	Introduction.....	55
2.2	Materials and methods .....	58
2.2.1	Materials .....	58
2.2.2	Buffer preparation.....	59
2.2.3	Microbubble dispersion preparation.....	59
2.2.4	Microscopy .....	60
2.2.5	Dynamic light scattering for size measurement .....	61
2.2.6	Surface tension measurement .....	63
2.3	Results.....	64
2.3.1	Bubble formation and stability over time .....	64
2.3.2	Impact of HFBII concentration on MBs.....	68
2.3.3	Multiple aeration.....	72
2.3.4	Effect of surface activity on MBs.....	73
2.4	Conclusion .....	79
<b>Chapter 3 :</b> .....		<b>80</b>
3.1	Introduction.....	80
3.2	Materials and methods .....	83
3.2.1	Materials .....	83
3.2.2	Preparation of Nanoparticles and microbubbles formation.....	83
3.2.3	Microscopy .....	85
3.2.4	PBCA NPs size and $\zeta$ - potential .....	85
3.2.5	Free Tyloxapol determination .....	86
3.3	Results.....	87
3.3.1	Impact of polymerization condition on NPs properties.....	87
3.3.2	MBs stability.....	96
3.3.3	Stability of MBs after freeze and thaw cycle .....	106
3.3.4	Determination of free Tyloxapol in the system .....	106
3.4	Conclusion .....	107

<b>Chapter 4 :</b> .....	<b>109</b>
4.1 Introduction.....	109
4.2 Materials and methods .....	113
4.2.1 Materials .....	113
4.2.2 Methods .....	113
4.2.3 PBCA NPs size and $\zeta$ -potential .....	116
4.2.4 Microscopy .....	116
4.2.5 Static light scattering .....	116
4.3 Results and discussion .....	117
4.3.1 Large bubble syringe .....	117
4.3.2 Effect of initial bubble size on final bubble size and foam height	133
4.4 Conclusion .....	136
<b>Chapter 5 :</b> .....	<b>139</b>
5.1 Introduction.....	139
5.2 Numerical approach .....	140
5.3 Results and discussion .....	149
5.3.1 Impact of NPs volume fraction in the inlet of dispersion, $\phi_p^i$ , on final bubble size .....	149
5.3.1 Impact of $W_d^i$ on $r_b^{o2}$ .....	154
5.4 Conclusion .....	154
<b>Chapter 6 :</b> .....	<b>156</b>
<b>References:</b> .....	<b>159</b>

## List of figures

- Figure 1.1:** Dispersed phase (medium 2) of radius  $r$  separated by a surface to surface separation  $h$  in a liquid continuous phase (medium 1)..... 3
- Figure 1.2:** (A): the concentration ( $c$ ) of coions and counterions at the vicinity of a negatively charged surface, where  $c_\infty$  is the bulk electrolyte concentration. (B): shows the decrease of electrostatic potential close to the surface, thickness of the double layer is shown as  $1/\kappa$  (Walstra 2003) ..... 8
- Figure 1.3:** Overlap of the electrical double layers between two particles at a distance  $h$  from each other. In (A) the double layers virtually do not overlap, and the electrostatic potentials  $\psi$  equal zero in the middle; in (B) the particles are closer and their electrical double layers do overlap, which causes the potentials to locally increase (Walstra 2003)..... 10
- Figure 1.4:** Schematic interaction energy versus distance profiles of DLVO interaction. The attractive van der Waals and the repulsive electrostatic potentials form the total interaction energy (Adair, Suvaci and Sindel 2001). ..... 11
- Figure 1.5:** The DLVO plot for the interaction of two MBs in water, EI: electrostatic interaction, VDW: van der Waals interaction. For modelling parameters see the text..... 13
- Figure 1.6:** Steric interactions between two bubbles can be divided into: a mixing contribution that involves interpenetration of the polymer chains and an elastic contribution that involves compression of the polymer layers. .... 15
- Figure 1.7:** The total free energy  $V$  relative to  $k_B T$  as a function of  $h$  (interparticle distance), between same sized spherical particles covered by a layer of polymer. Van der Waals attraction and steric interaction is considered for calculation (Walstra 2003). ..... 17
- Figure 1.8:** Schematic representation of foam with different liquid volume fraction (Langevin 2017)..... 19
- Figure 1.9:** Production of MBs, high shear mixing is used to emulsify the polymer (Bjerknes *et al.* 2000)..... 27
- Figure 1.10:** Microbubble preparation by coaxial electrohydrodynamic atomisation (CEHDA): (a) schematic of CEHDA apparatus; (b) CEHDA mode 1: bubble dripping; (c) CEHDA mode 2: coning; (d) CEHDA mode 3: continuous microbubbling.(Stride and Edirisinghe 2008)..... 29
- Figure 1.11:** Typical size distributions of MBs produced from a phospholipid suspension via sonication, CEHDA and a microfluidic T-junction device (Stride and Edirisinghe 2008). ..... 30
- Figure 1.12:** Film rupture due to solid particles. (A): hydrophobic particles, (B): particles from materials that can spread over the surface ..... 33
- Figure 1.13:** Silicone oil film profile between glycerol drops at various times after the formation of the dimple: experiments (symbols) and theory (lines). Note the very different magnitudes of the vertical and horizontal scales. Inset: comparison of experimental and theoretical optical interference fringe patterns of the silicone oil film at  $t = 1/4$  27 s when the capillary drive was stopped (Chan, Klaseboer and Manica 2011). ..... 36

<b>Figure 1.14:</b> Schematic representation of (A): homogenous, (B): Janus particle and (C): surfactant molecule.....	42
<b>Figure 1.15:</b> Illustration of classification of polymer nanoparticles nanospheres (A), nanocapsules containing oil (B) and water (C).....	43
<b>Figure 1.16:</b> Schematic representation of poly (alkyl cyanoacrylate) formation via the stepwise anionic polymerization mechanism in emulsion/dispersion. Initiation step (a), reversible propagation step (b), and reversible termination step (c). Adopted from: Nicolas and Couvreur (2009) .....	49
<b>Figure 1.17:</b> Solid spherical particle with contact angle $\theta$ in equilibrium at the oil – water interface.....	51
<b>Figure 2.1:</b> The structure of <i>T. reesei</i> hydrophobin HFBII; disulfide bridges are highlighted in yellow and the hydrophobic patch in red. Adopted from: Hakanpaa <i>et al</i> (2006).....	56
<b>Figure 2.2:</b> Schematic of image formation by confocal scanning laser microscope	61
<b>Figure 2.3:</b> Schematic diagram of Zetasizer Nano to measure particle/ bubble size	63
<b>Figure 2.4:</b> Schematic of Wilhelmy plate working mechanism.....	64
<b>Figure 2.5:</b> Represents the mean diameter of MBs during a period of 240 hours by microscope techniques (■), light scattering (●).....	65
<b>Figure 2.6:</b> Visual assessment of a sample made with 0.03wt% HFB II and 0.1wt% NaCas.....	67
<b>Figure 2.7:</b> Microscopy images of MBs stabilized by 0.03 wt% HFBII and 0.1 wt. % NaCas. ....	68
<b>Figure 2.8:</b> Comparison of mean diameter of MBs stabilized by 0.03 wt. % HFBII (■) and 0.06 wt. % HFBII (●) and 0.1 wt. % NaCas .....	69
<b>Figure 2.9:</b> Confocal microscopy image of MBs stabilized by 0.03 wt. % HFBII + 0.1 wt. % NaCas (A) and 0.06 wt. % HFBII + 0.1 wt. % NaCas (B) 16 days after MBs formed. Scale bar: 75 $\mu$ m .....	71
<b>Figure 2.10:</b> Volume % of MBs dispersion after each aeration step .....	72
<b>Figure 2.11:</b> Mean diameter of MBs stabilized by different concentration of NaCas when the concentration of HFBII remained constant at 0.03 wt.%. 0.1 wt.% NaCas (■), 0.05 wt.% NaCas (●) , 0.2 wt.% NaCas (▲) and 0.1wt.% NaCas in absence of HFBII (▼).....	74
<b>Figure 2.12:</b> Mean MBs diameters for the period of 10 days. NaCas (▼), Tween 20 (■), Tween 80 (●), Triton X-100 (▲), WPI (◄) and $\beta$ -lactoglobulin (◆).....	77
<b>Figure 2.13:</b> Air volume% of different systems.....	78
<b>Figure 2.14:</b> Air volume % as a function of surface tension.....	78
<b>Figure 3.1:</b> Schematic of a capillary cell and illustration of charged molecule movement when electric field is applied.....	86
<b>Figure 3.2:</b> Chemical structures of (A) Triton X-100, (B) Tyloxapol (Regev and Zana 1999) .....	90

- Figure 3.3:** Representative micrographs of MBs stabilized by different NPs, 24 h after aeration. Scale bar = 20  $\mu\text{m}$ . (A): BCA, Tyloxapol, pH 4 (B): ECA, Tyloxapol, pH 4 (C): BCA, Triton X-100, pH 4, (D): OCA, Tyloxapol, pH 4 (E): BCA, Tyloxapol, pH 2.2 (F): BCA, Tyloxapol, pH 6. Red arrows pointed at the non-spherical MBs ..... 95
- Figure 3.4:** Shows system 5 and 6, 24 hours after aeration, the turbid layer at the surface of the system 5 represents the MBs creamed. .... 96
- Figure 3.5:** Micrographs of MBs stabilized by PBCA NPs (made at pH 4, 1wt.% Tyloxapol), (A): 1hour, (B): 24 hours, (C): 1 week, (D) 70 days. Scale bar =20 $\mu\text{m}$  ..... 97
- Figure 3.6:** Histogram of MB size distributions at different storage times stabilized by PBCA (A) and PECA (B) NPs formed with 1wt.% Tyloxapol at pH 4 ..... 99
- Figure 3.7:** Volume% of MBs stabilized by PBCA NPs 15 min after aeration (■), and 48 h after aeration (▲), [Tyloxapol blank in 76% glycerol 15 minutes after aeration (●) and 48 hours after aeration (▼)]..... 100
- Figure 3.8:** CLSM micrographs of PBCA stabilized MBs ..... 102
- Figure 3.9:** SEM micrographs of PBCA NPs at the A/W of MBs. In (B), the particle contact angle is measurable..... 103
- Figure 3.10:** Representative SEM micrograph of PECA NPs at the A/W interface ..... 104
- Figure 3.11:** Representative SEM micrograph of PBCA NPs formed in absence of surfactant at the A/W interface ..... 104
- Figure 3.12:** SEM micrographs of (A): PBCA NPs, (B): PACA NPs and (C): PBCA NPs made in absence of surfactant and (D): nanoparticle size distribution based on SEM images ..... 105
- Figure 3.13:** Micrograph of PBCA stabilized MBs (system 5) after 1 cycle of freeze – thaw ..... 106
- Figure 4.1:** Schematic of (A): aeration by piston and bubble syringe and (B): bubble syringe, the air flows between wire and tube wall and comes out in a form of small monodispersed bubbles, (C): micrograph of initial bubbles ..... 115
- Figure 4.2:** Size distribution of MBs produced from standard PBCA dispersion. 1<sup>st</sup> foam (■), 2<sup>nd</sup> foam (●), 3<sup>rd</sup> foam (▲), 4<sup>th</sup> foam (◆) ..... 118
- Figure 4.3:** Micrograph of MBs aerated by Ultraturrax after 4 cycle aeration by cylinder, scale bar = 10  $\mu\text{m}$ ..... 119
- Figure 4.4:** CLSM micrograph of PBCA stabilized MBs, taken from 3<sup>rd</sup> aeration, diluted in glycerol (ratio 1:20).scale bar = 20  $\mu\text{m}$ ..... 121
- Figure 4.5:** Comparison of size distribution of 1<sup>st</sup> foam produced at different concentration of PBCA NP. PBCA standard (■), 0.15 % PBCA (●), 1 % PBCA (▲), 2% PBCA (▼), Centrifuged and redispersed in its supernatant again (◆) and supernatant only (◀)..... 122
- Figure 4.6:** Schematic of impact of particle size on MB size, both bubbles have the same % particle coverage..... 123
- Figure 4.7:** Shows the size distribution of aerated PBCA containing 0.01 M KCl (■), 0.1 M KCl (●) and 1 M KCl (▲). Foam height and  $d_{32}$  are also illustrated . 125

- Figure 4.8:** SEM micrographs of (A): PBCA stabilized microbubble produced during 4<sup>th</sup> cycle of aeration (B): PBCA stabilized microbubble in presence of 1M KCl produced during 1<sup>st</sup> cycle of aeration..... 127
- Figure 4.9:** Impact of NP fractionation on MB size distribution (A): aerated supernatant, (B): aerated supernatant + 1 M KCl. 1<sup>st</sup> foam (■), 2<sup>nd</sup> foam (●), 3<sup>rd</sup> foam (▲)..... 130
- Figure 4.10:** Schematic of impact of low concentration (A) vs high concentration (B) of NPs on bubble stabilization ..... 131
- Figure 4.11:** Comparison of 1st foam produced at different concentration of PBCA or different condition. (A) : size distribution PBCA standard (■), 0.15 % PBCA (●), 1 % PBCA (▲), 2% PBCA (▼), supernatant only (◆), PBCA + 0.1 M KCl (◄), PBCA + 1 M KCl (►), (B): foam height ..... 132
- Figure 4.12:** Long term stability of MBs (aerated PBCA standard), 24 h (■), 6 months (●), 9 months (▲) ..... 133
- Figure 4.13:** Size distribution after 24 hour when initial bubbles size were 386 μm, PBCA standard (■), supernatant (●) ..... 134
- Figure 4.14:** Represents the impact of initial bubble size on final bubble size distribution, large needle (■), small needle (●) ..... 135
- Figure 5.1:** Schematic of (A) a single particle, (B) a single bubble covered and stabilized by nanoparticles ..... 140
- Figure 5.2:** Schematic of continues aeration chamber with 2 entries for water, particles ●, and bubbles ●, and two exits for water, particles and stabilized bubbles. The chamber is equipped with a stirrer ..... 141
- Figure 5.3:** The shrinkage ratio defined as  $\frac{r_b^{o2}}{r_b^i}$  plotted versus initial size of bubbles,  $r_b^i$ , in a system with a large excess of stabilizing nanoparticles, taken from Ettelaie and Murray (2014). In such a system the shrinkage is determined by the rate of adsorption and not the number of available particles. .... 146
- Figure 5.4:**  $\varphi_p^i$  plotted against  $r_b^{o2}$  for different  $W_d^i$ : 1 ml / h (■), 2 ml / h (●), 3 ml / h (▲), 5 ml / h (▼), 10 ml / h (◆) and 25 ml / h (◄). All results are calculated assuming that injected bubbles have a size of 100 μm. .... 150
- Figure 5.5:** : The required volume fraction of particles ,  $\varphi_p^i$ , needed to achieve the final size indicated on x – axis.  $\varphi_p^i$  plotted against  $r_b^{o2}$  for different  $r_b^i$ , when  $W_d^i = 1$  ml / h and the number of injected bubbles was 10000 bubbles per second. .... 151
- Figure 5.6:**  $\varphi_p^i$  plotted against  $N_b^i$  for different  $W_d^i$ , when  $r_b^{o2} = 10$  μm. All the results are calculated assuming that initial bubble size is 100 μm. .... 152
- Figure 5.7:**  $\varphi_p^i$  plotted against  $r_b^{o2}$  for different  $N_b^i$  when  $W_d^i = 1$  ml / h. All the results are calculated assuming that initial bubble size is 100 μm. .... 153
- Figure 5.8:**  $W_d^i$  plotted against  $r_b^{o2}$  for different  $\varphi_p^i$  %. All the results are calculated assuming that initial bubble size is 100 μm and injection rate is 10000 bubbles per second. .... 154

## List of tables

<b>Table 1.1:</b> Differences between polymerization system (Rao and Geckeler 2011) .	47
<b>Table 2.1:</b> Surface tension measurement for different surfactants and proteins. HFBII (Cox <i>et al.</i> 2007), Triton-X- 100 (Robinson, Sutton and Reid 2014), Tween 20 and 80 (Kothekar <i>et al.</i> 2007), NaCas (Abascal and Gracia-Fadrique 2009), WPI and $\beta$ -lactoglobulin (Woodward <i>et al.</i> 2004).....	76
<b>Table 3.1:</b> Yield, size (d) and zeta potential of NPs formed under different conditions and the stability of the corresponding microbubbles (MBs) formed on aeration. All systems used BCA monomer except * = ECA, # = OCA.....	88
<b>Table 3.2:</b> Represents the size changes after NPs formed for the period of 20 days	92
<b>Table 4.1:</b> Shows the dimension and bubble size produced by each bubble syringe .....	114
<b>Table 4.2:</b> Foam heights of different PBCA concentration.....	118
<b>Table 4.3:</b> Shows the foam height of PBCA stabilized MBs in presence of different concentration of KCl.....	125
<b>Table 4.4:</b> PBCA NPs size and $\zeta$ – potential before and after centrifuge at 500 g	128
<b>Table 4.5:</b> Shows foam heights of centrifuged PBCA dispersions .....	129
<b>Table 4.6:</b> Shows the foam heights when initial bubbles size were 386 $\mu$ m .....	135

# Chapter 1 :

## Introduction

### 1.1 Objectives

Aqueous foams are widely used by variety of different industries: from foods to cosmetics, fire extinguishing, blast mitigation and oil recovery (Wilson 1989). Bubbles also are used to produce low weight porous materials for thermal insulation and medical implants. Over the past two decades bubbles have played an important role in medical fields as a carrier for drug delivery and ultrasound imaging (Ashby *et al.* 2002; Hench and Polak 2002). However, the thermodynamically unstable nature of liquid foams raises critical issues in all of these applications. Foam instability arises from the high interfacial energy (tension) of the gas–liquid interface, and constitutes a driving force for decreasing the total interfacial area of the foam through coalescence and disproportionation (dissolution and shrinkage) (Gonzenbach *et al.* 2006).

This thesis will explore Pickering stabilization of microbubbles (MBs) using two different particles namely hydrophobin (HFB II) and poly butyl cyanoacrylates (PBCA). The objective of this project is to provide a better understanding of the effect of HFBII and PBCA nanoparticles (NPs) on MBs formation and stability in order to optimize MB stability during the shelf life of a product. This is done by investigation of the effect of

HFBI concentration on MBs size and stability, also the impact of mixing HFBI with other surface active materials. The chemical and physical properties of different poly alkyl cyanoacrylates (PACA) on MBs stabilization have been investigated. The stability of MBs covered by PBCA NPs as a function of concentration, multiple aeration, ionic strength, and initial bubble size was also studied.

## **1.2 Colloidal phenomena**

Colloid generally refers to the dispersed phase of a two-component system in which the elements of the dispersed phase are too small (although vague, suggests a size range from  $\sim$ nm ( $10^{-9}$  m) to  $\sim$   $\mu$ m ( $10^{-6}$  m), to be easily observed by naked eye and whose motion is affected by thermal forces. When the continuous phase, the suspending medium, is liquid they do not readily sediment and cannot pass through a membrane (such as in dialysis). Colloids appear in food, emulsions, gels, coating and biological systems, examples of naturally occurring colloids are milk, blood and paint. Colloids can be solid or liquid or particles dispersed in solid, liquid or gas medium. Gases also can be dispersed in solid or liquid. Solid or liquid particles dispersed in gas are known as aerosol. The Brownian force and gravity are the two main forces acting on colloidal particles (Mewis and Wagner 2011).

## **1.3 Interaction forces that influence stability**

Colloidal interactions rule whether the individual emulsion droplets or bubbles remain as separate bodies or they associate with each other. The characteristic of any types of aggregation formed (e.g., size, shape and deformability) is also determined by these colloidal interactions (Dickinson 2010a; Dickinson 2013). The interaction between two bubbles can be described in terms of inter-bubble pair potential  $w(h)$ . This is the energy

required for to bring two bubbles from an infinite distant apart to a surface to surface separation of  $h$ .

In a system consisting of only two similar bubbles with radius  $r$  at a surface to surface separation of  $h$  (Figure 1.1), it is more convenient to assume there are only two types of interactions occur between bubbles, attractive and repulsive attractions.

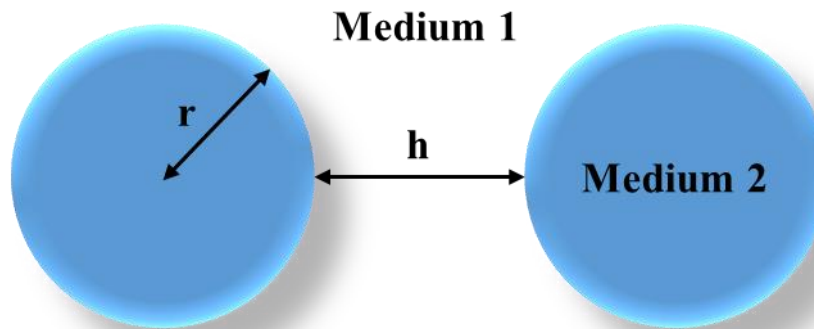


**Figure 1.1:** Dispersed phase (medium 2) of radius  $r$  separated by a surface to surface separation  $h$  in a liquid continuous phase (medium 1).

$$w(h) = w_{attractive}(h) + w_{repulsive}(h), \quad (1.1)$$

The overall interaction between bubbles depends on the magnitude and range of these two interactions. Different behaviour might occur depending on the nature of the interactions:

Repulsive interactions dominate at large separations where attractive interactions dominate at short separations. At long distances there are no effective interactions between the droplets. But when the droplets move toward each other the repulsive interactions dominate, however at a closer separations attractive interactions starts to dominate. Bubbles or any other particles tend to aggregate when the strength of the interaction is large compared to the thermal energy ( $|w(h_{min})| \geq kT$ ) (McClements 2016).

### 1.3.1 Van der Waals interaction

Atoms and molecules interact by so-called dispersion forces, as a consequence of the polarization of the electron cloud of one atom by the fluctuating electron cloud of another. This fluctuation polarization leads to an attractive force between the atoms. Colloidal particles are subject to similar effects, whereby the atoms of one colloid induce polarization in the atoms of another. The net effect of this fluctuating polarization is known as the van der Waals or dispersion force between the particles (Mewis and Wagner 2011). Van der Waals interaction is the weakest (ranging from 0.5 to 1 kcal/mol) of all intermolecular attractions between molecules and has a non-ionic nature. However, with a lot of Van der Waals forces interacting between two objects, the interaction can be very strong (Roy, Kar and Das 2015). Van der Waals interaction are always present and can be important both at small and large separations (up to 100 nm) however the van der Waals forces rapidly decay with distance between molecules (Walstra 2003).

The strength of the van der Waals interaction between particles is reduced because of a retardation. The origin of retardation is the time required for an electromagnetic field to travel from one particle to another and back. The frequency dependent contribution to the van der Waals interaction is the result of a transient dipole in one particle causes a dipole in another particle. These two dipoles then interact together. The retardation is more important for  $h$  values (particle distances) larger than 5 nm. Van der Waals interactions not only take place between two homogenous spheres that are separated by an intervening medium. In fact any stable colloidal particles will be covered by a thin layer of stabilizing molecules. This interfacial layer has a different physicochemical properties than either phases. The molecules at the surface of the stabilizing particles make the greatest contribution to overall van der Waals interaction. Therefore the composition of the interfacial layers can have a significant influence on the van der Waals

interactions, particularly at close separations. This is regarded to as influence of interfacial layer on van der Waals interactions (Walstra 2003).

For two spherical particles with radii  $r_1$  and  $r_2$  respectively separated at a distance  $h$  (distance between particle surfaces) and if  $h \leq r_1, r_2$ , then the energy ( $V$ ) of van der Waals is:

$$V_{vdW} = -\frac{A\bar{r}}{12h}, \quad (1.2)$$

Where

$$\bar{r} = \frac{2r_1r_2}{r_1 + r_2}, \quad (1.3)$$

So the repulsive energy is inversely proportional to interparticle distance. For two parallel homogenous plates, their size larger than  $h$  and thickness larger than 5 times  $h$ , the result is:

$$V_{vdW} = -\frac{A}{12\pi h^2}, \quad (1.4)$$

where  $V_{vdW}$  is expressed as  $\text{J m}^{-2}$ . The coefficient  $A$ , known as the Hamaker constant, is a function of the material of the particles as well as that of the suspending medium (and can also depend on the separation distance) (Walstra 2003).  $A$  ranges from about  $30 \times 10^{-20}$  J, for gold particles in water, to values of the order of  $1 \times 10^{-20}$  J or less, for inorganic and polymeric particles (Mewis and Wagner 2011).

In summary general features of van der Waals interactions are: 1) The interaction between two droplets in a continuous phase is always attractive. 2) the larger the droplets the stronger the van der Waals interaction. 3) The interaction is relatively long range, however the strengths of the interactions decrease as the distance between droplets

increases. 4) The strengths of the interaction depends on the physicochemical properties of the particles and continuous phase (Israelachvili 2011).

An accurate calculation of range and magnitude of van der Waals interaction is extremely difficult due to lack of all physicochemical data that are essential for calculation. Considering that the van der Waals interactions are strong and long range, and also that they are always attractive implies that any colloidal particles, including bubbles, always have a tendency to aggregate together in absence of repulsive interactions (Israelachvili 2011).

### **1.3.2 Electrostatic repulsion**

Any aqueous surface or interface carries an electric charge. It must be noted that the surface of pure water is negatively charged due to adsorption of  $\text{OH}^-$  ions. In salt solutions there is a strong preference for some ions, mainly anions to adsorb at the interface. In the case of food systems ionic surfactant and proteins are adsorbed to the interface, hence the surface charge significantly increases (Walstra 2003). Adsorption of any ionic substances available in a colloidal system (from either phases) to the particles surface can influence the surface charge density. Examples are multivalent mineral ion (e.g.,  $\text{Fe}^{3+}$ ,  $\text{Cu}^{2+}$ , and  $\text{Ca}^{2+}$ ), ionic surfactants (e.g., small molecule surfactants, fatty acids and phospholipids) or charged nanoparticles (e.g., silica dioxide) or charged biopolymers (e.g., polysaccharides and proteins). The driving force for adsorption of these charged ions is electrostatic or hydrophobic attractions depending on the type of species. For example ions with sufficient number of nonpolar groups such as proteins or ionic surfactants are mainly adsorbed via hydrophobic interaction where hydrophilic ions such as mineral ions are usually adsorbed via electrostatic interactions.

Electrostatic interactions can strongly influence the overall stability and physicochemical properties of a colloidal system. The sign and magnitude of electrical charges depends on

type of stabilizer and its concentration and the environmental conditions such as ionic strength, temperature and pH. Usually all the particles in a system are stabilized by same type of stabilizer, hence they all have same electrical charge. The electrostatic interaction between similarly charged droplets is always repulsive, acting against particle aggregation. Electrical characteristic of the interfacial layer and the ionic composition of the continuous phase strongly influence the electrostatic interactions (Hunter 2001).

If an excess charge is present at the interface it results into electrostatic surface potential  $\psi_0$ . This may lead to repulsion between two charged surfaces that are close together. Counterions (ion with opposite sign charge to that of particles at the interface) pile up close to the interface, while the coions are depleted (see Figure 1.2 A). This mechanism leads to formation of an electric double layer and the charge at the surface is compensated for (Walstra 2003).

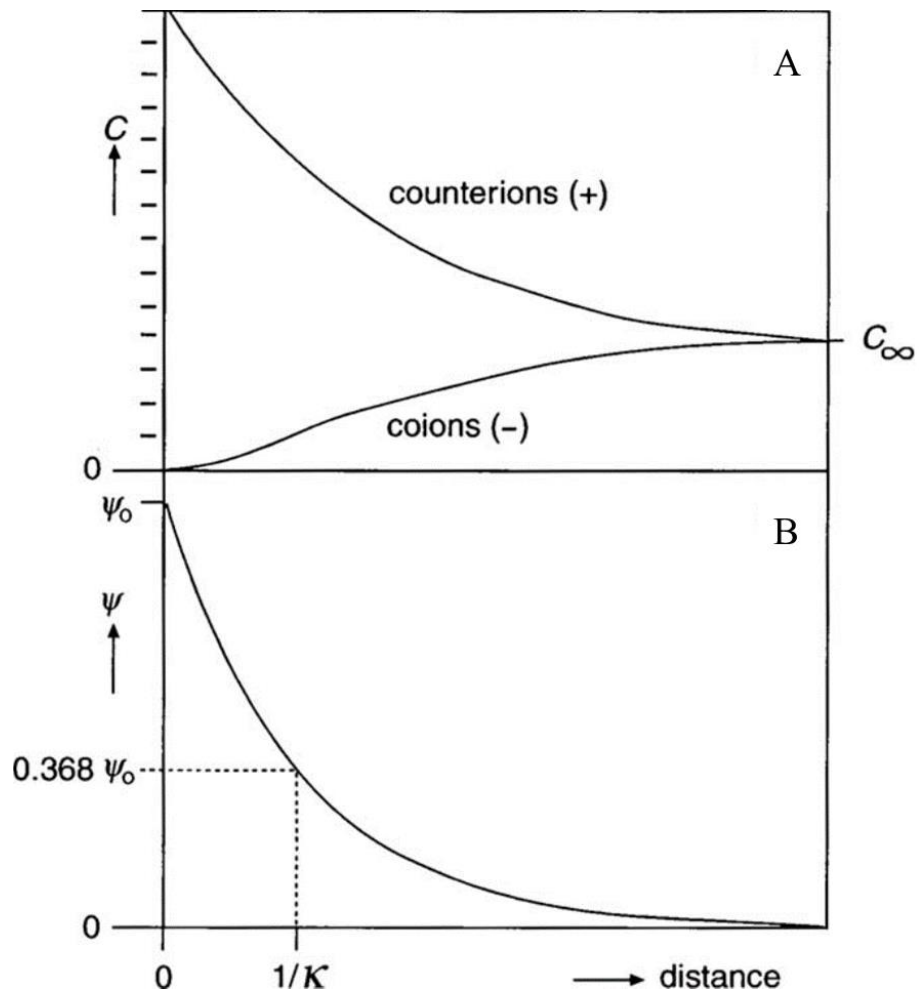


**Figure 1.2:** (A): the concentration ( $c$ ) of coions and counterions at the vicinity of a negatively charged surface, where  $c_\infty$  is the bulk electrolyte concentration. (B): shows the decrease of electrostatic potential close to the surface, thickness of the double layer is shown as  $1/\kappa$  (Walstra 2003)

The distribution of the ions is governed by two opposing effects. The attractive energy between ions of opposite charge pulls the counterions to the surface to neutralize the charge (whereas, the coions are pushed away from the surface). This is counteracted by the loss in mixing entropy that it would cause. The system will go toward a minimum in free energy, and from this principle the distribution of the ions can be calculated. The electrostatic potential decreases as the distance from the interface increases (see figure 1.2 B) (Walstra 2003).

The range of electrostatic interaction can be determined by Debye length ( $1/\kappa$ ). Debye length is a measure of how far the electrical properties of an interface are sensed within the bulk or simply is the nominal thickness of the electric double layer.

According to Debye – Huckel theory:

$$\psi = \psi_0 \exp(-\kappa h), \quad (1.5)$$

Where  $\psi_0$  is surface potential and  $h$  is the distance from the surface.

$$\kappa^{-1} = \sqrt{\frac{\epsilon_0 \epsilon_R kT}{e^2 \sum n_{0i} z_i^2}}, \quad (1.6)$$

where  $n_{0i}$  is the number of ionic species of type  $i$  in the bulk electrolyte (in molecules per  $m^2$ ),  $z_i$  is their valency,  $e$  is the elementary electrical charge ( $1.602 \times 10^{-19}$  C),  $\epsilon_0$  is the dielectric constant of a vacuum and  $\epsilon_R$  is the relative dielectric constant of the solution.

For an aqueous solution at room temperature  $\kappa^{-1} \approx 0.304/\sqrt{I}$  nm, where  $I$  is the ionic strength (mole/litre) (Israelachvili 2011; McClements 2016).

The double layer is not a static layer that adheres to particles. Ions and molecules diffuse in and out. When a charged particle is subject to an electrokinetic experiment (meaning that the particle is moving relative to the salt solution in which it is dispersed due to an externally applied electrostatic potential gradient) the slipping plane between the particle and liquid is close to geometrical particle surface. The zeta potential ( $\zeta$ - potential), which is the electrical potential determined in such an electrokinetic experiment (electrophoresis), is the potential at the slipping plane. It agrees with the value of  $\psi_0$ , required to calculate the electrostatic repulsion (Walstra 2003). If the electrostatic interaction between a charged surface and the counter-ions is weak the surface charge density is simply related to the surface potential, so the electrical properties of the surface are influenced by the presence of electrolyte in the aqueous phase. If it is assumed the surface charge density remains constant when salt is added to the aqueous phase, less

energy is required to bring the charge from infinity to particle surface through an electrolyte solution due to screening effects. If the electrical potential remains constant when the salt concentration is increased, the surface charge density must increase (Evans and Wennerström 1999).

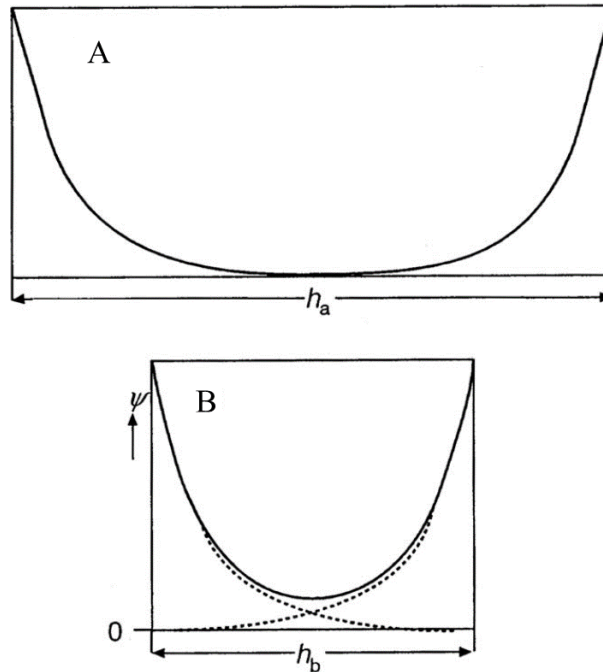


**Figure 1.3:** Overlap of the electrical double layers between two particles at a distance  $h$  from each other. In (A) the double layers virtually do not overlap, and the electrostatic potentials  $\psi$  equal zero in the middle; in (B) the particles are closer and their electrical double layers do overlap, which causes the potentials to locally increase (Walstra 2003).

When two particles (similarly charged) approach each other their counterion clouds overlap (Figure 1.3) hence the repulsive interaction increases this implies that work must be applied to bring particles closer to each other. Based on this increase in potential free energy can be calculated. However the mathematics of the theory is very complicated and gives results if the value of  $\psi_0$  is not too high, (below 30 mV). For spheres the relationship is :

$$V_{EI} = 2\pi\epsilon_0\epsilon_r r\psi_0^2 \ln(1 + e^{-\kappa h}) \approx 4.5 \cdot 10^{-9} r\psi_0^2 \ln(1 + e^{-\kappa h}), \quad (1.7)$$

Where the part after the  $\approx$  sign is only valid for water at room temperature ( in SI units).

Some general features of electrostatic interactions are: 1) The strengths of the interaction decreases with droplet separation, and it can be either short or long range depending on the ionic strengths and dielectric constant of the electrolyte solution that surrounding the droplets. 2) The strengths of the electrostatic interaction depend on the droplet size. 3) Electrostatic interactions could be either attractive or repulsive. If the droplets have similar charges it is repulsive and if the droplets have opposite charges it is attractive (opposite charges of droplets is rare) (McClements 2016).

### 1.3.3 DLVO theory

The DLVO theory was developed by Derjaguin, Landau, Verwey and Overbeek in the 1940s. The basic idea of the DLVO theory is that the stability of the lyophobic colloids in an aqueous system is determined by van der Waals attraction and electric repulsion via the following equation:

$$V_T = V_{vdW} + V_{EL}, \quad (1.8)$$

Where  $V_T$  is the total interaction free energy at any value of  $h$ . If there is no other interaction forces, then this equation is correct (Dickinson, Robson and Stainsby 1983; Walstra 2003)

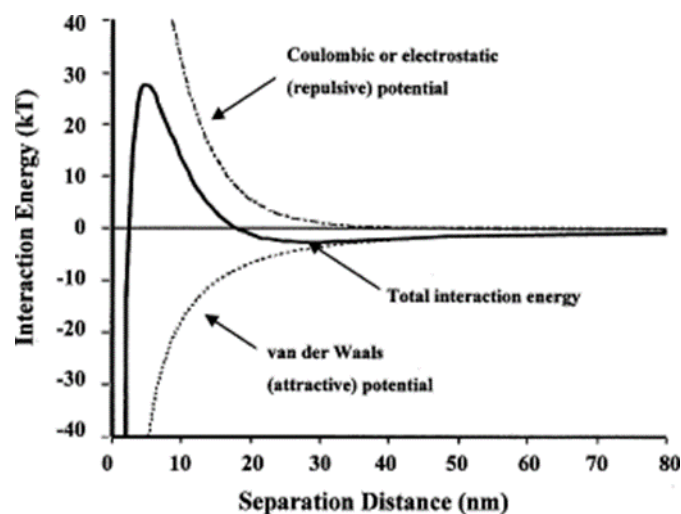


**Figure 1.4:** Schematic interaction energy versus distance profiles of DLVO interaction. The attractive van der Waals and the repulsive electrostatic potentials form the total interaction energy (Adair, Suvaci and Sindel 2001).

Figure 1.4 shows the interaction energy versus the separation distance of two charged particles. The attractive interaction energies arises from the van der Waals interactions. As the particles get closer together the van der Waals forces increases. Because no work is needed to bring the particles together the  $V_{vdW}$  is negative. The  $V_{EI}$  arises from the electric double layer that surrounds the two particles, when the distance between two particles decreases the  $V_{EI}$  starts to decay and as mentioned before energy is required to push the particles closer together, so the  $V_{EI}$  is positive. Variations in the ionic strength of the dispersion controls the range of the double layer interaction, while the van der Waals forces are insensitive to the ionic strength. Adding the van der Waals attraction and the electrostatic repulsion gives the total interaction energy at a particular separation distance. For low ionic strength, both particles have a net repulsion at large and intermediate separations. To approach one another requires that the kinetic energy of the particles due to thermal motion be larger than the finite energy barrier. The combination of two forces dictates the stability of the colloidal dispersion (Adair, Suvaci and Sindel 2001).

The DLVO theory is very useful in predicting stability against aggregation for inorganic systems. However, in food and many other organic systems, the DLVO is insufficient to calculate the total interaction, because in most cases steric interactions (raised from protruding polymer chains around particles) also influence the stability (Walstra 2003).

### 1.3.3.1 DLVO theory example

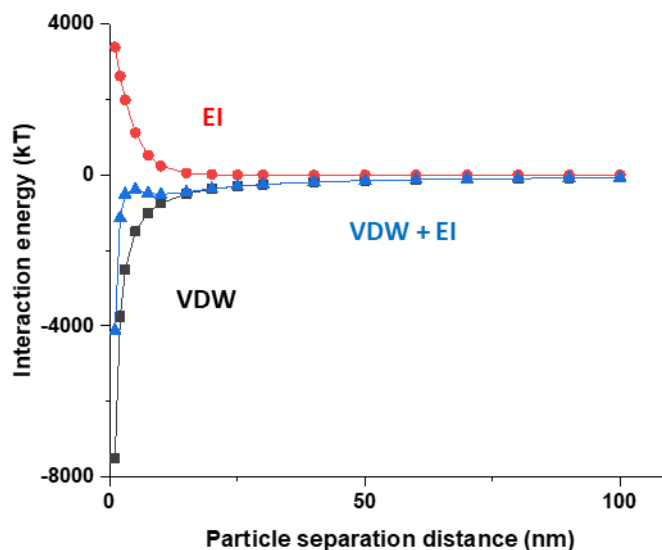


**Figure 1.5:** The DLVO plot for the interaction of two MBs in water, EI: electrostatic interaction, VDW: van der Waals interaction. For modelling parameters see the text.

Interaction of two bubbles are generally described in the context of DLVO theory as described above. Figure 1.5 depicts an interaction energy vs particle separation distance plot based on DLVO theory for the interaction of two MBs (radius  $10\ \mu\text{m}$ ) in an aqueous dispersion of PBCA. The use of  $10\ \mu\text{m}$  as a bubble radius is based on our results of MB production (see chapter 3 & 4). The MB radius influences the magnitude of van der Waals and electrostatic interaction energies in the same relative magnitude. For the calculation of interaction energies  $A = 3.7 \times 10^{-20}\ \text{J}$ ,  $\epsilon_r = 80$ ,  $T = 298\ \text{K}$  and  $\psi_0 = -24\ \text{mV}$  was taken into account. The Debye length was equal to  $3\ \text{nm}$  at  $0.01\ \text{M}$  ionic strength. Increasing the ionic strength to  $1\ \text{M}$  resulted into very small Debye length ( $1/\kappa = 0.3\ \text{nm}$ ) that was associated with strong screening surface charge. The Figure 1.5 clearly shows that van der Waals interaction dominates the overall interaction curve, and electrostatic repulsion is so short ranged that can be neglected this is through when MBs are not stabilized. Since the MBs (stabilized by PBCA NPs) dispersion are a stable system, it can be concluded that DLVO is not able to fully explain the MB interaction when they are stabilized by

PBCA NPs. Due to attachment of PBCA NPs to the surface of MBs the minimum distance between two MBs was at least 160 nm (the radius of a PBCA NP is 80 nm) so at this range of distance van der Waals interaction can be neglected too because the hard core potential energy between particles are several times larger than the van der Waals attraction.

#### **1.3.4 Steric repulsion**

When a layer of proteins, particles or surfactants adsorb to an air – water interface the long range interactions occur and prevent particles from moving closer to each other, it means the interaction forces reduce the risk of aggregation and coalescence (Napper 1977). When two particles move toward each other their interfacial layers starts to overlap and interact together. Steric interactions are a result of this intermingling or compression of the interfacial layer. At close separation steric interactions are strongly repulsive and hence prevent aggregation. This is called steric stabilization. It must be stressed that the overall magnitude and sign of the steric interactions are dependent on the characteristic of the interfacial layer. Steric stabilization is effective when a steric barrier layer is formed by polymer chains that are either freely adsorbed or grafted onto the colloidal surface. Grafted means that one end of molecules strongly attached onto a particle (Walstra 2003). Steric interaction can be divided in to two components: mixing and elastic contributions (see Figure 1.6). The mixing contribution occurs as a result of intermingling of the stabilizing molecules within the interfacial layers as they overlap. The elastic contribution is due as a result of compression of interfacial layer (Hunter 2001).

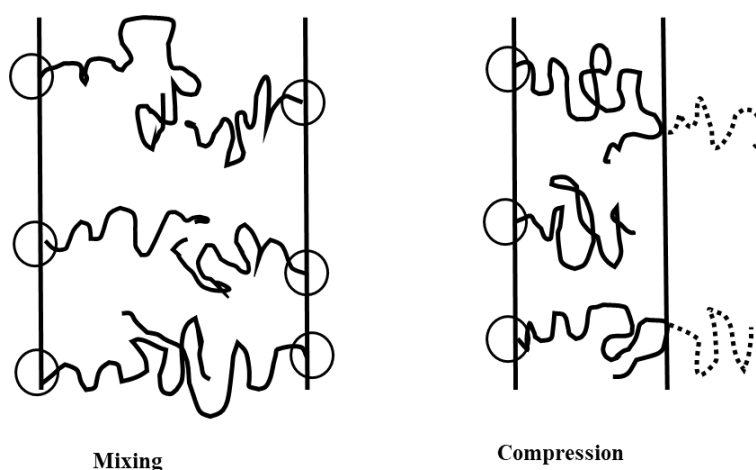


**Figure 1.6:** Steric interactions between two bubbles can be divided into: a mixing contribution that involves interpenetration of the polymer chains and an elastic contribution that involves compression of the polymer layers.

If the interfacial layer are compressed without any interpenetration of polymer molecules, the interaction is elastic. When the interfacial layer is compressed then there is less space available for polymer molecules to occupy, hence their configuration entropy is reduced and this is not thermodynamically favoured, thus this type of interaction is always repulsive (McClements 2016).

The quality of the solvent determines the whether the mixing contribution is attractive or repulsive. Interpenetration of polymer results into local increase in concentration of polymer. In a good solvent increase in concentration of polymer is thermodynamically unfavourable as it reduces the number of the polymer- solvent contacts and leads to repulsive interaction. However in a poor solvent it is thermodynamically favoured as it increases the number of polymer – polymer contact. This leads to an attractive interaction between the droplets (McClements 2016).

If the second particle gets very close to the first particle and restricts the volume in which the protruding polymer chains can be, this means that the number of conformations that a chain can assume is restricted, so the entropy of these chains is lowered, therefore the free energy is increased, hence a repulsive force will act. The repulsive free energy is very

large: several times  $k_B T$  for each polymer chain involved, and the number of polymer molecules in the gap between two particles will often be of order  $10^3$ . This means that at very close approach (for example for  $h < \delta$ ) the repulsive energy between the particles will always be positive and large; it increases sharply with decreasing value of  $h$ .

However, when two particles approach each other, mixing of both polymer layers will occur for  $h < 2\delta$ , i.e., before volume restriction comes into play. This means that the mixing entropy will decrease, and this then would also lead to repulsion. It occurs most of the time but not always, as it depends on the solvent quality for the polymer chains. As mentioned above if the quality of the solvent is low, just high enough to allow the chains to protrude into the liquid, the attractive energy between polymer segments may be large enough to more than compensate for the decrease in mixing entropy, thereby causing attraction. Another way to explain these mechanisms is by considering the osmotic pressure in the liquid between approaching particles. If the pressure increases in the gap between the particles, solvent will be drawn into the gap to lower the osmotic pressure again, so there will be repulsion (Walstra 2003).

A model known as self-consistent field model can calculate the conformation of the molecules in the polymer layer, and as a result it can also calculate the steric interaction energy. The free energy of the polymer layer is then minimized by considering all possible conformations of the polymer chains. The theory requires knowledge of the magnitude of variables that is not mostly available. These variables that affect the polymer conformation are polymer properties (i.e., chain length, chain stiffness and branching), solvent quality and also density and distribution of electric charges and ionic strength. Figure 1.7 is an example of total free energy. in this example the van der Waals attraction is also considered.

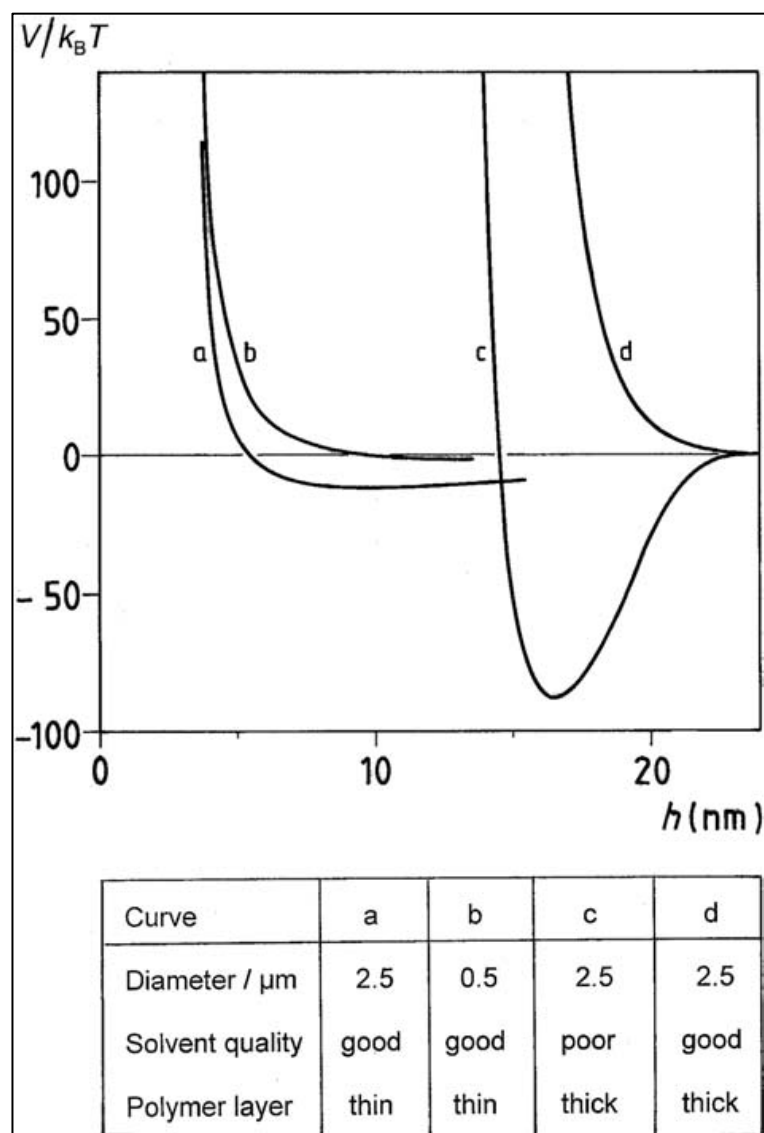


**Figure 1.7:** The total free energy  $V$  relative to  $k_B T$  as a function of  $h$  (interparticle distance), between same sized spherical particles covered by a layer of polymer. Van der Waals attraction and steric interaction is considered for calculation (Walstra 2003).

If the solvent has a poor quality then a deep energy minimum occurs, which causes a strong attraction. Curve (c) and (d) correspond to same polymer but with different solvent composition.

An effective steric stabilizer must have number of physicochemical properties: 1) High coverage of the droplet surface. 2) It must have an amphiphilic nature so it has an affinity for both phases, with some parts that protrude into the bulk phase, and some that protrude or adsorb strongly to the dispersed phase. 3) The continuous phase must be a good solvent

for the parts of the stabilizer that protrude into it. 4) The steric repulsive interaction must be able to act over a distance comparable to the van der Waals interactions. This means that stabilizers with the ability to form thick layer (e.g., gum arabic) are more effective steric stabilizers compared to the ones that form thin layers at the interface (e.g., globular proteins) (Dickinson 2003).

## 1.4 Foams, bubbles

Bubbles are generated by dispersing gas in a continuous phase, where the continuous phase is usually liquid (Pugh 1996; Ettelaie *et al.* 2003; Binks and Horozov 2005). The liquid phase could be solidified later by cooking or freezing; examples are bread and ice cream (Murray and Ettelaie 2004). Polyhedral foam is referred to polyhedral bubbles that are packed together. Bubbly foam refers to well dispersed spherical bubbles (Xu *et al.* 2008).

Bubble interfaces and the film around them partly reflect the rays of light impinging upon the foam/ bubble dispersion. The multiple reflections of light in all different directions scatter the incident light in a very efficient way so the foam/ bubble dispersion is seen white. Smaller bubbles have more interface therefore reflect more light and look whiter compared to larger bubbles (Bergeron and Walstra 2005).

The ratio of gas to liquid is an important factor determining the foam structure characteristics. The gas volume fraction ( $\varphi$ ) can be used to quantify this ratio. When the gas volume fraction is small, sometimes the system is called aerated rather than a foam. If the gas volume fraction is  $\leq 0.63$  the foam is considered as a wet foam while high gas volume fraction  $\geq 0.8$  is called dry foam (Figure 1.8). When  $\varphi$  is high bubbles are forced to contact and form polyhedral bubbles (Bergeron and Walstra 2005; Weaire and Hutzler 1999). Here often the distinction between the different types of foam is not made and the word foam is used for all bubble dispersions.

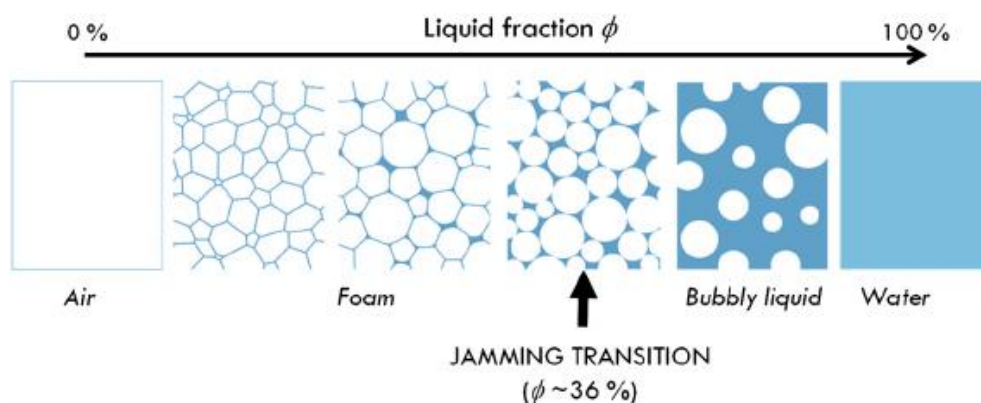


**Figure 1.8:** Schematic representation of foam with different liquid volume fraction (Langevin 2017)

In the late 1960's Claude R. Joyner noticed that dye injection into patient's heart ventricles improved the contrast of the ultrasound signals. Later on it was found that contrast enhancement arises from formation of very fine bubbles (few micrometre ) at the needle tip (Kremkau *et al.* 1970). After this, microbubbles (MBs) become an interesting topic for medical applications (Unger *et al.* 2002; Borden *et al.* 2006; Ferrara, Pollard and Borden 2007; Sirsi and Borden 2009) and also variety of other industries ranging from food (Haedelt, Beckett and Niranjana 2007; Tchuenbou-Magaia *et al.* 2011; Rovers *et al.* 2016), coating, cosmetic and oil recovery to light weight microporous structure which has application in medical and engineering fields (Gonzenbach *et al.* 2006).

MBs are perceived as a new ingredient for food industry, to enhance sensory properties, improve food texture, design novel products and reduce fat content (Zúñiga and Aguilera 2008; Tchuenbou-Magaia, Norton and Cox 2009; Tchuenbou-Magaia *et al.* 2011; Rovers *et al.* 2016).

## 1.5 Surface behaviour of surfactants, proteins and nanoparticles

### 1.5.1 Surface tension

When a surface-active substance is added to water, it spontaneously adsorbs at the surface and decreases the surface energy. A monolayer is formed, with the polar parts of the

surface active molecules in contact with water and the hydrophobic parts in contact with air. The decrease in surface tension is identified as the surface pressure,  $\Pi$ , equation **1.9**

$$\Pi = \gamma_w - \gamma, \quad (1.9)$$

where  $\gamma_w$  is the surface tension of pure water. It is difficult to measure the amount because the majority of the surface active molecules are usually still dissolved in bulk water. Thermodynamics predicts that the surface concentration  $\Gamma$  is related to the bulk concentration,  $c$ , (equation **1.10**):

$$\Gamma = -\frac{1}{kT} \frac{\partial \gamma}{\partial \ln c}, \quad (1.10)$$

Where  $k$  is the Boltzmann constant and  $T$  is the absolute temperature. This equation is known as the Gibbs adsorption equation. It works reasonably well for surfactants that adsorb reversibly from dilute solutions (Langevin 2008).

Equation **1.10** is less helpful when proteins adsorb, because their adsorption is essentially irreversible. Also, proteins partially change the conformation during adsorption to expose their hydrophobic parts to the air. Therefore the surface and bulk proteins are different. Proteins surface concentration can be estimated via neutron or X-ray reflectivity (Langevin 2008).

Flexible proteins such as  $\beta$ -casein change their conformation more easily compared to globular proteins, such as  $\beta$ -lactoglobulin. Flexible proteins adsorb more rapidly to the surface and in larger amounts ( $2 - 3 \text{ mg m}^{-2}$ ) compared to their globular counterparts ( $1 - 2 \text{ mg m}^{-2}$ ). In addition, flexible proteins creates larger surface pressure, hence in principal they can displace the globular proteins from the interface. However, in practice, the adsorbed layer is dominated by the protein that adsorbs first at the surface, related to the quasi-irreversibility of protein adsorption (Dickinson 1999).

Small surfactant molecules can also displace the proteins from the surface because can pack more tightly and produce a larger surface pressure. If the concentration of the surfactant is not high enough then a layer of protein surfactant can be formed, with the protein and surfactant forming separate surface domains. Displacement of protein by surfactant is much easier when the surfactant is added to the solution just after adsorption, when the protein molecules have had less chance to unfold and cross-link. It is possible to displace the protein from the interface by two different mechanism: a) the replacement mechanism, surfactant are more effective than proteins or protein – surfactant complex, in lowering the interfacial free energy. b) the solubilization mechanism, protein – surfactant complex is more soluble in water than the protein itself, therefore protein desorption increases as a result (Dickinson 1999).

Surface layers of nanoparticles at the air – water interface have been less explored compared to proteins and surfactants. However the surface layers of nanoparticles at oil – water interface has been studied more extensively. Monodisperse spherical particles can form hexagonal close-packed networks with well-defined contact lines when jamming at the interface (Subramaniam *et al.* 2006). The origin of the forces that keep particles packed together has been debated for many years. These forces are shown to have a dipolar origin and partial wetting of particles by aqueous phase stops them from sticking irreversibly together. When the particles are not completely hydrophobic or hydrophilic they adsorb irreversibly to the interface, and form monolayers. If the monolayers are compressed they buckle and when the monolayers decompressed, they break into isolated domains with the particles remaining in a compact state (Safouane, Langevin and Binks 2007).

### **1.5.2 Dynamic surface tension**

As previously discussed, when a new surface is formed molecules from the bulk adsorb to form a layer. Free surfaces are created by using devices such as liquid jets or drops.

Dynamic surface tension devices are used to measure surface tension as a function of time. When the adsorption is controlled by diffusion, at short times the surface concentration can be calculated via the following equation (Langevin 2008).

$$\Gamma = 2\sqrt{\frac{Dt}{\pi}}c, \quad (1.11)$$

For low molecular weight (MW) surfactants typical equilibrium surface concentrations are of the order of one molecule per nm<sup>2</sup>. For bulk concentrations in the millimolar (mM) range, the adsorption times are  $\approx 10$  ms. The adsorption time for bulk concentration around 0.1 mM increases to 1 s (Ybert and Meglio 2000).

In case of proteins it must be noted that adsorption at air – water interface is much slower than adsorption at oil – water interface. It has been suggested that proteins may adsorb more reversibly at the air – water interface than at oil – water interface (Beverung, Radke and Blanch 1999). After the initial diffusion step, a long reorganization step takes place in the protein monolayer. This reorganization step is usually longer in case of globular proteins as their unfolding process at the surface needs greater energies. For example for concentration in the order of 0.1 g L<sup>-1</sup> the reorganization takes between 1 and 2 hours. The reorganization process is quicker for flexible proteins because they have little or no secondary structure. Another important factor that impacts the structural change is the population of the protein at the surface. When the concentration of adsorbed protein is low then they have more space to unfold. Therefore the proteins that adsorb early have a greater opportunity to unfold and have less exchangeable with bulk phase proteins (Dickinson 1999). A third process, surface gelation, happens at longer time scales. Surface gelation occurs as the partially unfold proteins cross-link via H-bonds, hydrophobic bonds, etc. As a result of cross-linking the adsorption irreversibility is increased. Late-adsorbed proteins usually participate in forming secondary protein layers,

i.e., multilayers. The formation of multilayers causes formation of a rigid skin around the bubble (Li, Zhang and Yan 2001).

In case of nanoparticles, most studies have been made using the particle spreading procedure. Adsorption from solution has been studied for mixture of surfactants and particles. The adsorption rate is quite slow similar to proteins (Ravera *et al.* 2006).

When the adsorption process is finally complete, surface tension values are similar for surfactants and proteins, though usually lower for surfactants. However the foam stability can be totally different. So the surface tension appears not to be the main factor determining foam stabilization. Surface viscoelasticity is more important in terms of controlling the foam stability (Langevin 2008).

### **1.5.3 Surface viscoelasticity**

It is generally accepted that emulsion and foam stability are related to the viscoelastic properties of the adsorbed monolayer at the air- water or oil- water interface (Langevin 2000). Viscoelasticity is a property of materials that exhibit both viscous and elastic characteristic when undergoing deformation. Viscous materials such as water resist shear flow and strain linearly with time when a stress is applied. On the other hand elastic materials strain when stretched and immediately return to their original state once the stress is removed. Levich (1962) recognised that monolayers exhibit surface viscoelasticity. Gibbs was the first to show that liquid interfaces are not as sharp as mathematical surfaces, therefore he introduced “surface excess” properties. Surface viscosity and elasticity can be defined as excess properties. Elastic and viscous parameters can be categorised under compression parameters and shear parameters, with a modulus  $G$  and a surface viscosity  $\eta_s$ . Different types of devices are available to measure shear and compression parameters. Oscillating disks and channel viscometers are the most popular devices to study the surface shear properties. Surface light scattering, moving

barrier devices and oscillating bubbles has been widely used to study the compression properties of monolayers at the surface. Large frequency variations of the viscoelastic coefficients, have been observed in different systems particularly in case of dilatational rheology of soluble monolayers because of the coupling with bulk. A model has been developed to explain the frequency variations of the viscoelastic coefficient. The assumption of this model is that upon on compression, some of the surface active molecules dissolve into water underneath the monolayer to restore the equilibrium surface concentration. After the monolayer expansion the molecules comeback to the surface again. The compression viscoelasticity of protein monolayers is similar to that of low molecular weight surfactants, but the elastic modulus is a little larger for globular proteins. The difference in shear parameters is much larger. For example the surface shear viscosity of  $\beta$ -casein and  $\beta$ -lactoglobulin are around  $1 \text{ mNsm}^{-1}$  and  $1 \text{ Nsm}^{-1}$  respectively. These values are much larger than that of surfactant solutions which are in the region of  $1 \text{ }\mu\text{Nsm}^{-1}$  (Langevin 2008).

It must be noted that the viscoelastic properties of nanoparticle layers are not well explored and there are a very limited number of studies particularly in case of nanoparticle layers at the air – water interface. One of the difficulties in measuring the viscoelastic properties of nanoparticle monolayers is that they are solid-like materials with non-zero shear modulus, therefore the standard data analysis is not valid (Zang *et al.* 2010).

Surface viscoelastic measurements are performed on macroscopic surfaces and the range of strains and stresses applied do not reflect the conditions of practical foam formation and evolution. For example bubble break- up involves large deformations and high strain rates. It follows that the linear surface viscoelastic regime does not have a great relevance to foam properties (Bos and Vliet 2001). For example the viscoelasticity of protein monolayers have been studied and it is significantly non-linear and dependent on the magnitude of strain and strain rates. Few techniques are available to study the monolayer

rheology under non-equilibrium conditions and large deformations and deformation rate. The overflowing cylinder technique is one example of useful equipment to study the dilatational viscoelasticity of surface monolayers. The advantage of the overflowing cylinder is that the expansion behaviour of the liquid surface is of a pure dilatational nature, so surface shear cannot influence the measurement (Prins 1999).

## **1.6 Microbubble generation techniques**

Air and water are two immiscible fluids. It is important to note that pure liquids cannot foam unless a surface active material is present. When a gas bubble enters into the pure liquid it will burst immediately after the liquid drains (Pugh 1996). Gas, liquid, surface active materials and energy are the four necessary ingredients to make foam. When foam is generated the interfacial area between the phases is increased thus the interfacial free energy is increased. Surface active materials play an important role in foam formation by lowering the surface tension. Lowering the surface tension reduces the Laplace pressure thereby facilitating break up bubbles to smaller ones (Walstra 2003; Walstra 1989). The Laplace pressure is the pressure difference between the inside and the outside of a curved surface that forms the boundary between a gas region and a liquid region (Martinez *et al.* 2008).

### **1.6.1 Sonication**

A wide range of techniques have been developed to generate MBs with different sizes e.g., from 0.1 – 50  $\mu\text{m}$ . One of the most common way of producing MBs is via sonication. In this method gas is dispersed in a suspension of coating material such as protein polymer or surfactant, by applying high intensity ultrasound (Unger *et al.* 1998; Zhao *et al.* 2005). Sonication process involves two main mechanisms, a suspension of microbubble is produced and their surface covered by a layer of surfactant or protein. Then surface layer

is chemically modified due to high pressure and temperature caused by inertial acoustic cavitation of the system (Suslick *et al.* 2000). For example if a protein is used as the coating material it can cross-link via superoxide formed from sonolysis of the water (Suslick and Grinstaff 1990). In the case of surfactants it has been shown that their structure is also modified as result of high temperature and pressure (Wang, Moser and Wheatley 1996). However the structure alteration is not completely explained or understood yet. This surface modification improves the microbubble stability.

### **1.6.2 High shear mixing**

Another well-known method for generation of microbubble is using high shear, especially for microbubbles that are stabilized by polymer coating. The high shear is mainly used for emulsification of polymer (see Figure 1.9). In this method the polymer, usually dissolved in an organic solvent, is emulsified in an aqueous phase that contains a suitable stabilizer. The volatile solvent evaporates and the polymer adsorbs to the surface of formed droplets. These droplets are freeze dried after the remaining solvent is washed away (Bjerknes *et al.* 2000). What is left is hollow/ partially hollow microspheres depending on how porous the polymer shell is. The porosity determines whether it is possible to remove the solvent (liquid) inside the microspheres. Microbubble size depends on the initial size of droplets, and coalescence of microspheres during the process. Additional filtration is required to narrow down the size distribution (Bjerknes *et al.* 2000).

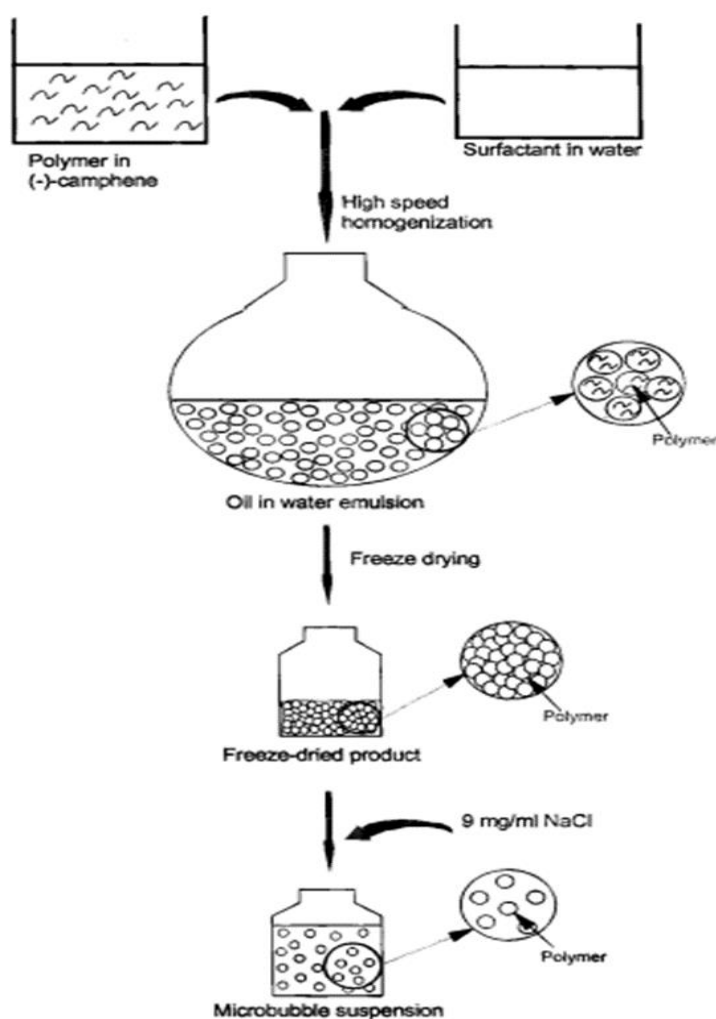


**Figure 1.9:** Production of MBs, high shear mixing is used to emulsify the polymer (Bjerknes *et al.* 2000)

### 1.6.3 Membrane processing

In this method the components are forced through a porous membrane (Joscelyne and Trägårdh 2000). Microbubbles are produced by adding gas to the system as a dispersed gas phase. An alternative way of forming microbubble by this technique is making liquid droplets that can form microbubbles later by using the freeze drying process (Bao *et al.* 2007) as described in the previous section: 1.6.2. Membrane emulsification offers greater control on microbubble size and therefore the size distribution becomes much narrower compared to high shear mixing or sonication techniques. It is possible to form almost monodispersed microbubbles via this technique. However the process is strongly

influenced by membrane parameters such as stiffness, wettability and pore size distribution (Kukizaki and Goto 2006).

#### **1.6.4 Coaxial electro hydrodynamic atomisation**

Coaxial electro hydrodynamic atomisation (CEHDA) is a relatively new technique to produce microbubbles. In this technique two liquids form a coaxial jet. Then, uniform droplets are formed by atomisation of the coaxial jet. Encapsulation can be performed if two immiscible liquids are used. Figure 1.10 shows a schematic CEHDA apparatus. The figure shows that the apparatus has two needles; each of these needles is connected to a syringe pump. Each of the syringe pumps supplies one of the fluids. The electrical potential difference between the needles is equal to few kilovolts, which is applied by a power supplier. To produce microbubbles the inner needle is filled with gas while the outer needle is filled with suitable coating material. CEHDA has three different electro hydrodynamics modes of flow (Stride and Edirisinghe 2008).

By varying applied voltage, liquid flow rate and gas flow rate within a specific range, it is possible to produce microbubbles with desired size and uniformity. The advantage of this technique is that microbubbles are produce by a single step processing method (Stride and Edirisinghe 2008).

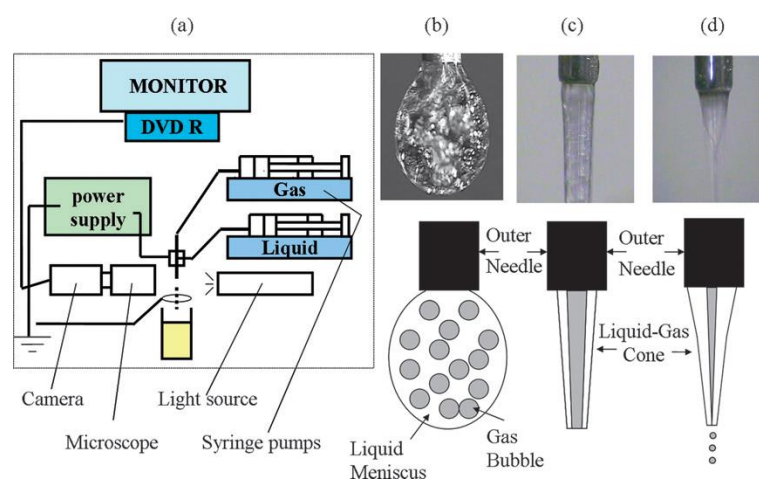


**Figure 1.10:** Microbubble preparation by coaxial electrohydrodynamic atomisation (CEHDA): (a) schematic of CEHDA apparatus; (b) CEHDA mode 1: bubble dripping; (c) CEHDA mode 2: coning; (d) CEHDA mode 3: continuous microbubbling. (Stride and Edirisinghe 2008)

### 1.6.5 Microfluidics

It is possible to highly control the size and uniformity of microbubbles by employing microfluidic devices to produce microbubbles (Whitesides 2006). Microfluidic devices initially have been used to produce monodispersed liquid droplets and only recently used to produce microbubbles (Garstecki *et al.* 2004). Two different types of microfluidics that have been used are flow focusing units (soft lithography techniques are used) (Hettiarachchi *et al.* 2007) and mechanically assembled units that consist of capillaries that form a T- Junction in a polymeric block. (Pancholi *et al.* 2008).

The initial cost of lithographic etching equipment is high, but subsequent running costs are comparatively low. However, in order to obtain monodisperse bubbles in the size range (1–10  $\mu\text{m}$ ), this type of device requires very fine channels ( $\approx 7 \mu\text{m}$  diameter) and hence must be operated under very clean conditions. In addition, high surfactant concentrations and low liquid viscosities are necessary to reduce the liquid and air pressures required. This can result in relatively low production rates and multiple devices are therefore required to produce microbubble yields comparable with the techniques described in the previous section. Yield cannot be increased simply by increasing the gas

flow rate as this leads to a loss in monodispersity (Hettiarachchi *et al.* 2007). The cost of producing and operating a single T-junction device is considerably lower, since it does not require clean room conditions and consists simply of an acrylic block embedding three fused silica capillaries. The capillaries are detachable and their separation can be adjusted to control the size of the orifice and hence that of the bubbles produced. Thus a single device can be used to produce a range of bubble sizes. Due to its construction, the T-junction device is also less prone to deformation (Pancholi *et al.* 2008). Similar to CEHDA, microfluidic devices produce the bubbles in a single step. In addition multi-layer coating is possible by using microfluidic devices. In contrast with CEHDA, microfluidic devices are working under a very limited range of pressure and flow rate conditions. Figure 1.11 shows typical size distribution of MBs made via different techniques.

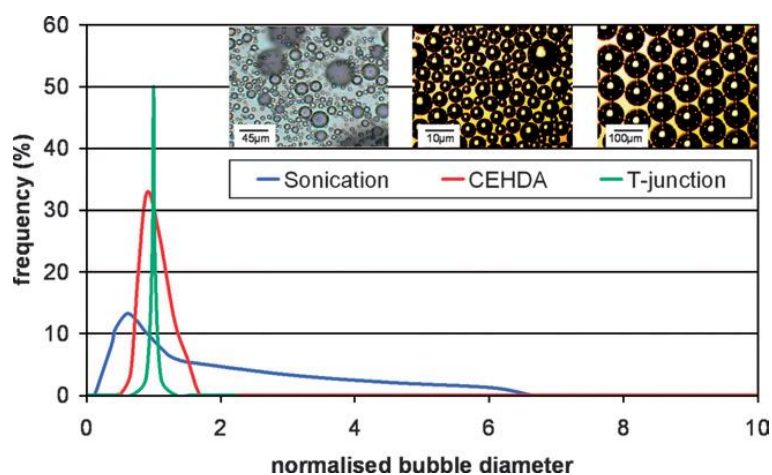


**Figure 1.11:** Typical size distributions of MBs produced from a phospholipid suspension via sonication, CEHDA and a microfluidic T-junction device (Stride and Edirisinghe 2008).

## 1.7 Significance of the Laplace pressure

In principle any system will tend to move towards a system of low free energy. At a surface the total free energy is proportional to the surface area. When a bubble is being created inside a liquid there is a difference in surface area and surface pressure which tends to create a force. In order for the surface tension to cancel out this force, the surface must adopt a curved shape. The result of the formation of a curved interface is a jump in pressure between the liquid and gas barrier. This difference in pressure across the curved surface is called the Laplace ( $\Delta P$ ) pressure and is defined by the following equation:

$$\Delta P = P_{inside} - P_{outside} = \gamma \left( \frac{1}{r_1} + \frac{1}{r_2} \right), \quad (1.12)$$

where  $\gamma$  is the surface tension,  $r_1$  and  $r_2$  are the radii of the curved surfaces and  $P$  is the pressure. In the case of a spherical bubble, where radius is  $r$ , the pressure difference between the inside and outside would be given by:

$$\Delta P = \frac{2\gamma}{r}, \quad (1.13)$$

as in this case  $r_1 = r_2$  (Walstra 1989; Dickinson 1992).

From this equation it is noted that smaller bubbles have higher Laplace pressure inside them. The Laplace pressure has a key role in destabilizing foams (Dickinson 1992).

## 1.8 Foam/ bubble stability

Similar to emulsions, foams are thermodynamically unstable (Dickinson 1992; Weaire and Hutzler 1999). As mentioned previously in section 1.6, energy is required for foam formation and creating bubble surfaces. This energy is equal to  $\gamma A$ , where  $\gamma$  is the surface tension and  $A$  is the fresh surface area created. Because the area is not minimized the

consequence is that foams are thermodynamically unstable. The most stable configuration is produced if each bubble takes a shape with minimal area. The shape to minimize the area is spherical for isolated bubble and polyhedral cells when the gas volume fraction is high. The lowest energy polyhedral shape is an unsolved mathematical problem (Weaire and Hutzler 1999).

As soon as bubbles are formed they undergo several changes due to film thinning, film rupture and bubble shrinkage (Hotrum *et al.* 2002; Dickinson 1992). Overall, the rate of deterioration of a foam depends on the kinetics of coalescence, disproportionation and drainage (Dickinson 1992; Ettelaie *et al.* 2003; Pugh 1996). It must be noted that although these are separate mechanisms they are dependent on each other up to some extent.

### **1.8.1 Drainage**

Complete separation of gas and liquid media occurs as foams age (Bergeron and Walstra 2005), drainage of the liquid between the gas bubbles occurring due to large density difference between the two phases and gravity (Langevin 2008). The liquid drains through capillary channels, hence the bubbles in the system are pushed closer together which can cause coalescence to take place. The rate of drainage depends on the viscosity of the liquid phase and could be slowed down by increasing viscosity of the liquid phase (Langevin 2008).

### **1.8.2 Coalescence**

Coalescence occurs when two or more bubbles are in close proximity and merge together to form one single bigger bubble, due to the film around the bubble(s) rupturing. Coalescence can take place numerous times between bubbles but also between a bubble and the open air at the surface of products (Martinez *et al.* 2008). Coalescence eventually leads to complete loss of foam structure and loss of gas from the product (Ettelaie *et al.* 2003).

Film stability is therefore an important aspect of foam stability. The mechanisms of film rupture for young and thick films are very different from that of old, thin films (Walstra 1989). Evaporation of water can cause thin films to rupture, especially if the bubbles are present at the surface of the foam. Once the thickness of a film reaches  $\approx 10\text{nm}$ , the film can spontaneously rupture. Thin films usually correspond to older films however film drainage coupled with water evaporation results in film thinning (Martinez *et al.* 2008). When the young/ fresh film forms if there is a thinner spot, the surface locally enlarges and causing a locally higher surface tension. As a result the liquid flows to the thin region and gives the self-stabilizing Marangoni mechanism if surfactant (surface active material) is present. If the concentration of surfactant is very low film rupture occurs in thick and young films (Walstra 1989).

Hydrophobic particles can also cause film rupture. This can only happen if the film has thinned enough so the particles can bridge the film or if the particles are relatively hydrophobic. The area in contact with the particle has a much higher curvature resulting in the Laplace pressure becoming positive. The difference in pressure causes the water to flow away from the higher pressure region which causes even further film thinning resulting in film rupture (Figure 1.12 A). However the adsorption of hydrophobic particles does not always induce film rupture (Walstra 1989).

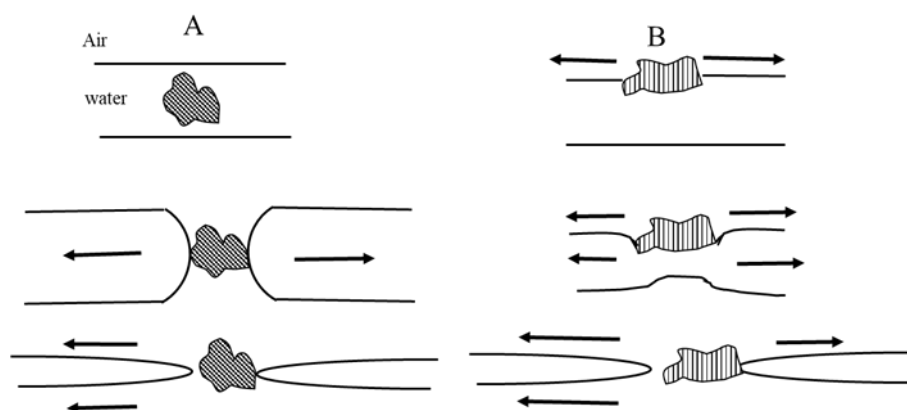


**Figure 1.12:** Film rupture due to solid particles. (A): hydrophobic particles, (B): particles from materials that can spread over the surface

If the film contains oil droplets with ability to spread over the surface, these spreading droplets can cause liquid to flow along with them. If the spreading continuous extensively and the foam is not thick enough the film may rupture (Figure 1.12 B). In this case the particle has to be larger than film thickness, but also needs to reach the surface. In other words that the film between particles and air has to rupture. This probably happens more readily if the particle is large and has an irregular shape. Oil droplets containing fat crystals reach the surface more readily. This appears to be the principal behind the de-foaming of emulsions. Another necessary prerequisite is that the spreading droplet has the ability to lower the surface tension of the film surface, otherwise it cannot spread (Walstra 1989).

#### **1.8.2.1 Dimple formation**

Foams undergo changes and evolve as they age through different mechanisms: drainage due to gravity and coarsening as a result of gas transfer between bubbles due to capillary pressure differences and bubble coalescence because of the rupture of liquid film between adjacent bubbles. Foam drainage is rather well understood however coarsening is less well understood in particular coalescence (physico-chemical aspects) is still unclear. In particular the role of surface-active agents remains unclear. Recent advances were made in the bubble coalescence topic. In particular the role of surface-active agents remains unclear (Langevin 2015). The first model describing film rupture of liquid films was first proposed by Sheludko (1967) and Vrij (1966).

When a droplet or a bubble approaches a liquid interface, the thin continuous phase film between them drains away under the action of the applied force which is initially gravitational or inertial. As the film becomes thinner, electrostatic repulsive forces may reduce the drainage rate. When the film is very thin, London-van der Waals attractive forces cause the film to rupture, so that coalescence occurs (Hartland, Yang and Jeelani

1994). In other words as two bubbles approach at a velocity  $V$  and when the distance  $h$  between their surfaces becomes small, these surfaces deform and become flatter. The flattening occurs when the hydrodynamic pressure  $P_{hyd}$  at the film center exceeds the capillary pressure  $P_{cap}$  in the bubbles. It is only then that films form. For spherical bubbles of radius  $r$  and no-slip boundary conditions,  $P_{hyd} > P_{cap}$  when  $h$  is less than a distance  $h^*$ :

$$h^* \sim r \sqrt{\frac{\eta V}{\gamma}}, \quad (1.14)$$

where  $\gamma$  is the surface tension and  $\eta$  the liquid viscosity. When there are no forces between film surfaces, it can be shown that the flattened region deforms and that a dimple always form (see Figure **1.13**). In fact, there are always van der Waals forces between film surfaces, but dimples are formed in this case as well, excepted when the velocity  $V$  is very small, in that case a pimple is formed. At very high velocities, the bubbles may rebound after the collision (Chan, Klaseboer and Manica 2011).

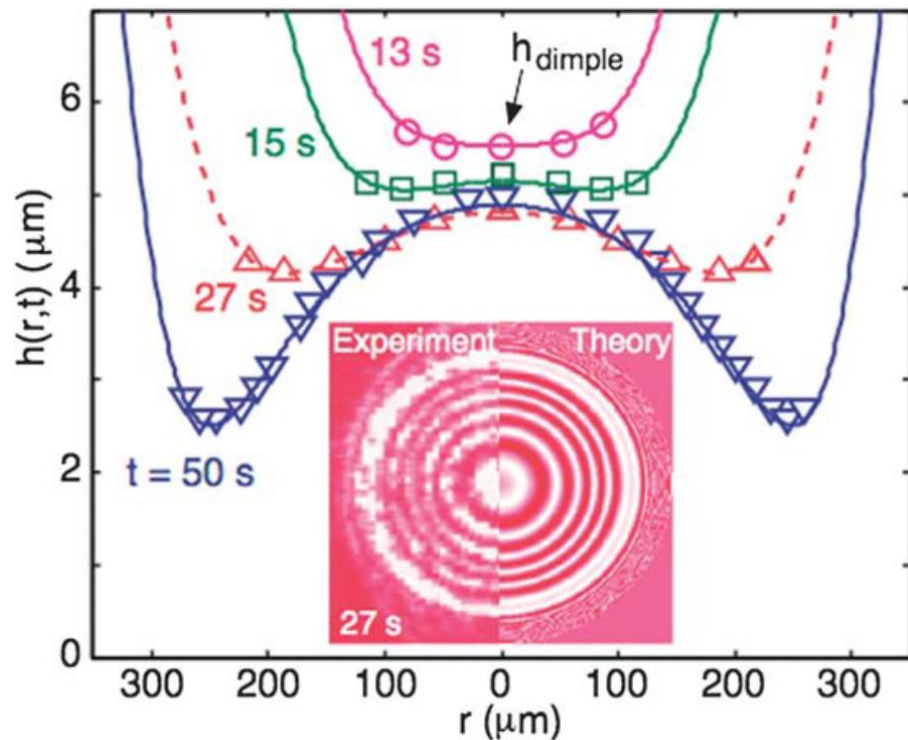


**Figure 1.13:** Silicone oil film profile between glycerol drops at various times after the formation of the dimple: experiments (symbols) and theory (lines). Note the very different magnitudes of the vertical and horizontal scales. Inset: comparison of experimental and theoretical optical interference fringe patterns of the silicone oil film at  $t = 27$  s when the capillary drive was stopped (Chan, Klaseboer and Manica 2011).

### 1.8.2.2 Gibbs – Marangoni effect

When two fluid interfaces approach one another the liquid in the continuous phase is forced out of the narrow gap that separates the droplets. As the liquid is forced out, some of the stabilizing molecules are also dragged along. As a result, the concentration of stabilizer decreases in some regions of the interface. This causes a surface tension gradient at the interface, which is thermodynamically unfavourable. Because of the surface tension gradient, the stabilizer molecules tend to flow to the regions of low stabilizer concentration and high interfacial tension, dragging along some of the liquids in the bulk continuous phase with them, acting against thinning of the liquid film and non-homogeneous surface coverage. This reduces the probability of coalescence. This is known as the Gibbs – Marangoni effect and is particularly more important in the case of low molecular weight surfactant molecules that are mobile at the interface. It is less important in the case of

biopolymers or nanoparticles where the adsorbed entities are relatively immobile at high surface coverage (Bergeron and Walstra 2005; Pugh 1996). The Gibbs – Marangoni effect is particularly important in the case of foam and bubble dispersions as a self-healing mechanism that improves stability, where the dimensions of the interfaces are relatively large but deformation is not so fast as to preclude this mechanism operating (Walstra 1989).

### **1.8.3 Disproportionation**

The process of diffusion of gas molecules from small bubbles to larger bubbles in a system is called disproportionation. Disproportionation is the greatest challenge in stabilising microbubbles. Surfactant monolayers, even when they are well packed cannot completely prevent disproportionation process since the packing is dynamic and air molecules can easily pass through gaps that continuously form and close when the monolayer is fluctuating (Disalvo 1988).

Disproportionation is responsible for coarsening of gas bubbles in a system since large bubbles grow larger at the expenses of the dissolving and disappearance of smaller gas bubbles. Disproportionation significantly reduces the shelf life of the product. Ostwald ripening in emulsions, has the same origin driven by chemical potential gradients but disproportionation happens much faster compared to Ostwald ripening due to four main reasons: a) Higher interfacial tension between gas and water interfaces compared to interfacial tension between oil and water interfaces. b) Gases are more soluble in water than lipids. c) Gases have much higher molar volume in comparison with oils. d) Gas bubbles are usually in contact with air at the surface of a product, which behaves like a huge air bubble.

A life time of a bubble with radius  $r_i$ , is estimated to be  $\tau r_i^3$ , where  $\tau$  is a constant, which has the units of  $\text{s m}^{-3}$ , defined as:

$$\tau = \frac{P_0}{6\gamma S D_g R_g T}, \quad (1.15)$$

Where  $P_0$  is the pressure in the gas above the liquid–gas interface and  $S$  is the solubility constant of the gas in the liquid.  $T$  is the temperature,  $R_g$  is the ideal gas constant,  $\gamma$  is the gas-water surface tension and  $D_g$  is the diffusion coefficient of the molecules of the dispersed phase in the continuous medium.

If  $P_0= 100$  kPa and  $T=298$  K,  $\gamma= 0.07$  N m<sup>-1</sup>,  $D_g = 2 \times 10^{-9}$  m<sup>2</sup> s<sup>-1</sup>,  $S= 7 \times 10^{-6}$  mol N<sup>-1</sup> m<sup>-1</sup> for air in water,  $R_g$  equals 8.31 J K<sup>-1</sup> and  $\tau$  is  $6.872 \times 10^{15}$  s m<sup>-3</sup>. Therefore for a bubble with radius equals to 0.1 mm life time is about 2 hours and for a bubble radius 1 μm life time is very short – a few milliseconds (Dickinson *et al.* 2002; Ettelaie *et al.* 2003).

### 1.9 Mechanism to overcome foam/ bubble instability

There are ways in which very fine MBs can be made more stable. One way of stabilisation is by covering the surface of gas bubbles by surfactants that have the ability to crystallize after being adsorbed on the bubble surfaces (Fairley 1992). However it must be mentioned that in food system these type of surfactants are very limited and there is always an adsorption competition between these surfactants and other amphiphilic molecules that are present in the system (Ettelaie and Murray 2015).

Even in case of non-food materials surfactant monolayers, even when they are well packed, cannot completely prevent disproportionation process. The adsorption of surfactants is reversible. As mentioned earlier the air molecules can pass through the layer gaps when the monolayer is fluctuating. Time scale of these fluctuation is very short (e.g., few micro/ milliseconds) (Disalvo 1988).

Surface active molecules with the ability of forming an elastic film such as proteins can be used to slow down disproportionation. Proteins are widely used by food industry to stabilize foams. It is important to make a distinction between foamability (the ease and

extent of foam formation) and foam stability (the rate of loss of foam structure once formed). Foamability depends on the protein having the capacity for rapid adsorption and unfolding at the interface, where foam stability depends on the ability of protein to form a strong, cohesive and flexible film to reduce the gas permeability hence inhibit disproportionation. Proteins with good foamability are not necessarily good foam stabilizer and vice versa (Dickinson 1989).

There is a complicated relation between protein structure and its foaming ability (Damodaran 2005). One example of widely used protein as a foam stabilizer is egg albumen. It can coagulate and form a protein network at the interfaces (Dickinson 2006). A protein known as lysozyme is also found in egg white but unlike ovalbumin it is not an effective foaming agent, unless it is dry heated at 80 °C (Desfougeres *et al.* 2008). Aggregates of soluble or insoluble  $\beta$ -lactoglobulin improved the foam stability (Rullier, Novales and Axelos 2008). In general the ability of proteins in stabilizing foams is increased when they become less soluble because their interfacial visco-elastic film forming capacity is increased as a result of losing solubility (Damodaran 2005). However if the proteins become too insoluble and the form aggregates that are too large, they do not adsorb efficiently.

A study by Dickinson (Dickinson *et al.* 2002) proved that film forming proteins that have different viscosities and interfacial elasticity have the same effect on microbubble dissolution. None of these proteins can completely stop shrinkage but only slowdown 2 or 3 times.  $\beta$ -lactoglobulin unfolds and cross-links at the interfaces forming strong films, but start to wrinkle while the bubble still undergoes shrinkage, eventually non-spherical particles of protein, a few micron in size, remain in the system. These particles become smaller with time as they may break up or re-dissolve in the system. Egg white protein ovalbumin is an exception as it spontaneously forms solid particles on the surface of bubble. These aggregates of ovalbumin are visible at the very beginning of shrinking

process. Walstra (2003) has confirmed that proteins can stabilise foams only if they coagulate at the interface of the bubbles and form a solid network.

Another technique to overcome disproportionation is using gases such as decafluorobutane and SF<sub>6</sub>, which is very insoluble in water. These are commonly used in medical imaging as contrast agents and generating MBs with size of 3 – 4 μm (Krause 2002). This method is not used in food production because these gases are expensive and also are associated with safety issues.

Perhaps the best route to prevent disproportionation and also coalescence is to stabilise small gas bubbles by adsorption of nanoparticles to their surface. This way of stabilization is known as Pickering stabilisation and is used to stabilise emulsions as well as foams. It has been established that Pickering stabilized bubbles can remain stable against disproportionation for long period of time e.g., days or weeks, whereas the protein stabilized bubbles collapse in few hours (Kostakis, Ettelaie and Murray 2007). The main advantage of Pickering systems over other more traditional stabilization methods is its surfactant-free preparation, which is highly relevant for medical and skincare applications (Arditty *et al.* 2003; Frelichowska *et al.* 2009).

It should be noted that like other methods of stabilisation, emulsions and foams stabilised this way are still thermodynamically unstable but the energy involved in displacement of these particles from the surface of bubbles can be few thousands of  $k_B T$ , where  $k_B$  is the Boltzmann constant and  $T$  is the temperature (Aveyard *et al.* 2000; Du *et al.* 2003).

## **1.10 Pickering stabilization**

### **1.10.1 Particles/ nanoparticles**

Colloidal particles are intrinsic part of system where the finely divided matter (particles) is dispersed in a liquid or gas. The particle size ranges from a few nanometre (nm) to tens

of micrometres ( $\mu\text{m}$ ), hence covering a broad size domain (Evans and Wennerström 1994; Binks and Horozov 2006; Dickinson 2010b).

These particles are not necessarily solid but may include bacteria cells, bacteria spores and microgels, for example (Lam, Velikov and Velev 2014). Similar to surfactants, surface active particles spontaneously accumulate at the interface of two immiscible phase (liquid – liquid or liquid – air). In many of these systems the particles participate in the stabilization of the multi-phase structure by providing a physical barrier to emulsion droplet coalescence. This type of stabilization is called ‘Pickering stabilization’ after the pioneering work of Pickering [and also Ramsden (1904)] more than a century ago (Pickering 1907). Over the last five decades the behaviour of particles at liquid interfaces extensively studied (Sheppard and Tchekedjian 1968; Aveyard *et al.* 2000; Paunov, Binks and Ashby 2002; Tyowua, Yiase and Binks 2017). Only recently it has been shown that colloidal particle with the right degree of hydrophobicity can also remarkably increase the stability of foams (Du *et al.* 2003; Alargova *et al.* 2004; Binks and Horozov 2005), before then particles were mainly used as antifoaming agent (Denkov *et al.* 2000) and there were only few studies on microbubble stabilization by irregularly shaped quartz particles (Johnson and Wangersky 1987).

Surface active particles may have a uniform surface but another class of surface active particles is commonly called ‘Janus’ particles (see Figure 1.14). Janus particles have two distinct hydrophobic and hydrophilic regions in their surface. Janus particles are amphiphilic similar to surfactant molecules (Binks and Horozov 2006). Janus particles have considerable advantages for use in emulsion [foam] stabilization, but their production is more challenging compared to conventional particles (Böker *et al.* 2007).

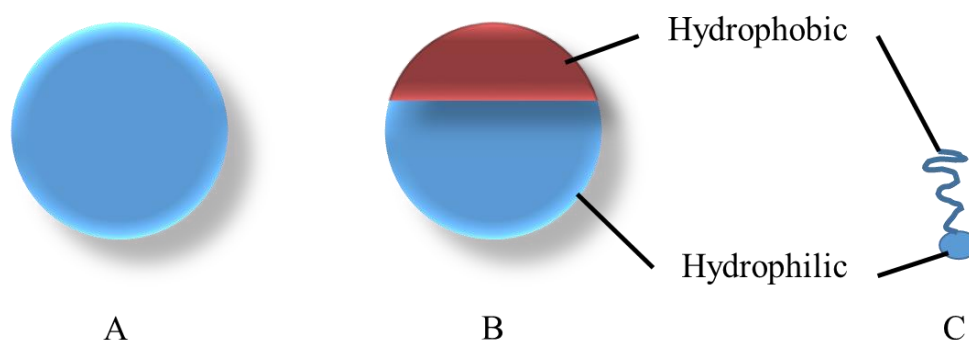


**Figure 1.14:** Schematic representation of (A): homogenous, (B): Janus particle and (C): surfactant molecule.

The basic mechanisms underlying the stabilizing effect of nanoparticles are still not completely understood. From one side the increased stability is related to the presence of particles in the foam lamellae or, in the case of emulsions, in the liquid film between approaching droplets. In those cases, particle engulfment exerts a remarkable resistance to thinning, as also observed for micelles (Wasan, Nikolov and Aimetti 2004). Other mechanisms may be related to the formation of liquid bridges between particles (Kralchevsky and Denkov 2001).

### 1.10.2 Definition and classification of polymer nanoparticles

Most of the research into Pickering stabilized systems until recent years has been focused on using inorganic particles such as silica particles due to their well-defined spherical shape, surface tunability, cheap price, availability in different size and narrow size distribution (Binks and Horozov 2005; Lam, Velikov and Velev 2014). During the past few years polymer nanoparticle (PNP) have attracted significant interest due to their unique properties that meets a wide range of applications and market needs ranging from electronics and photonics, conducting materials, pollution control, medicine and biotechnology (Rao and Geckeler 2011; Crucho and Barros 2017). PNP is a collective term given for any type of polymer nanoparticles, but specifically for nanocapsules and nanospheres. Nanocapsules are vesicular systems made of a polymeric membrane which

encapsulates an inner liquid core (water or oil) at the nanoscale. Nanospheres are matrix particles – their entire mass is solid and molecules can be adsorbed at their surface or encapsulated in the particle (Rao and Geckeler 2011). Figure 1.15 shows a schematic representation of PNPs.

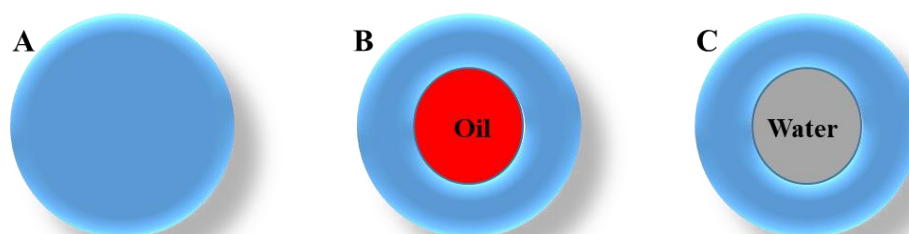


**Figure 1.15:** Illustration of classification of polymer nanoparticles nanospheres (A), nanocapsules containing oil (B) and water (C).

### 1.10.3 PNP preparation techniques

PNPs are made by different preparation techniques. The preparation techniques chosen is based on the PNP application, size requirement, their physiochemical characteristics etc. (Nasir, Kausar and Younus 2015). Preparation methods can be classified into two main groups: namely those made by polymerization of the monomer and those made from preformed polymers (Allouche 2013).

#### 1.10.3.1 PNP production via pre-formed monomers

Techniques such as salting out, solvent evaporation, nanoprecipitation, dialysis and super critical fluid (SFC) technology can be used to make PNPs from pre-formed polymers. These techniques do not involve any polymerization process. On the other hand direct synthesis of PNPs is possible by employing techniques such as emulsion polymerization, mini emulsion polymerization, surfactant free polymerization and interfacial polymerization. Polymerization techniques are employed to design nanoparticles with specific characteristic for a particular application (Rao and Geckeler 2011).

### 1.10.3.2 PNP production via polymerization

Emulsion polymerization is the most common technique used to produce a wide range of specialty polymers. In this method water is used as the dispersion medium. Using water is environmentally friendly and allows excellent heat dissipation from the system. Based on presence or absence of surfactant emulsion polymerization can be classified as conventional and surfactant free.

#### **Emulsion polymerization**

Conventional emulsion polymerization accounts for the majority of worldwide PNP production ( $>20 \times 10^6$  tones/year) (Asua 2004). Water, monomer (low water solubility), surfactant and water soluble surfactant are the ingredients of conventional emulsion polymerization. At the end of polymerization reaction the PNPs are containing thousands of polymer chains. The size of an individual PNP obtained by this method is around 50 – 300 nm. The emulsion stabilization may be electrostatic, steric or electro-steric, displaying both stabilizing mechanisms. Initiation occurs when a monomer molecule dissolved in the continuous phase collides with an initiator molecule that may be an ion or a free radical. Alternatively, the monomer molecule can be transformed into an initiating radical by high-energy radiation, including  $\gamma$ -radiation, ultraviolet or strong visible light. Phase separation and formation of solid particles can take place before or after the termination of the polymerization reaction (Kreuter 1982; Chern 2006).

Conventional emulsion polymerization systems utilize varying quantities of surfactants that usually need to be eliminated from the final product which can be difficult to do. Removal of surfactants is a time-consuming process that increases the cost of production. Moreover, increasing environmental and energy concerns cannot be effectively addressed because of these drawbacks (Rao and Geckeler 2011).

As an alternative, emulsion polymerization has been performed in the absence of added emulsifier, often referred to in literature as surfactant-free, emulsifier-free, or soap-less emulsion polymerization. This technique has received considerable attention for use as a simple, green process for PNP production without the addition and subsequent removal of the stabilizing surfactants. Producing a monodisperse and controlling particle size are the main unsolved problems of surfactant free emulsion polymerization (Zhang *et al.* 2001).

Poly alkyl cyanoacrylate (PACA) nanoparticles and particularly poly butyl cyanoacrylate (PBCA) NPs have been used as MBs stabilizer in recent years (Harris, Depoix and Urich 1995; Schmidt and Roessling 2006; Olbrich *et al.* 2006). Alkyl cyanoacrylates are an unusual class of polymerizable monomers, because they have two strong electron withdrawing groups in the  $\alpha$ -carbon of their double bond; these groups are cyano (CN) and ester (COOR). Alkyl cyanoacrylate monomers are remarkably reactive toward weak bases, e.g. water, alcohol and amine, or anions e.g. iodided, alcoholate, and hydroxide. Poly alkyl cyanoacrylates nanoparticles are generally synthesised via emulsion polymerization (Nicolas and Couvreur 2009; Behan, Birkinshaw and Clarke 2001).

### **Mini-emulsion polymerization**

Mini-emulsion polymerization has been a subject of interest over the past few years as it allows production of a wide range of functional organic or inorganic nanomaterials (Asua 2002; Yildiz and Landfester 2008). However, the mini-emulsion method is still limited due to its use at high temperature (Crespy and Landfester 2009). Mini-emulsion formulation commonly consists of water, monomer, initiator, surfactant and co-stabilizer. Unlike emulsion polymerization, the particles do not form spontaneously during the mini-emulsion polymerization but require high shear mixing (e.g., ultrasound) to break up the emulsion droplets into smaller ones. At the end of the polymerization, only a fraction of

the initial number of monomer droplets become polymer particles (Delgado and El-Aasser 1990) . Another key difference between emulsion polymerization and mini-emulsion polymerization is the use of low molecular weight co-stabilizers. Mini-emulsion are thermodynamically unstable and have an interfacial tension much greater than zero and require a high shear mixing to reach a steady state (Crucho and Barros 2017).

### **Microemulsion polymerization**

Microemulsion polymerization is a relatively new technique for producing smaller particles (10 – 100 nm ). Although emulsion and microemulsion polymerization appear to be similar because both methods produce colloidal polymer particles of high molar mass, they are entirely different. Microemulsions are optically transparent due to the small size of nanoparticles. Another major difference between emulsion and microemulsion arises from the amount of surfactant used to stabilize the systems. Much higher concentrations of surfactant is required for microemulsion polymerization (at least 10% of the total weight). The high concentration of surfactant is required to stabilize a large internal interfacial area. The particles are completely covered with surfactant because of the utilization of a high amount of surfactant. Presence of high amount of surfactant is a drawback that can significantly restrict the use of micro-emulsion polymerization. High concentrations of surfactant is not desirable in most of nanoparticle applications. Using polymerizable surfactant is a possible way to combat this issue (Pavel 2004). Emulsion polymerization and microemulsion polymerization are also entirely different in terms of kinetics. Emulsion polymerization exhibits three reaction rate intervals, whereas only two are detected in microemulsion polymerization. Both particle size and the average number of chains per particle are considerably smaller in micro-emulsion polymerization. In microemulsion polymerization, an initiator, typically water-soluble, is added to the aqueous phase of a thermodynamically stable microemulsion containing swollen micelles. The polymerization starts from this thermodynamically

stable, spontaneously formed state, which possess an interfacial tension at the oil/water interface close to zero. Initially, polymer chains are formed only in some droplets, as the initiation cannot be attained simultaneously in all micro-droplets. Later, the osmotic and elastic influence of the chains destabilize the fragile micro-emulsions and typically lead to an increase in the particle size, the formation of empty micelles, and secondary nucleation. Very small particles coexist with a majority of empty micelles in the final product (Rao and Geckeler 2011). Table 1.1 illustrates the summary of the differences between different polymerization techniques.

<b>Characteristic</b>	<b>Emulsion</b>	<b>Mini-emulsion</b>	<b>Microemulsion</b>
<b>Thermodynamic stability</b>	Non stable	Non stable	Stable
<b>Stability period</b>	Seconds to months	Hours to months	Infinite stability
<b>Droplet size range</b>	1 – 10 $\mu\text{m}$	20 – 200 nm	$\approx 10$ nm
<b>Polydispersity</b>	Low	Very low	Very low
<b>Average Particle size</b>	50 – 300 nm	10 – 30 nm	10 – 100 nm

**Table 1.1:** Differences between polymerization system (Rao and Geckeler 2011)

### **1.10.3.3 Formation of poly alkyl cyanoacrylate (PACA) NPs via emulsion polymerization**

Alkyl cyanoacrylates are highly reactive monomers that have excellent adhesive properties. Shorter alkyl chain cyanoacrylate such as methyl ester is used as “Superglue”, whereas longer chain cyanoacrylates such as butyl cyanoacrylate are available as biodegradable tissue adhesive for surgical applications (Nicolas and Couvreur 2009).

The polymerization rate is very high. Presence of traces of any of the mentioned compounds in the reaction medium is enough to initiate the polymerization. For this reason handling alkyl cyanoacrylates is very difficult at their pure form. Usually small amount of acidic stabiliser e.g. sulfonic acid, SO<sub>2</sub>, etc. are added to the monomer in order to make it more stable.

PACA NPs are synthesised by one of the three main mechanisms of polymerization: 1: anionic, 2: radical and 3: zwitterionic. However under conventional experimental conditions, anionic and zwitterionic polymerization are more predominant than radical polymerization mechanism due to remarkable reactivity of alkyl cyanoacrylates. So in both homogeneous (solution or bulk) and heterogeneous (emulsion or microemulsion) anionic and zwitterionic are responsible for the polymerisation. Free radical polymerisation is believed to be the main mechanism during chain growth step. (Nicolas and Couvreur 2009). Figure 1.16 represents formation of PACA NPs via the stepwise anionic polymerization mechanism in emulsion/dispersion.

Literature contains various conflicting results for particle size and molecular weight. A study reports various sizes for produced nanoparticles, where the only variable in producing these nanoparticles was the monomer source. Another study has reported a three-fold variation in the reactivity of six different batches of butyl cyanoacrylate monomer, due to varying amount added polymerisation inhibitor such as sulfonic acid (Behan, Birkinshaw and Clarke 2001).

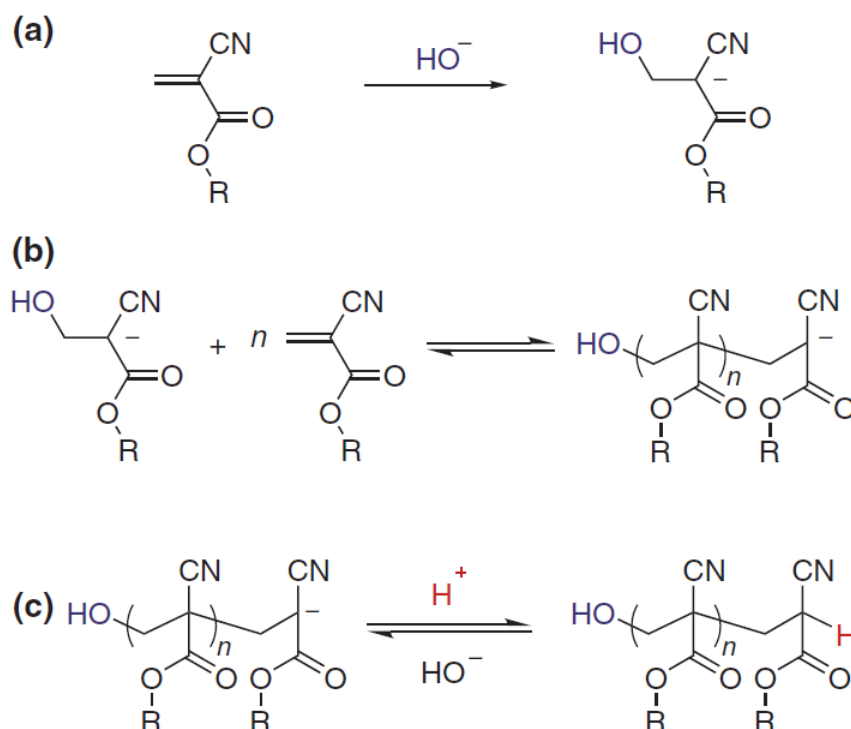


**Figure 1.16:** Schematic representation of poly(alkyl cyanoacrylate) formation via the stepwise anionic polymerization mechanism in emulsion/dispersion. Initiation step (a), reversible propagation step (b), and reversible termination step (c). Adopted from: Nicolas and Couvreur (2009)

In late 1970s, Couvreur (Couvreur *et al.* 1979) showed a simple way of producing nanoparticles. The method includes dropwise addition of alkyl cyanoacrylate to the acidic solution of HCl (pH between 2 and 3) that contains either a non-ionic or macromolecular surfactant under stirring condition (Nicolas and Couvreur 2009; Behan, Birkinshaw and Clarke 2001). Since then PACA NPs have been studied in great detail in order to establish the main parameters that control the polymerisation kinetics as well as the nanoparticle characteristic. Based on these studies it has been shown that the concentration and nature of the surfactant have a significant effect on particle size, on the other hand the type of monomer as well as surfactant influence the molar mass of the produced polymer particles. Monomer concentration and pH are found to be responsible for the colloidal properties of the obtained nanoparticles (Nicolas and Couvreur 2009).

#### **1.10.4 Food grade nanoparticles**

In terms of nanoparticles to be used in food, extra consideration is needed, for example nanoparticles must be food grade with correct sizes and right contact angle to stabilize air bubbles. Fat crystals are often considered as food grade Pickering particles; however it is more effective in stabilising water in oil emulsion rather than stabilising oil in water or foams. Another candidate for food grade nanoparticle is ethyl cellulose, but considering the size of these particles it can only stabilise relatively large bubbles around few tens of microns (Ettelaie and Murray 2014).

A promising food grade nanoparticle is a fungal protein called hydrophobin. Hydrophobins have attracted attention of researchers in regards to their foamability and foam stability properties (Cox, Aldred and Russell 2009; Wang *et al.* 2013; Burke *et al.* 2014; Tucker *et al.* 2015; Dimitrova *et al.* 2017). Hydrophobin is a compact globular protein that shows characteristics of a small Janus NP upon adsorption to an interface because it does not unfold after adsorption and remains spherical (Burke *et al.* 2014).

#### **1.10.5 Contact angle**

A key parameter when dealing with solid particles at interfaces is three phase contact angle,  $\theta$ . This is the angle between the tangents to the solid surface and the liquid – liquid or liquid – gas interface measured through one of the liquids (usually water if this is one of the liquids) in each point of the three phase contact line where the solid meets two fluids. Figure **1.17** shows the contact angle of spherical particle at interface.

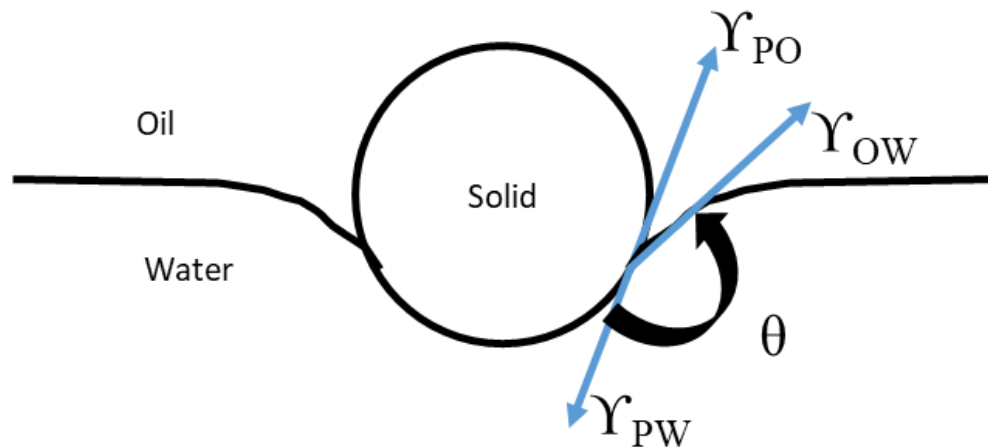


**Figure 1.17:** Solid spherical particle with contact angle  $\theta$  in equilibrium at the oil – water interface

The contact angle depends on the surface free energies (interfacial tension) at the particle – water ( $\gamma_{pw}$ ), particle – oil ( $\gamma_{po}$ ) and oil – water ( $\gamma_{ow}$ ), interface according to Young's equation:

$$\cos \theta = \frac{\gamma_{po} - \gamma_{pw}}{\gamma_{ow}} , \quad (1.16)$$

If particles equally wet by both phases ( $\gamma_{po} = \gamma_{pw}$ ) the contact angle is  $90^\circ$ . Hydrophilic particles are preferentially wet by water ( $\gamma_{po} > \gamma_{pw}$ ) hence  $0^\circ \leq \theta < 90^\circ$ . Hydrophobic particles are preferentially wet by oil ( $\gamma_{po} < \gamma_{pw}$ ), so  $90^\circ < \theta \leq 180^\circ$  (Binks and Horozov 2006).

When a small spherical particle at a planar oil – water interface is in its equilibrium state the surface free energy of the system,  $G$  is the minimum and is given by:

$$G = \gamma_{ow}A_{ow} + \gamma_{pw}A_{pw} + \gamma_{po}A_{po} , \quad (1.17)$$

Where  $A_{OW}$  is the area of oil- water interface,  $A_{PW}$  and  $A_{PO}$  are areas of the particle – water and particle – oil interfaces respectively.

This expression can be used to calculate the energy needed to remove a particle from the interface between two fluids. For a spherical particle:

$$G = -\Delta E = \pi r^2 \gamma_{OW} (1 - |\cos \theta|)^2, \quad (1.18)$$

Where  $r$  is the radius of the particle,  $\gamma_{OW}$  is the interfacial tension between the immiscible (oil- water in here) phases, and  $\theta$  is the three phase contact angle. This expression – for spheres – asserts that the closer the contact angle of the particle at the interface to  $90^\circ$  and the larger the particle, the more energetically favourable the adsorption (Lam, Velikov and Velev 2014).

As mentioned previously particles have applications as a foam stabilizers or antifoaming agents in surfactant-stabilised aqueous foams. Highly hydrophobic particles are mainly used as antifoam agent as they take part in bridging - de-wetting mechanism, while hydrophilic particles are used to stabilize foams by packing at the air-water interface; therefore film drainage slows down, stabilizing the foams. In addition hydrophilic particles reduce disproportionation. The stability of these foams depends not only on the type of used particles, but also on size, concentration shape and hydrophilicity of the particle (Binks and Horozov 2005).

It is possible to control the foam stability by altering the level of hydrophobicity and hydrophilicity of the nanoparticle surface. Contact angle values equal or close to  $0^\circ$  are not favoured because the adsorption energy of the particle at the air/water interface is very low, and particles remain dispersed in the aqueous phase (Binks and Murakami

2006). Contact angles between  $43^{\circ}$ –  $90^{\circ}$  are associated with highest yield of foam stabilization for silica particles (Binks and Murakami 2006; Wong *et al.* 2011).

### **1.10.6 Capillary interactions between solid particles at interface**

When solid particles floating at the fluid – fluid interface attract one another even in the absence of gravity. Emulsion and foams are stabilized by the formation of this coherent skin made of particles at the interface (Lucassen 1992). The stability and behaviour of the Pickering stabilized interface strongly depends on the microstructure formed by adsorbed particles. This microstructure is determined by interactions between the particles at the interface which can be different from those in the bulk. Indeed, in addition to the colloidal forces that particles experience in the bulk, adsorbed particles experience lateral capillary forces due to interface deformation as a result of their presence (De Corato and Garbin 2018). The liquid phase forms a capillary bridge between particles. Then the capillary force is directed to the planes of the contact lines on the particle surface. The normal capillary –bridge forces can be either attractive or repulsive (Kralchevsky and Denkov 2001).

## **1.11 Overview**

It is difficult to cover all aspects of Pickering stabilization, therefore the focus of this review has been on the less explored aspects of Pickering stabilization of MBs in food and non-food systems, putting this into the context of general colloidal stability aspects. The focus of Chapter 2 is on Pickering stabilization of food grade MBs by employing HFBII in presence of other surface active proteins and low molecular weight surfactants with particular attention to the relationship between foam stability and surface tension of the proteins / surfactants. Chapter 3 looks at the properties of synthetic NPs as a MB stabilizers for comparison. The funding indicates how monomer type, surfactant type and pH of the aqueous phase impact the properties on NPs and determine its suitability for

MB stabilization. The aeration conditions such as the initial size of MB, size and physiochemical properties of NPs and ionic strengths and their impact on MBs formation, size and stability are discussed in Chapter 4. In Chapter 5 the essential considerations to design a continuous method of MBs formation and stabilization is discussed.

## Chapter 2 :

# Hydrophobin Stabilized Microbubbles for Food Applications

### 2.1 Introduction

Most of the proteins show some degree of surface activity and can be classified as a surface active polymers. They have polymeric and polyelectrolyte characteristic. They can easily adsorb to almost any interfaces and therefore widely used to stabilize emulsions, foams and other dispersions (Murray 2011; Tucker *et al.* 2015). The adsorption of protein in a mixture with other protein or surfactant has been intensively studied (Krägel *et al.* 1999; Mackie *et al.* 2001; Radulova *et al.* 2012; Burke *et al.* 2014). Hydrophobins are a group of very small surface active proteins (7 – 10 kDa) that produced by filamentous fungi (Wösten 2001; Linder *et al.* 2005; Cox *et al.* 2007). They are classified as the most surface active proteins with the ability to self-assemble themselves at the interfaces or hydrophobic – hydrophilic surfaces. This behaviour helps the fungi to form an aerial structure (Wessels 1996; Hakanpaa *et al.* 2006). Hydrophobins have a robust globular structure. Eight cysteine residues are responsible for hydrophobin rigid structure as they form four intermolecular disulfide bridges (Hakanpaa *et al.* 2006).

Hydrophobins can be divided into two groups based on their solubility. Hydrophobin class I are extremely insoluble in water and form a rod shape aggregates only dissolve in strong acids. Class II hydrophobins such as HFBI (7.5 kD) and HFBII (7.2 kD), from the filamentous fungus *Trichoderma Reesei* (Figure 2.1), are more soluble in aqueous solution and can be dissolved in ethanol or SDS (Linder *et al.* 2002; Linder *et al.* 2005; Lumsdon, Green and Stieglitz 2005).

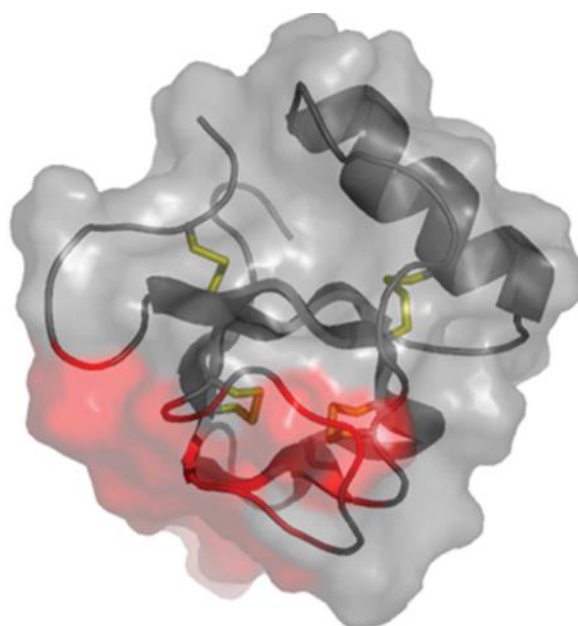


**Figure 2.1:** The structure of *T. reesei* hydrophobin HFBII; disulfide bridges are highlighted in yellow and the hydrophobic patch in red. Adopted from: Hakanpaa *et al.* (2006)

HFBII monomer has a hydrophobic patch ( $\approx 12 - 19\%$  of the total surface) on its surface. The driving force for self-assembly of hydrophobin at the interface is the concealment of the hydrophobic patch. Usually HFBII is found in a dimeric state and conceal 34% of the hydrophobic patch compared to monomers, this is energetically more favourable. HFBII can form monolayer at the air – water or oil – water interface due to exposing of the hydrophobic patch to the hydrophobic phase and create a more stable energetic state as the hydrophobic patch can be completely concealed (Butko *et al.* 2001).

In contrast with other globular proteins, HFBII doesn't unfold after adsorption to a surface. HFBII strongly adsorbs to the interface and form a closely packed layer which results into a very strong mechanical film. It has been demonstrated that HFBII is a great foam stabilizer and prevent disproportionation quite effectively and stabilize bubbles for at least several months (Murray *et al.* 2005; Cox, Aldred and Russell 2009). Furthermore HFBII is shown to act more like a Janus particles (Cox *et al.* 2007).

Although HFBII proved to be an outstanding foam stabilizer but its extraction and purification is highly expensive, therefore makes it difficult to be used in a commercial product. In addition HFBII seems not to be a good foaming agent. Therefore the focus of this work is to investigate the foam stabilization properties of a mixture of HFBII and other surface active proteins such as sodium caseinate not only to make using HFBII more feasible and cost effective but also to see how presence of this protein affect HFBII functionality as a foam stabilizer.

Milk proteins are widely used in food industry to stabilize foams and emulsions (Dickinson 1999; Marinova *et al.* 2009). Generally milk proteins are classified into two groups: flexible and globular proteins. Flexible proteins such as  $\alpha_{s1}$ - casein,  $\alpha_{s2}$ - casein,  $\kappa$ -casein,  $\beta$ - casein, calcium caseinate and sodium caseinate (NaCas), have no tertiary structure due to presence of large number of proline residue (Heth and Swaisgood 1982; Creamer and MacGibbon 1996). Caseins accounts for 80% of total milk protein. Globular protein can be extracted after casein sedimentation. This globular proteins are called whey proteins. The whey proteins have disulfide bridges which help them to keep their globular shape even after adsorption to the interface (Marinova *et al.* 2009).

Caseins are small amphiphilic molecules that have both hydrophobic and hydrophilic groups on their peptide chain. About 70 % of the chain is hydrophilic and charged while the rest is non polar and hydrophobic, depending on the type of casein the hydrophobic

and hydrophilic regions are distributed differently (Creamer and MacGibbon 1996). When random coil protein such as casein adsorb to the interface the hydrophobic parts of their flexible polymer chain is orienting to the air (train) while the hydrophilic parts orientating to the water phase (loops). This structure of adsorbed protein is known as loop- train model (Wierenga and Gruppen 2010).

Milk proteins such as  $\beta$ -caseinate and its substitute are not able to completely stop the disproportionation, therefore they are not considered as good foam/microbubbles stabilizer (Dickinson *et al.* 2002). Bubbles stabilized by sodium dodecyl sulphate,  $\beta$ -lactoglobulin and  $\beta$ -casein are not stable, their life time is only few minutes and they will shrink until they disappear. Burke *et al.* (2014) has studied the interaction between  $\beta$ -casein and HFB II at the air- water interfaces. The results show that bubbles stabilized by a mixture of HFB II and  $\beta$ -casein are stable for a long period of time at least several days as  $\beta$ -casein is increasing the viscosity of HFB II film. Their results suggest that the interaction between two proteins at the interfaces is not electrostatic or hydrophobic and it might be related to how HFB II and  $\beta$ -casein pack at the interface. Their results also shows that there is a synergy between the HFB II and  $\beta$ -casein at the interface up to a certain ratio of HFB II:  $\beta$ -casein. In theory this suggests that  $\beta$ -casein adsorbs to the air – water interface much quicker than HFBII. During the adsorption of HFBII,  $\beta$ -casein is likely to desorb from air water interface, so bubbles will be stabilized by HFB II.

## **2.2 Materials and methods**

### **2.2.1 Materials**

Class II Hydrophobin (HFBII) previously sourced and used by Burke *et al.* (2014) was supplied by Unilever (Colworth, UK), provided in an ammonium acetate buffer solution. It was then freeze dried and stored in a vacuum oven (Gallenkamp) at 40°C for 18h, in order to remove the water and buffer, to enable solutions to be prepared at specific pH

values. The HFBII was reconstituted in pure water at concentration of 1.44 wt% and stored frozen. Water from a Milli-Q apparatus (Millipore, Watford, UK), was used throughout. Sodium caseinate (NaCas) was supplied by Fronterra LTD (Auckland, New Zealand). Glycerol was supplied by Fischer scientific (Loughborough, England). All the chemicals used to make the buffer (sodium phosphate, sodium chloride and potassium phosphate), sodium azide ( $\text{NaN}_3$ ) and Nile blue were supplied by Sigma-Aldrich (Poole, UK). The lactose-free whey protein isolate powder was provided by Davisco Foods International (Le Sueur, Minnesota, USA). Tween 20, Tween 80, Triton™ X-100, Tyloxapol and  $\beta$ -Lactoglobulin from bovine milk purchased from Sigma-Aldrich (Poole, UK).

### **2.2.2 Buffer preparation**

All solutions were prepared in a phosphate buffer using 0.05 mol phosphate buffer + 0.05 mol sodium chloride. By dissolving 1.72 g of sodium phosphate, 2.92 g of sodium chloride and 1.87 g of potassium phosphate in one litre of deionized water, to reach pH  $7 \pm 0.05$  via addition of few drops of  $1 \text{ mol dm}^{-3}$  NaOH as necessary. The buffer was kept for several days in the fridge and fresh buffer was made every two weeks.

### **2.2.3 Microbubble dispersion preparation**

The buffer was heated to ambient temperature before dissolving NaCas with it. HFBII was rapidly thawed in cold water before mixing into the different solutions. Both 0.1 wt. % NaCas and 0.03 wt. % HFBII (or 0.06 wt. % HFBII for samples with higher concentration) solutions were prepared by weight. The proteins and sodium azide (acts as a biocide) were first dissolved in the required amount of buffer and then 76 % glycerol was added. The solution was then sheared mixed using an Ultra-Turrax T25 (Janke & Kunkel, IKA Labortechnik) at 24,000 revolutions per minutes (rpm) for one minute. The

MBs dispersion were stored in glass tubes covered by plastic lid to prevent evaporation. The dispersions were stored at 4°C.

In subsequent experiments the NaCas was replaced by Tween 20, Tween 80, Triton X-100, Tyloxapol or  $\beta$ -Lactoglobulin at the same concentration (0.1 wt. %) or the concentration of NaCas was changed to 0.025, 0.05, 0.2 or 0.4 wt. %. In all these experiments the concentration of HFBII was 0.03 wt. %. The change in surfactant type or concentration was to investigate the impact of NaCas replacement by other surface active material on microbubble stabilization.

Some samples (0.1 wt. % NaCas and 0.03 wt. % HFBII) were subjected to multiple aeration at different time intervals. The density and therefore air content (volume fraction) of aerated samples was measured via a high precision oscillating U-tube densitometer (DMA 4500, Anton-Paar, Graz, Austria) at 25°C. In all cases of density measurement a 0.1 wt. % NaCas in 76% glycerol solution sample was used as a blank.

#### **2.2.4 Microscopy**

Images used for MBs size analysis were taken by an optical light microscope, using 10, 20 and 40 x objective lens and fitted with a Nikon SMZ-2T (Tokyo, Japan) digital camera. For each measurement around 1 ml of MB dispersion were transferred into well slide (diameter 19 mm and depth 3 mm) and sealed with a coverslip (0.17 mm thickness). Sample were diluted as appropriate – to give as far as possible a single layer of bubbles clearly visible just below the coverslip. Digital images of the bubbles were analysed ImageJ software (version 1.51s, USA). A Leica TCS SP2 confocal laser scanning microscope (CLSM) was also used in fluorescent mode to obtain images bubbles stabilized by HFBII and NaCas. Then 1 droplet of Nile blue was stirred gently into the dispersion to stain the proteins. Dyed samples were scanned at room temperature using a 40 x objective lens, exciting the dye with the 540 nm Ar laser line and emission

wavelength 625 nm Images were recorded at a resolution 1024 x 1024 pixels. Figure 2.2 shows schematic of image formation by CLSM.

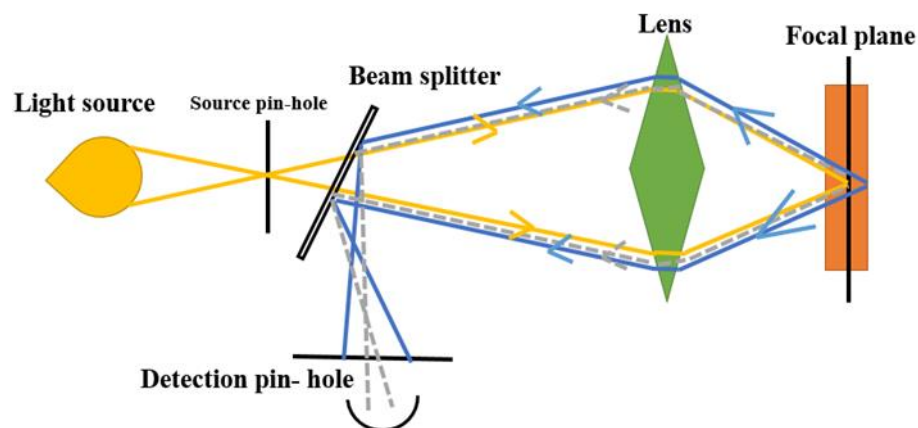


**Figure 2.2:** Schematic of image formation by confocal scanning laser microscope

### 2.2.5 Dynamic light scattering for size measurement

A Zetasizer Nano- ZS (Malvern instruments, Worcestershire, UK) was used to measure the size of microbubbles at different time interval. Samples were diluted 1:10 (wt/wt) in MilliQ water (pH 6 -7) prior to measurement and transferred into disposable PMMA cells for size distribution measurement. The refractive index of water and MBs were set at 1.33 and 1.00 respectively.

A Zetasizer measures the particle/ bubble size based on Dynamic light scattering (DLS) principals. DLS uses a laser as a light source in order to illuminate the sample particles/microbubbles within a cell. The two most commonly used methods in commercial instruments are photon correlation spectroscopy (PCS) and Doppler shift spectroscopy (DSS). In theory most of the laser beam passes straight through the sample, however the presence of particles will cause light scattering. Therefore dilution of samples is required in order to prevent the effect of multiple light scattering. The intensity of the scattered light is measured via a detector which is then passed through a correlator.

The correlator compares the light scattering intensity at successive times in order to derive the rate at which the intensity is varying. This information is then passed on to the computer where the Zetasizer software is able to convert the data into the particle/microbubble size distribution by using a mathematical model (Figure 2.3). DLS measures the Brownian motion and relates it to the particles/microbubbles size by measuring the intensity of fluctuation in the scattered light. Brownian motion is the movement of particles/microbubbles due to the random collision with the molecules of the liquid that surround the particle. An important feature of the Brownian motion is that small particles/microbubbles move faster than large particles/microbubbles (McClements 2016).

The relationship between the size of the particle and its speed (due to Brownian motion) is defined in the Stokes-Einstein equation:

$$D = \frac{k_B \cdot T}{6\pi\eta r}, \quad (2.1)$$

Where D is the diffusion coefficient,  $k_B$  the Boltzmann's constant, T the temperature in Kelvin,  $\eta$  the viscosity and r the radius of the particle/ bubble. The Stokes-Einstein theory is based on the hypothesis that the particle is spherical (McClements 2016).

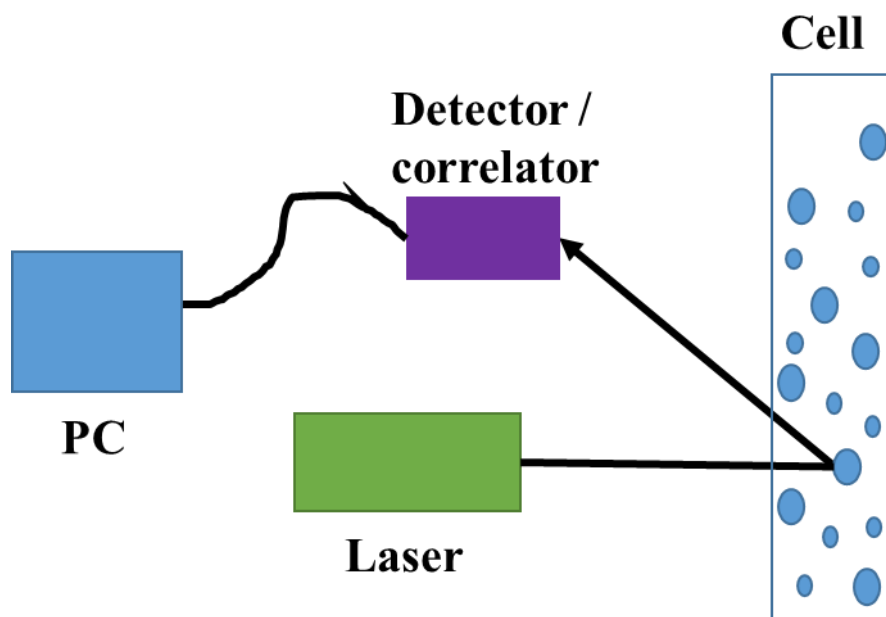


**Figure 2.3:** Schematic diagram of Zetasizer Nano to measure particle/ bubble size

### 2.2.6 Surface tension measurement

The surface tension of surfactant or protein solutions in MilliQ water were measured using the Wilhelmy plate technique via a Krüss K10S1 tensiometer (Hamburg, Germany). A roughened platinum plate was used, rinsed with deionized water and if necessary acetone also, then passed through a blue Bunsen flame and left to cool before each measurement. The plate is moved towards the surface until the meniscus connects with it (Figure 2.4). The force acting on the plate due to its wetting is measured by a tensiometer or microbalance.

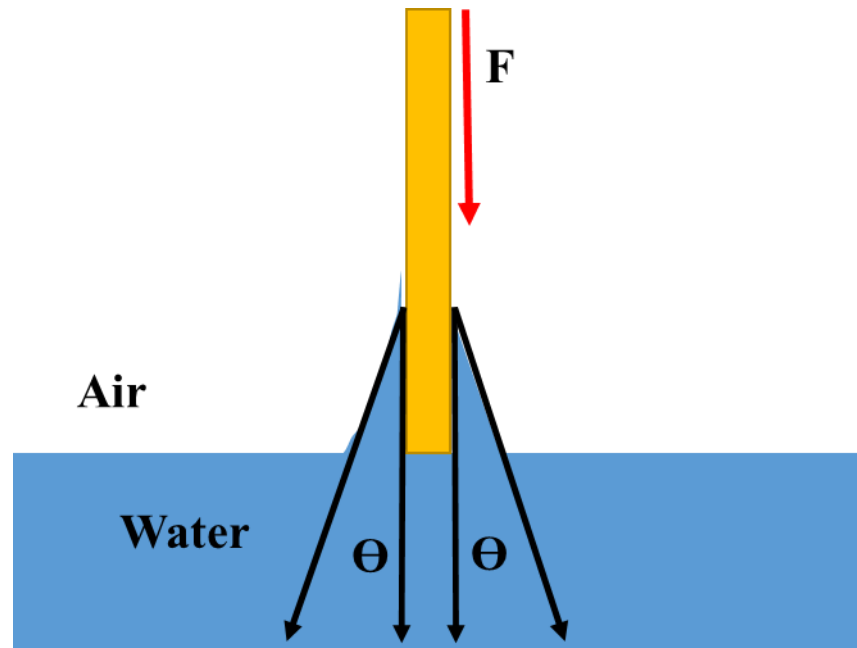


**Figure 2.4:** Schematic of Wilhelmy plate working mechanism

To determine the surface tension  $\gamma$  the Wilhelmy equation is applied. If the plate has a width  $l$  and its weight is  $W_{plate}$ , then the force  $F$  needed to detach it from the liquid surface equals:

$$F = W_{total} = W_{plate} + 2l\gamma \cos \theta, \quad 2.2$$

Multiplying by 2 is required because the surface tension acts on both sides of the plate.

The thickness of the plate is neglected. If the liquid wets completely the plate, then  $\cos \theta = 1$  and the surface tension is expressed by:

$$\gamma = \frac{W_{total} - W_{plate}}{2 \cdot l}, \quad 2.3$$

## 2.3 Results

### 2.3.1 Bubble formation and stability over time

The stability of MBs stabilized by a combination of sodium caseinate and HFB II over time has been investigated. Three batches each containing 0.03 wt. % HFB II and 0.1 wt.

% NaCas has been made as mentioned in the sample preparation section (2.2.3). An unpublished work done by Torres and co-worker found that addition of 76% glycerol to the protein solution made of 0.03 wt. % HFBII and 0.1wt. % NaCas provides the right viscosity for obtaining stable MBs. After formation of microbubble the mean diameter ( $d_z$ ) of microbubbles in each batch was determined by dynamic light scattering technique using Malvern Zetasizer.

In order to measure the size of MBs via microscopy technique a small amount of aerated dispersion was deposited in a well slide and observed using an optical microscope at regular interval time. At least five images were taken per each sample at each specific time for the period of 48 hours. Mean diameter ( $d_m$ ) of MBs was calculated by measuring diameters of at least 100 microbubbles per sample at a specific time. Figure 2.5 compares the mean diameter of MBs measured by light scattering technique and microscopy imaging.

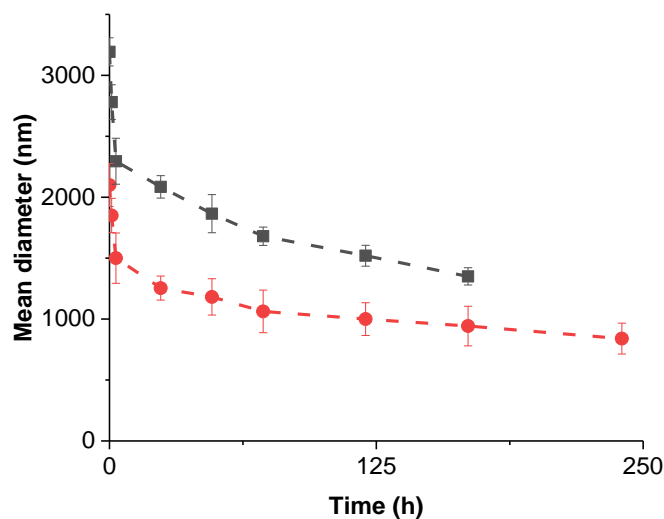
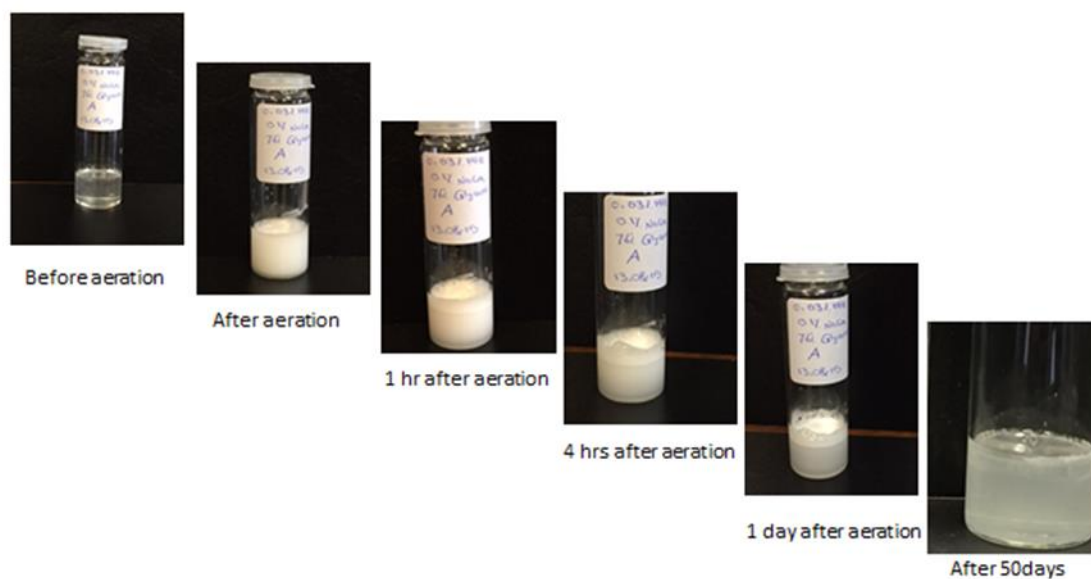


**Figure 2.5:** Represents the mean diameter of MBs during a period of 240 hours by microscope techniques (■), light scattering (●)

Both techniques showed that MBs were shrunk rapidly just after their formation especially within the first 24 hours after their formation. Then the rate of shrinkage slowed down. The light scattering results shows that after almost 72 hours the bubbles were not undergo any further shrinkage and the mean diameter remained more or less constant after 72 hours. The same observation has been reported by others (Dimitrova *et al.* 2017). It can be hypothesized that the rate of size changing corresponds to the point that the HFBII [particles] reach their packing density at the bubble surface, therefore the surface area available for gas diffusion reduces significantly, additionally the effective interfacial tension reduce significantly as a result of a decrease in the surface to volume ratio (Mohamedi *et al.* 2012).

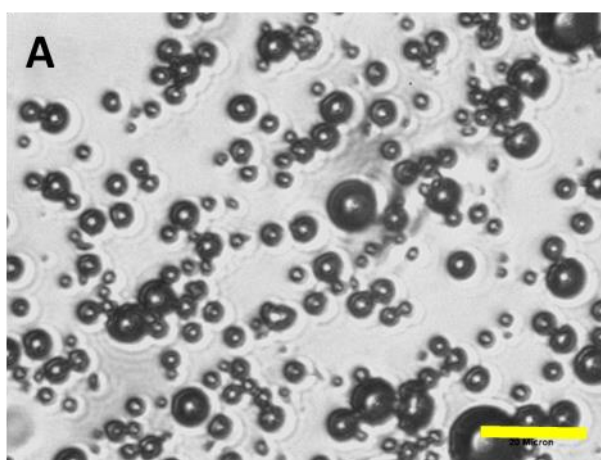
Despite the general agreement between the two measurement techniques, the mean diameters measured via light microscope images were larger than what was recorded by Zetasizer. This difference can arise from limitations associated with optical light microscopy. Light microscopy can only detects objects with diameter 1 $\mu$ m or larger at highest magnification and the depth of the field is restricted. So it can only detects the MBs that are at the surface. In addition taking microscopy images and analysing the images can be very time consuming. In here only 250 MBs diameter were measured at each time for obtaining the mean diameter where Zetasizer measures diameters of at least millions of MBs.

The initial fast shrinkage of MBs were explained by Burke *et al.* (2014). They suggested that bubbles shrink very rapidly until surface completely stabilizes by the HFBII. As HFBII forms a very dense layer around the bubbles their size doesn't change.



**Figure 2.6:** Visual assessment of a sample made with 0.03wt% HFB II and 0.1wt% NaCas

The aerated dispersions were visually assessed. Figure 2.6 illustrate that presence of MBs makes the dispersion white and cloudy because the refractive index of MBs. The image shows that MBs were stable even 50 days after the aeration. The long term stability of MBs is a result of Pickering stabilization.



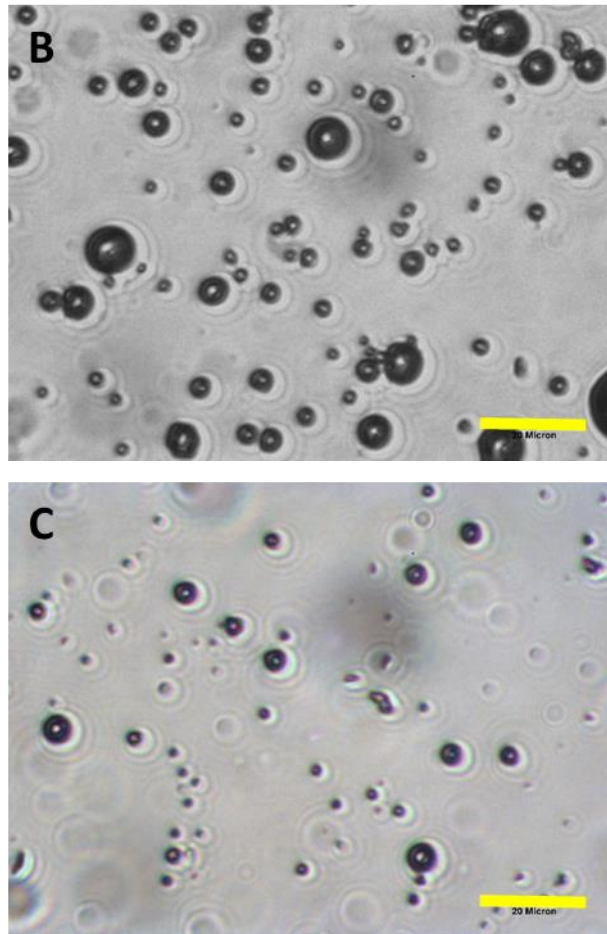


**Figure 2.7:** Microscopy images of MBs stabilized by 0.03 wt% HFBII and 0.1 wt. % NaCas.

1 hour (A), 24 hours (B) and 168 hours (C), scale bar: 20  $\mu\text{m}$

Microscopy images (Figure 2.7) confirm that MBs were very polydispersed and the polydispersity increased by time due to disproportionation. High shear mixing techniques always produce a polydispersed MBs dispersions (Stride and Edirisinghe 2008).

### 2.3.2 Impact of HFBII concentration on MBs

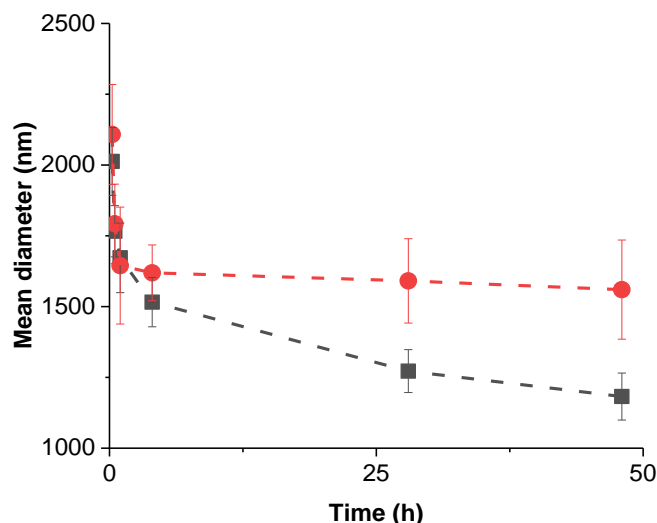


**Figure 2.8:** Comparison of mean diameter of MBs stabilized by 0.03 wt. % HFBII (■) and 0.06 wt. % HFBII (●) and 0.1 wt. % NaCas

Impact of increasing the concentration of HFBII on MBs stability was studied. For this experiment the concentration of HFBII was doubled (0.06 wt. %) while the concentration of NaCas remained constant (0.1 wt. %). Figure 2.8 shows the results of MBs diameter changes versus time. The mean diameter were measured using a Zetasizer. The result shows that at both High and low concentration of HFBII, MBs were shrunk very rapidly after their formation. However the MBs stabilized at higher concentration of HFBII stopped from further shrinkage just after 3 hours. MBs stabilized at lower concentration were slowly shrinking even after 48 hours. This results suggest at higher concentration of HFBII microbubbles stabilized faster by HFBII. Therefore they didn't shrink further. CLSM images of MBs (Figure 2.9) confirms that MBs dispersion with higher concentration of HFBII were more stable and less dissolution of gas after 16 days. The CLSM images also confirmed that bubbles stabilized at higher concentration of HFBII were having a larger diameter. A theoretical study of particle stabilized microbubbles also show that the final size of microbubbles depends on number of available nanoparticles as

well as the adsorption rate of these nanoparticle at the surface of microbubbles. (Ettelaie and Murray 2015).

CLSM images also revealed that some of the bubbles are not spherical. Presence of none spherical bubbles in a system is a sign of Pickering stabilization as the adsorbed particles (in here HFBII) strongly adsorbed to the interface and crumple as the bubble shrunk (Bala Subramaniam *et al.* 2005).

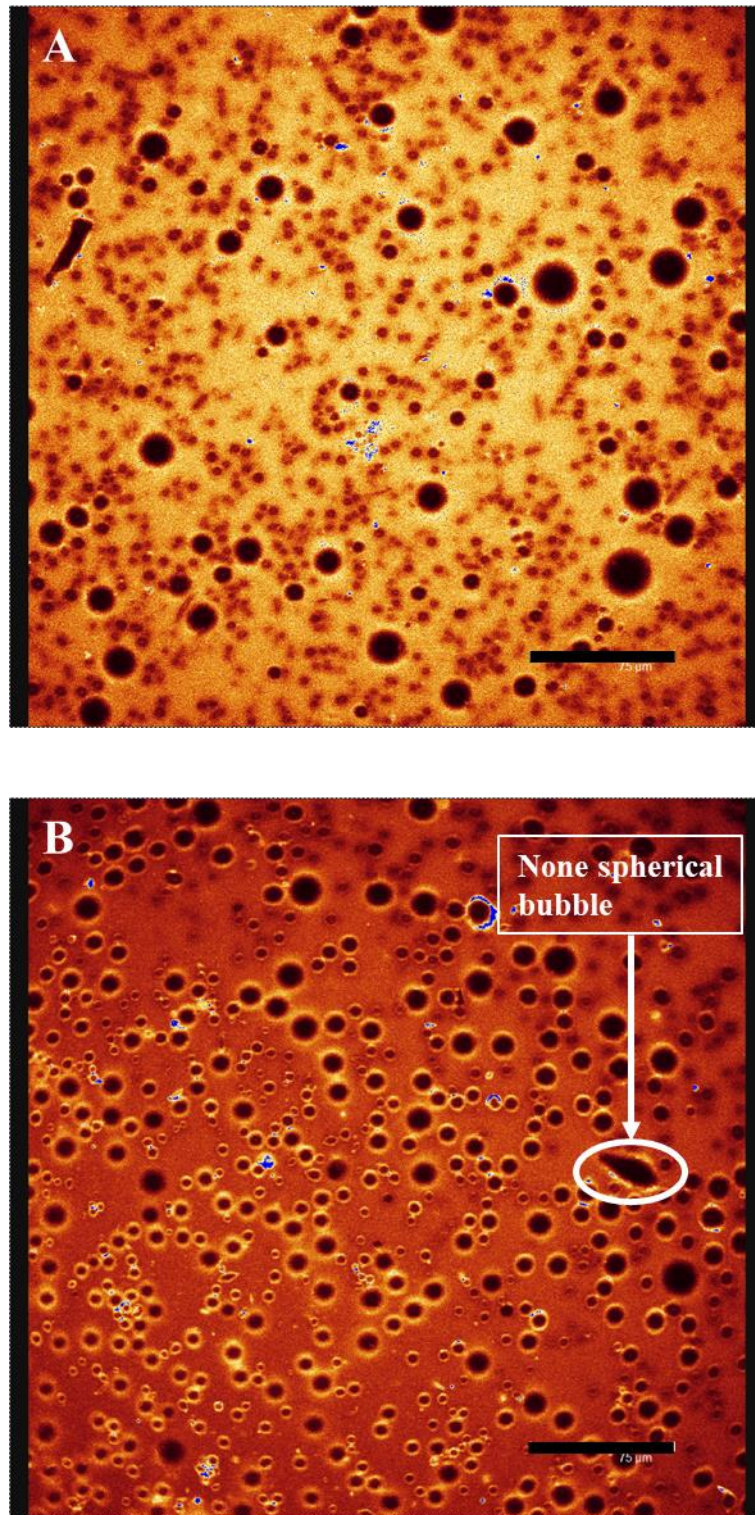


**Figure 2.9:** Confocal microscopy image of MBs stabilized by 0.03 wt. % HFBII + 0.1 wt. % NaCas (A) and 0.06 wt. % HFBII + 0.1 wt. % NaCas (B) 16 days after MBs formed. Scale bar: 75μm

### 2.3.3 Multiple aeration

The volume fraction of MBs stabilized by 0.03 wt. % HFBII and 0.1% wt. % NaCas were calculated from the density measurement of MBs dispersions. The density measurement was carried out 15 minutes after each 3 aeration step. There was 1 hour interval time between the aeration steps. The objective of this experiment was to find out if multiple aeration can lead to increase in MBs volume fraction or has a reverse effect on stabilized MBs and cause them to coalesce. Figure 2.10 represent the volume fraction of multiple aeration.

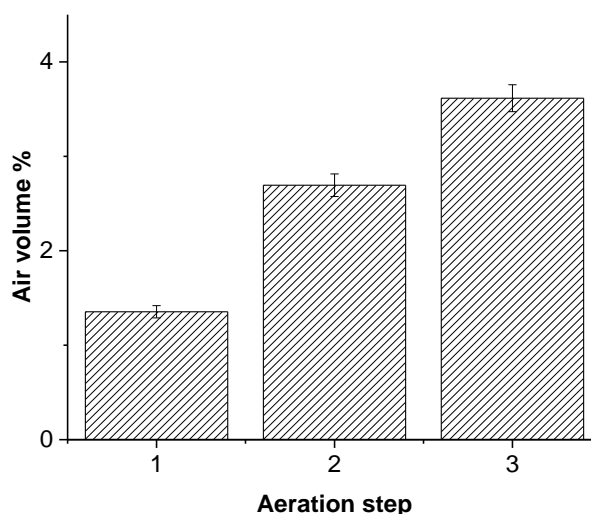


**Figure 2.10:** Volume % of MBs dispersion after each aeration step

The volume fraction of MBs after first aeration is not very high and on average it's only 1.6% of the total volume of dispersion this could be due to slow rate of particle adsorption into the air – water interface (Ettelaie and Murray 2015). MBs with a relatively small diameter 2-3  $\mu\text{m}$  have a very short life time e.g. few seconds. So the results of first aeration volume fraction showed that the MBs were stabilized by particle like HFBII. The volume fraction increased by increasing the aeration step, this shows that already formed and stabilized MBs could survive high shear mixing conditions. The further increase in

MBs volume fraction after each step of aeration means that more bubbles could form and stabilize by adding more steps of aeration. So adding enough aeration steps could lead to generation of MBs dispersion with a relatively high volume fraction of air. This can be very useful for industries that try to increase the air volume fraction of their products. Due to lack of time the multiple aeration were carried out for only 3 steps of aeration. It would have been very interesting to find out how many aeration steps required to achieve highest MBs volume fraction.

#### **2.3.4 Effect of surface activity on MBs**

After finding out that increase in concentration of HFBII could increase the stability of MBs and halt disproportionation in the system it was worth trying to find out what would be the impact of increasing/decreasing the concentration of NaCas on MBs formation and stabilization. Figure 2.11 represents the mean diameter of MBs (measure by Zetasizer) stabilized by 3 different concentration of NaCas, 0.05, 0.1 and 0.2 wt. %, when the concentration of HFBII was 0.03 wt. % for all 3 systems. The system made of 0.1wt. % NaCas with no HFBII was used as a blank.

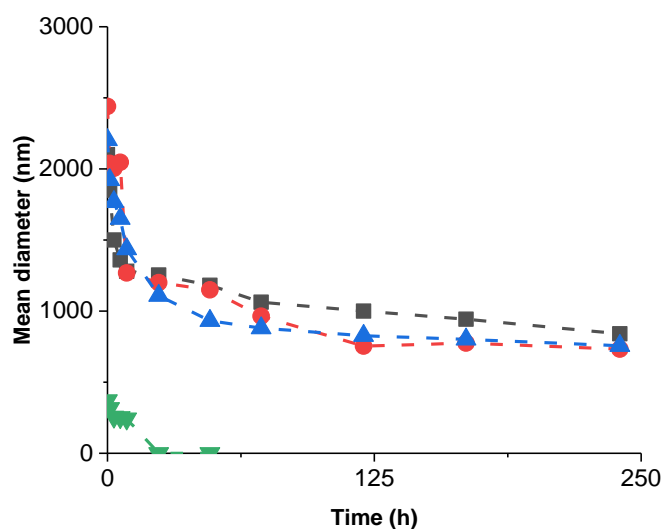


**Figure 2.11:** Mean diameter of MBs stabilized by different concentration of NaCas when the concentration of HFBII remained constant at 0.03 wt.%. 0.1 wt.% NaCas (■), 0.05 wt.% NaCas (●), 0.2 wt.% NaCas (▲) and 0.1 wt.% NaCas in absence of HFBII (▼)

The results didn't show any significant difference in the MBs size between different systems MBs shrunk at higher rate at the beginning of their formation and after few hours the rate of shrinkage slowed down. However the system with no HFBII wasn't stable and all the MBs were dissolved after 9 hours.

One conclusion for this behaviour could be that the difference in NaCas wasn't enough to make a significant change. Therefore 2 more systems (0.025 and 0.4 wt. % NaCas) were studied to see the impact of high/low concentration of NaCas on MBs.

The results didn't show any significant difference on the MBs size and stability over the period of 10 days. This led us to measure the density of the different systems after 48 hours to investigate if there is any difference between them. The results were very interesting and showed that an increase in concentration of sodium caseinate could increase the volume fraction of MBs. This results suggests that presence of more NaCas in the system means more MBs could be possibly stabilized without affecting the size of MBs. As mentioned earlier bubbles with this sorts of size have a very short life time of

less than few second so it is important that MBs stabilize very quickly before they dissolve completely. This results are in agreement with a previous study that suggested MBs are initially stabilized by casein before HFBII displace the casein and stabilize the bubble more permanently (Burke *et al.* 2014). The next step of this work was to identify the impact of replacing the NaCas by other surface active proteins or surfactants. The answer to this is very important and shows how other surface active material interact with HFBII at the air- liquid interface and how their competency affect the MBs. The surface active proteins and surfactant chosen for this experiment were Tween 20, Tween 80, Triton x-100, whey protein isolate (WPI) and  $\beta$ -lactoglobulin. They were used in 0.1 wt. % concentration to replace the NaCas. The MBs dispersion were made as described in sample preparation section.

The reason for selecting this specific surfactants and proteins was to make sure that a range of surface active material with higher and lower surface tension examined. Table 2.1 shows the surface tension measured for the different proteins and surfactants.

<b>Surfactant/Protein</b>	<b>Concentration (wt. %)</b>	<b>Measured Surface Tension (mN/m)</b>	<b>Surface Tension (mN/m)  according to literature</b>
<b>HFB II</b>	0.03	32	35
<b>Triton-X-100</b>	0.1	30.8	30
<b>Tween 20</b>	0.1	33	35
<b>Tween 80</b>	0.1	36	39.7
<b>WPI</b>	0.1	59	59
<b>NaCas</b>	0.2	49.5	50
<b>NaCas</b>	0.1	49.5	50
<b>NaCas</b>	0.05	49.5	50
<b>β- lactoglobulin</b>	0.1	57	55

**Table 2.1:** Surface tension measurement for different surfactants and proteins. HFBII (Cox *et al.* 2007), Triton-X- 100 (Robinson, Sutton and Reid 2014), Tween 20 and 80 (Kothekar *et al.* 2007), NaCas (Abascal and Gracia-Fadrique 2009), WPI and β-lactoglobulin (Woodward *et al.* 2004).

The mean diameter of the generated MBs made by different surfactants/ proteins and HFBII was measured by Zetasizer (Figure 2.12). The results were very similar for different surfactant or proteins used in combination with HFBII. They all had a faster rate of MBs shrinking at the beginning followed by a period of much slower rate after 48 – 72 hours. This behaviour observed for all different system studied here. The results are in an agreement with a recent paper that studied the impact of combing HFBII with other

proteins. The study found that adding other proteins, up to 94 % of total protein weight fraction, doesn't affect the HFBII adsorption. Addition of higher amount of protein could change the protein packing at the air – water interface and therefore affect the foam stability (Dimitrova *et al.* 2017).

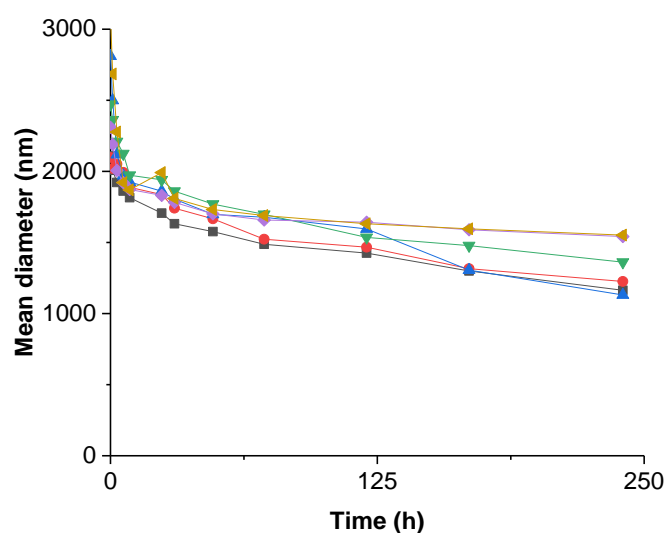


**Figure 2.12:** Mean MBs diameters for the period of 10 days. NaCas (▼), Tween 20 (■), Tween 80 (●), Triton X-100 (▲), WPI (◀) and β-lactoglobulin (◆)

So the better way to investigate the correlation of surface tension and MBs were by measuring the density 48 hours after MBs formed. Figure 2.13 represents the volume fraction corresponded to different systems. The results shows a direct correlation between surface tension of the surface active surfactant / proteins and MBs volume fraction. Figure 2.14 illustrate the air volume fraction plotted against surface tension. The results shows that increasing the surface tension led to an increase in volume fraction until it reached its optimum and then the volume fraction started to decrease after this optimum point. If the surfactant is too surface active (lower tension) then this dominates the particles too much and lowers the volume fraction. Optimum surface tension (β- lactoglobulin) gave the highest volume fraction. Whereas if the surfactant is not surface active enough (higher

tension) not enough bubbles will be formed in the first place. NaCas on its own is not an effective foam stabilizer (Dickinson *et al.* 2002). The air volume fraction of dispersion made by 0.1 wt. % in absence of HFBII was close to zero, 48 hours after aeration.

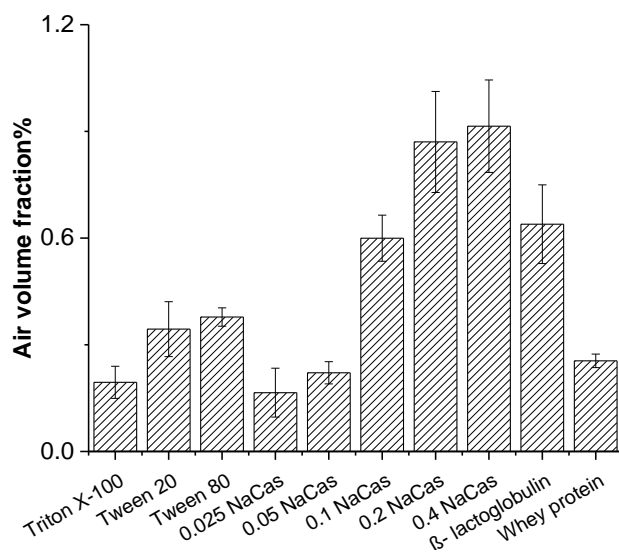


**Figure 2.13:** Air volume% of different systems

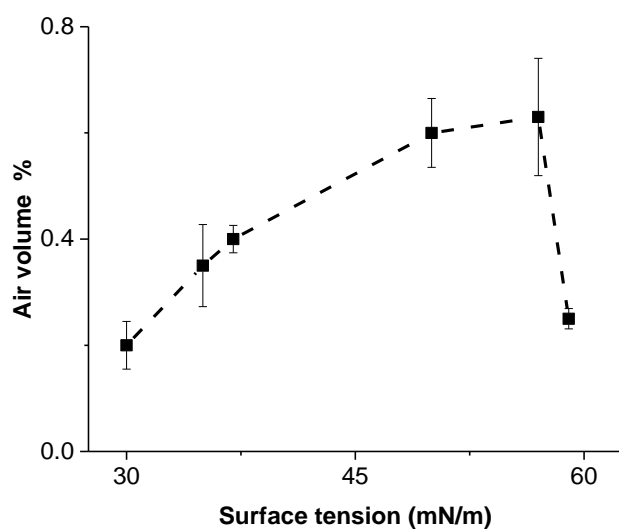


**Figure 2.14:** Air volume % as a function of surface tension

## 2.4 Conclusion

The MBs stability, size and volume fraction was investigated to see if HFBII can stabilize MBs in presence of other surface active materials such as proteins and surfactant. Our results shows that HFBII can stabilize MBs for a long period of time and prevents disproportionation. Nanoparticles can stabilize foams for several days whereas even best proteins stabilize bubbles for several minutes (Dickinson *et al.* 2002). The results are on agreement with previous studies investigating the foam stabilization ability of HFBII (Cox *et al.* 2007; Burke *et al.* 2014; Dimitrova *et al.* 2017).

Our finding also shows that the HFBII is responsible for longer stability of MBs as the system made with no HFBII were not stable and MBs dissolved within few hours. In addition HFBII proved to be responsible for the MBs final size. As the MBs stabilized at higher concentration of HFBII had shrunk less. It is possible to say that HFBII acts like a nanoparticles and prevents them from disproportionation for a long period of time. On the other hand NaCas is more responsible for initial stabilizing of bubbles so more MBs could be stabilized therefore the final volume fraction increases.

More importantly the results shows how different surface active material impact MBs formation and stability when used in combination with HFBII. Surface activity plays an important role on increasing the volume fraction so increasing the surface activity of the surfactant/ protein up to a certain value improves the foam volume fraction. However it reaches to a point that any increase in the surface activity have a negative effect on foam volume fraction.

## Chapter 3 :

# Poly Alkyl Cyanoacrylate Impact on Microbubble Stabilization

### 3.1 Introduction

MBs are widely used not only in food products but also in material coating, cosmetics, crude oil recovery, fabrication of lightweight materials for use in medical and engineering field (Gonzenbach *et al.* 2006), targeted drug delivery and gene therapy (Ferrara, Pollard and Borden 2007) and sonochemistry (Ashokkumar *et al.* 2007; Brotchie, Grieser and Ashokkumar 2010; Wood, Lee and Bussemaker 2017).

In chapter 1 the unstable nature of MBs was discussed in detail. The driving force for MBs instability is the Laplace pressure. Difference in Laplace pressure leads to rather quick dissolution of MBs, known as disproportionation. The only effective way to prevent disproportionation is Pickering stabilization of MB via nanoparticles.

Most studies of Pickering stabilized bubbles have used inorganic particles as stabilizer, partly because the effects of different shape and size can be tested but also a wide variety of chemical agents exist for modifying the particle surface chemistry and therefore contact angle (Binks and Horozov 2005). However over the past few decades there has

been an increased interest in finding Pickering nanoparticles for medical applications as well as food products (Dickinson 2010b; Lam, Velikov and Velev 2014).

Polybutyl cyanoacrylates (PBCA) nanoparticles have extensively used as MBs stabilizer over the past few years (Harris, Depoix and Urich 1995; Palmowski *et al.* 2008; Fokong *et al.* 2011; Mørch *et al.* 2015). This is mainly because of their ease of preparation, ability to adsorb to many drugs, long term stabilization of MBs and their biodegradability and biocompatibility (Douglas *et al.* 1984; Xiong *et al.* 2011). Poly butyl cyanoacrylate (PBCA) were first used by Schering AG to stabilize MBs for ultrasound imaging (Harris, Depoix and Urich 1995).

Alkyl cyanoacrylates are a group of highly reactive monomers, with excellent adhesive properties. Shorter chains alkyl cyanoacrylates such as ethyl (ECA) are mainly used as household adhesive, e.g., super glue (Nicolas and Couvreur 2009). Longer chains such as butyl cyanoacrylates (BCA) and octyl cyanoacrylates (ECA) are extensively used as medical glue to close open wounds or hold tissues together (King and Kinney 1999). Couvreur and co-workers (Couvreur *et al.* 1979) produced a simple technique to generate alkyl cyanoacrylate nanoparticles by dropwise addition of monomer to water in the presence of surfactant solution at pH 2 – 3. The previous techniques of polymerisation usually contained harsh chemicals and subsequently required several purification steps once they had been made. However, there are many conflicting results in the literature concerning the ideal conditions for polymerisation of alkyl cyanoacrylates to particles. In addition, as pointed out by (Yordanov, Abrashev and Dushkin 2010) the emulsion polymerization route via surfactant micelles should be distinguished from the alternative dispersion polymerization route using polymeric surfactants.

Despite high number of studies on PBCA NPs as MBs stabilizing agent mainly for medical applications (Pirker *et al.* 1996; Olbrich *et al.* 2006; Liu *et al.* 2011; Fokong *et*

*al.* 2011) it seems there are no systematic studies showing why PBCA NPs are a good MBs stabilizers.

Part of the confusion may arise from using different cyanoacrylate monomers, different sources of the same monomer with different purity and inhibitor, and also different polymerization conditions (Müller *et al.* 1992; Behan, Birkinshaw and Clarke 2001). Different monomers seem to produce NPs with different properties (Sulheim *et al.* 2016). Douglas *et al.* (1984) reported that pH and monomer concentration are the main factors that determine the properties of produced PBCA NPs. They concluded that particle size increases as a result of increase in pH of polymerization media. A relatively simple two step technique to produce stable MBs via PBCA NPs was developed by Schmidt and Roessling (2006). The first step was producing PBCA NPs by polymerization of BCA monomer in aqueous phase at low pH and in presence of Triton X-100. The second step was aerating the system to produce stable MBs. They investigated the effect of BCA concentration, polymerization temperature and stirring speed on MBs size and formation. By optimizing the polymerization conditions the PBCA formation yield reached 97%. Temperature had a little impact on MB formation and size while increase in monomer concentration resulted in producing larger NPs. Higher stirring speed formed smaller MBs and longer aeration time led to higher bubble volume fraction.

Despite these previous studies the impact of different monomer and concentration, surfactant type and concentration and other variable polymerization parameters on MB formation and stabilization are largely unknown. The aim of this work is to study the nature of these poly alkyl cyanoacrylates (PACA) NPs under different polymerization conditions and their effect on MBs formation and stability.

## **3.2 Materials and methods**

### **3.2.1 Materials**

De-ionized Milli-Q water (Millipore, Watford, UK) was used. Glycerol (purity 99.5%) was purchased from Fischer Scientific (Loughborough, UK). Butyl cyanoacrylate (BCA) monomer was supplied by Chemence (Corby, UK). Ethyl cyanoacrylate (ECA) monomer was purchased from Loctite (Henkel, Slough, UK) and octyl cyanoacrylate (OCA) monomer was supplied by Liquid Skin (Chemence, Corby, UK). Tyloxapol®, Triton X-100®, and AnalR HCl (37%), used to adjust the pH, were supplied by Sigma Aldrich (Gillingham, Dorset, UK). An Amicon® stirred cell (EMD Millipore Corporation, USA) fitted with 30 kDa Ultracel® filter were purchased from EMD Millipore Corporation (Hertfordshire, UK). Nile Red was purchased from Sigma-Aldrich (Steinheim, Germany). Xanthan gum, supplied by Sigma-Aldrich (Poole, UK), SP701PA clear casting resin, containing 1% catalyst was purchased from Trylon Ltd (Northants, UK). Glass specimen tubes (100 x 26mm) used to store the samples, were obtained from Scientific Laboratory Supplies Ltd (Nottingham, UK).

### **3.2.2 Preparation of Nanoparticles and microbubbles formation**

Butyl cyanoacrylate (BCA), ethyl cyanoacrylate (ECA) and octyl cyanoacrylate (OCA) were polymerised by anionic polymerisation to produce poly butyl cyanoacrylate (PBCA), poly ethyl cyanoacrylate (PECA) and octyl cyanoacrylate (POCA) nanoparticles (NPs), respectively. The optimum monomer concentration according to Schmidt and Roessling (2006) is 1.4 wt. %. Monomer was therefore added drop-wise up this concentration, in preliminary experiments to 1% Triton X-100 in deionized water, at pH 2.2 under mild stirring (at 500 – 700 rpm) using a magnetic stirrer and magnetic followers (PTFE covered, 25mm long). i.e., following their procedure. Under these

conditions the typical polymerization time, taken as the time when there appeared to be no further change in NP size (within experimental error, measured as described below) was 30 min. In order to determine the NP yield, a sample of polymerized material was filtered through a Whatman No. 3 filter paper (pore size 6 $\mu$ m) and the material retained was weighed, after drying. The polymer yield was defined as the wt.% fraction of monomer transformed into the material retained on the filter.

For preparation of microbubble (MB) dispersions, a sample (25 ml) of NP dispersion was aerated for 2 minutes via an Ultra-Turrax T25 mixer at room temperature at 24000 rpm. In subsequent experiments Triton X-100 was replaced with Tyloxapol and polymerization at pH 4 was also tested. To some dispersions glycerol was added to give 76% glycerol prior to aeration as above. These samples were also then subjected to multiple aeration at different time intervals. The density and therefore air content (volume fraction) of aerated samples was measured via a high precision oscillating U-tube densitometer (DMA 4500, Anton-Paar, Graz, Austria) at 25°C. The glycerol also served to increase the viscosity sufficiently to reduce any coalescence of bubbles in manipulation the sample into the densitometer. In all cases of density measurement a 1wt% Tyloxapol in 76% glycerol was used as a blank.

In order to remove the excess surfactant a sample of PBCA NPs were centrifuged in a Universal 320 centrifuge (Hettich, Tuttlingen, Germany) at 2370g for 35 minutes. The supernatant was removed carefully and sedimented particles were transferred to a clean beaker and deionized water (pH 4) was added, stirred gently by a spatula for 10 minutes, followed by 1 minute sonication in a Kerry Ultrasonic Bath (Hitchin, UK) of 1 litre capacity at 60 Hz.

### 3.2.3 Microscopy

The same procedure was used as described in 2.2.4. In order to increase the viscosity of the MB dispersions and immobilize bubbles so as to more clearly image the adsorbed particles, xanthan gum solution (0.1 wt%) was added. Nile red was used to stain the PBCA NPs when CLSM was used. The dye was excited with the 488 nm Ar laser line and emission wavelength 525 nm during the CLSM scanning.

Selected samples were also imaged via scanning electron microscopy (SEM) via an FEI Nova450 SEM (Eindhoven, The Netherlands). Approximately 5 droplets of MB dispersion were stirred inside silicone moulds filled with the clear casting resin and allowed to set for at least 24 hours. The solid samples were fractured using a sharp blade. Samples were coated with a thin layer of iridium (2 nm) via a Cressington 208HR sputter coater. Samples were imaged at 3 kV.

### 3.2.4 PBCA NPs size and $\zeta$ - potential

The particle size distribution (PSD) and  $\zeta$ - potential of the NP dispersions were measured by dynamic light scattering at 25 °C using a Zetasizer Nano- ZS (Malvern instruments, Worcestershire, UK). Samples were diluted 1:10 (wt/wt) in MilliQ water (pH 6 -7) prior to measurement and transferred into disposable PMMA cells for PSD measurement. The refractive index of water and PBCA were set at 1.33 and 1.46 respectively. For  $\zeta$ - potential measurements the diluted dispersions transferred to DTS 1070 measurement cells.

A Zetasizer measures the electrophoretic mobility of the particles then calculates the  $\zeta$ - potential by applying Henry's equation:

$$U_E = \frac{2\varepsilon z f(\kappa\alpha)}{3\eta} , \quad 3.1$$

Where  $U_E$  is electrophoretic mobility,  $z$  is the  $\zeta$ - potential,  $\varepsilon$  is dielectric constant,  $\eta$  is the viscosity and  $f(\kappa\alpha)$  is the Henry's function. The units of  $\kappa$  are reciprocal length and  $1/\kappa$  is the thickness of the electrical double layer (the Debye length),  $\alpha$  is the particle radius therefore  $\kappa\alpha$  is the ratio of particle radius to double layer thickness. For particles in aqueous media the maximum value of  $f(\kappa\alpha)$  is 1.5 (Smoluchowski approximation). A classical electrophoresis system uses a capillary cell with electrodes at both ends to which an electric field is applied (Figure 3.1). Particles move towards the electrode, until they reach a constant velocity as a result of applied electric field and viscosity.

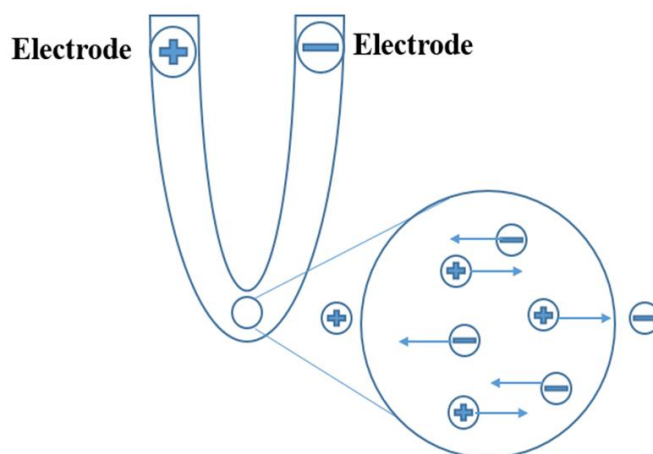


**Figure 3.1:** Schematic of a capillary cell and illustration of charged molecule movement when electric field is applied

### 3.2.5 Free Tyloxapol determination

Tyloxapol concentrations in water can be determined by spectrophotometry, the phenol ring giving strong absorbance at 270 nm. However, PBCA particles also absorb at this wavelength, so care had to be taken to separate NPs from Tyloxapol, via filtration. Serial dilution of Tyloxapol in water was used to obtain a standard curve. The same solutions were also re-measured after passing through a 30 kDa Ultracel filter in the Amicon stirred cell apparatus. NPs dispersions that also contained Tyloxapol were diluted (1:500) and

passed through the same filter to remove the NPs. Tests showed that this filter had a pore size sufficiently small to retain NPs of all the sizes produced but allow the free surfactant to pass through. The absorbance of all solutions was measured at 270 nm at 25°C in a 3 ml quartz cuvette.

### **3.3 Results**

#### **3.3.1 Impact of polymerization condition on NPs properties**

There is no general agreement in literature on how polymerization conditions such as surfactant type and concentration, monomer type and pH affect the PACA NPs in terms of physiochemical properties. Hence the impact of these parameters were tested and summarised in Table **3.1**. 11 different system were studied.

System No.	Surfactant and concentration	pH	NP Yield/ %	<i>d</i> / nm	$\zeta$ /mv	MB stability
1	0.1 wt.% Triton-X100	2.2	$\leq 15 \pm 5$	$140 \pm 7$	-20	None
2	1 wt.% Triton-X100	2.2	$\leq 30 \pm 3$	$110 \pm 2$	-20	$\geq 2$ weeks
3	10 wt.% Triton-X100	2.2	$\leq 10 \pm 2$	$140 \pm 5$	-21	None
4	1 wt.% Triton-X100	4	$\leq 30 \pm 3$	$100 \pm 10$	-20	$\leq 2$ months
5	1 wt.% Tyloxapol	4	$\geq 50 \pm 5 \%$	$150 \pm 30$	-24	$\geq 2$ months
6	No surfactant	4	$\geq 70 \pm 2 \%$	$90 \pm 5$	-61	None
7	1 wt.% Tyloxapol (added after particle formation)	4	$\geq 70 \pm 2 \%$	$90 \pm 5$	-34	None
8	1 wt.% Tyloxapol	2.2	$\leq 20 \pm 3 \%$	$105 \pm 10$	-19	$\geq 2$ months
9	1 wt.% Tyloxapol	6	$\geq 40 \pm 3\%$	$131 \pm 5$	-28	$\geq 2$ months
10	1 wt.% Tyloxapol*	4	$40 \pm 6 \%$	$90 \pm 10$	-33	2-5 days
11	1 wt.% Tyloxapol#	4	$50 \pm 10 \%$	25-151	-30	2-5 days

**Table 3.1:** Yield, size (*d*) and zeta potential of NPs formed under different conditions and the stability of the corresponding microbubbles (MBs) formed on aeration. All systems used BCA monomer except \* = ECA, # = OCA.

Triton-X100 was used first and the effect of its concentration on polymerization of BCA studied. The pH and monomer concentration were kept constant at 2.2 and 1.4 wt.%, respectively. Table 3.1, systems 1 to 3, show the effect of Triton-X100 concentration on the yield, mean diameter (*d*) and zeta potential of the NPs formed. (Note the pH of the

diluted dispersions during these measurements was pH 4 to 6). It is seen that the zeta potential was largely unaffected across 0.1 to 10 wt.% Triton-X100, at around  $-20$  mV. Triton-X100 is a non-ionic surfactant and so in itself is not expected to impart any charge if adsorbed to the NPs, whilst the monomer is anionic. The monomers are neutral (and fairly insoluble) in these pH ranges so that the negative zeta potential is therefore mostly likely due to adsorbed impurities (possibly some traces of de-esterified acrylates). The NP diameter ( $d$ ) was also not greatly affected by the Triton-X100 concentration during the polymerization, although 1 wt.% gave slightly lower  $d$  (110 nm) than 0.1 and 10 wt.% (140 nm). Overall then, it seems that although the BCA polymerization is supposed to proceed via an emulsion polymerization route and initiation within the surfactant micelles (Nicolas and Couvreur 2009; Behan, Birkinshaw and Clarke 2001), the final NP properties do not seem very sensitive this surfactant concentration.

Other workers (Budde *et al.* 2003) have used Tyloxapol as the surfactant rather than Triton-X100. Tyloxapol is an oligomer of Triton-X100 and as such is expected to have a lower critical micelle concentration and higher affinity for the interface. The structures of Triton-X100 and Tyloxapol are illustrated in Figure 3.2 (Regev and Zana 1999). It is reported to consist of an average of 3 to 8 (average 7) Triton X100 molecules with their head groups linked together via a single methylene group (Dharaiya, Aswal and Bahadur 2015); with a molecular weight of 1709 to 5263 Daltons.

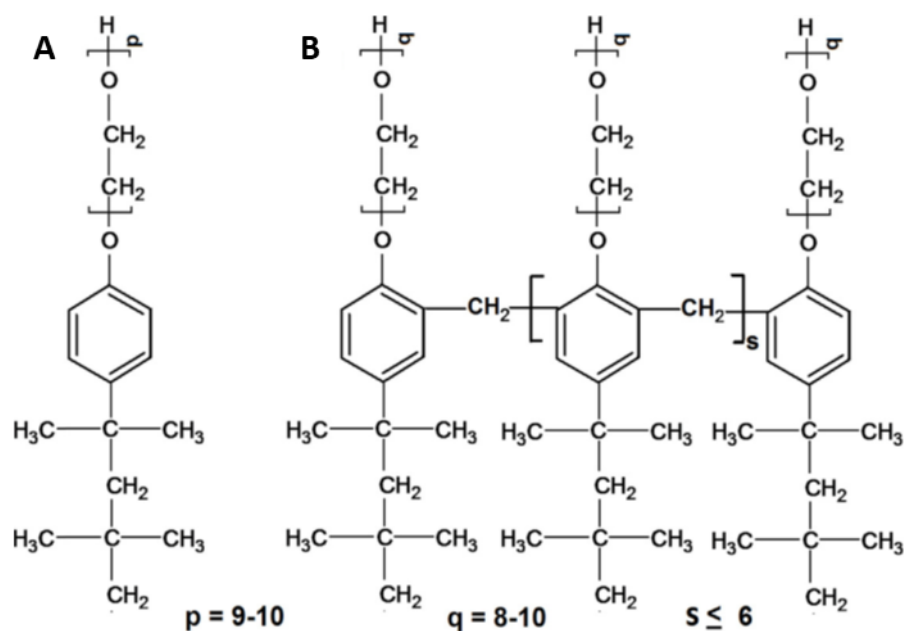


**Figure 3.2:** Chemical structures of (A) Triton X-100, (B) Tyloxapol (Regev and Zana 1999)

Polymerization of BCA in the presence of 1 wt.% of either surfactant was therefore carried out for comparison of NP properties. Polymerization was carried out at pH 4 in line with other studies (e.g., (Budde *et al.* 2003) with Tyloxapol and polymerization was also attempted in the absence of any surfactant as a control. Table 3.1, systems 4 to 7 show the properties of the NPs produced and also an indication of the stability of the MBs produced by aerating these dispersions, as described above.

Tyloxapol (system 5) gave slightly larger NP diameter ( $d$ ) than TritonX-100 (system 4) but a higher NP yield (50 % cf. 30% for Triton-X10). At first sight this higher yield is probably explained by the Tyloxapol giving greater NP stabilization due to (i) its higher molecular weight and therefore more effective steric stabilization, and/or (ii) greater coverage due its higher molecular weight and affinity for the interfaces and/or (iii) the slighter higher (more negative) zeta potential imparted by Tyloxapol ( $-24$  mV) versus Triton-X100 ( $-20$  mV). However, very interestingly, no surfactant at all (system 6) gave a similar NP sizes ( $90 \pm 5$  nm), a *higher* yield than either surfactant and NPs with a zeta potential almost twice as negative ( $-61$  mV) as with surfactant. Possibly some sort of

dispersion polymerization mechanism is responsible, or the polymerizing monomer acts as some sort of surfactant or stabilizer. However, these NPs were no use whatsoever at stabilizing MBs, possibly due to their higher negative charge, making them too hydrophilic. This suggests that the surfactant is not essential to BCA NP formation but plays some other role in controlling the NP surface active properties at the A/W interface. Excess surfactant is of course present when the NP dispersions are aerated, but control experiments aerating 1% Tyloxapol or Triton-X100 on their own did not give any stable MBs (Any bubbles formed appeared to have completely disappeared with less than 3 h). This is expected, since only particles are able to prevent disproportionation of MBs over long periods of time. Furthermore, adding 1 %Tyloxapol to the NP dispersion formed in the absence of surfactant *after* NP formation gave a system (system 7) which reduced the magnitude of the zeta potential to from  $-61$  to  $-34$  mV but these particles were still not able to stabilize MBs. The lowering of the zeta potential by the non-ionic surfactant must be due to its adsorption and shifting of the plane of shear further away from the surface of the particles where the charge density due to surface polymer chains is lower. The magnitude of this final zeta potential was not quite as low as that of the NP formed in the presence of Tyloxapol ( $-24$  mV), which suggests there might be a critical value of zeta potential that determines the surface activity of the NPs, but certainly simple Tyloxapol adsorption to the NPs cannot create this condition: Tyloxapol only imparts good MB-stabilizing properties when it is present *during* BCA polymerization. PBCA NPs formed in absence of any surfactant were not very stable and started to grow in a slow rate. Table 3.2 shows the size changes of PBCA NPs formed in absence of surfactant.

[Tyloxapol] added after NP formation/ wt.%	Diameter/ nm				
	10 mins	1 h	1 day	10 days	20 days
0	95	100	123	155	155
1	92	92	92	92	92

**Table 3.2:** Represents the size changes after NPs formed for the period of 20 days

Addition of 1 wt.% Tyloxapol to the PBCA NPs formed in absence of surfactant (system 6) halted the further increase in particle size see table 3.2. This suggests the added Tyloxapol adsorbed to the surface of the already formed particles and stabilized them against aggregation or growing.

In addition, samples of the optimum system 5 were subjected to centrifugation (see Methods section) to separate the PBCA particles from the remaining bulk Tyloxapol solution present during their formation. From the mass of the pellet it was estimated that  $\geq 90\%$  (0.158 g out of 0.175g) of the PBCA particles present in the sample as a whole were separated from the supernatant. This pellet was then re-dispersed in MilliQ water at pH 4 (using a spatula and stirring by hand for 10 minutes, followed by 1 minute sonication as described in methods section). The mean size and zeta potential of the dispersed material were measured as  $360 \pm 10$  nm and  $-34 \pm 1$  mV, respectively i.e., different to the pre-centrifuged particles. However, when this dispersion was aerated no stable MBs formed. This shows that the excess surfactant is necessary to lower the surface tension and help stabilize bubbles until sufficient NP coverage is achieved so as to inhibit their further shrinkage, i.e., some co-adsorption of NPs and surfactant must take place during the early stages of bubble formation. Addition of 1wt.% NaCas to the re-dispersed PBCA NPs, did not result in the formation of stable bubbles. Centrifugation might also

possibly change the properties of PBCA NPs so they were not effective as bubble stabilizers. Further investigation is required to understand why these centrifuged PBCA NPs could not stabilize MBs even after addition of NaCas as a foaming agent or Tyloxapol. In contrast aeration of the supernatant which must have contained a very low concentration of NPs led to formation of MBs. The concentration of MBs produced by aeration of supernatant was way less than that of aerated PBCA NP dispersion.

Since the polymerized NPs had a negative charge, it was expected that the pH of polymerization might affect the size and surface charge of the resultant NPs – and both of these factors would affect the NP contact angle and surface activity. Various workers seem to recommend different pH values. BCA was therefore also polymerized at pH 2.2 (system 8) and pH 6 (system 9), where the charge on the monomer should be significantly different. Since Tyloxapol seemed to give the best particles for MB stabilization 1 wt.% Tyloxapol was used as surfactant. Comparison of systems 8 and 9 with system 5 (pH 4) in Table 1 shows that pH had a significant effect on the yield of PBCA NPs, but not their size or MB-stabilizing capabilities. The yield increased when the pH was increased from 2.2 to 4 and decreased again slightly at pH 6, whilst MBs stabilized by all 3 systems appeared equally stable - for at least 2 months there was very little change in mean bubble size (see later). The optimum pH, i.e., for highest PBCA NP yield was therefore taken as pH 4.

Finally, although polymerization of in the presence of 1 % Tyloxapol at pH 4 seemed to give the optimum NPs for MB stabilization in the case of BCA (across all the conditions investigated thus far), it was thought worthwhile to investigate if any other monomers were advantageous, since there is no obvious reason why polymerization of the butyl derivative should give better NPs for MB stabilization than other alkyl cyanoacrylates. Two relatively easily available monomers are ethyl cyanoacrylate (ECA) and octyl cyanoacrylate (OCA), that have also been investigated by others (Couvreur *et al.* 1979;

Nicolas and Couvreur 2009; Sulheim *et al.* 2016) although no details of NP yields were given. Polymerization of both was attempted under the optimum conditions for BCA, i.e., 1.4 wt% monomer, pH 4 with 1 wt% Tyloxapol and the results (systems 10 and 11) are also shown in Table **3.1**. Comparison with BCA (system 5) shows that all 3 monomers gave similar yields under these conditions, although ECA gave slightly lower yields than BCA or OCA. ECA gave similar NP sizes to BCA (slightly smaller in fact) but the OCA particle size was very irreproducible, with most of the material present as very large aggregates and a representative value for POCA NPs could not be determined. Most significantly, only the PBCA particles were able to give high MB stability, PECA and POCA material gave bubbles that disappeared completely via coalescence and/or dissolution in less than 2 to 5 days, whereas PBCA-stabilized MBs were stable for at least 2 months. It is noteworthy that the size and zeta potential of the PECA particles were  $90 \pm 10$  nm and  $-33$  mV, respectively, very close to the values ( $90 \pm 5$  nm and  $-34$  mV) of the PBCA particles formed without surfactant but with Tyloxapol added afterwards (system 7). The latter particles also did not give good MB stability, again suggesting that such zeta potentials are too high in magnitude, making the particles too hydrophilic for a high enough contact angle and energy of desorption at the A/W interface.

The micrographs in Figure **3.3** illustrate the appearance and different stabilities of the MBs formed with some of these systems. Figure **3.4** shows system 5 and 6, 24 hours after aeration.

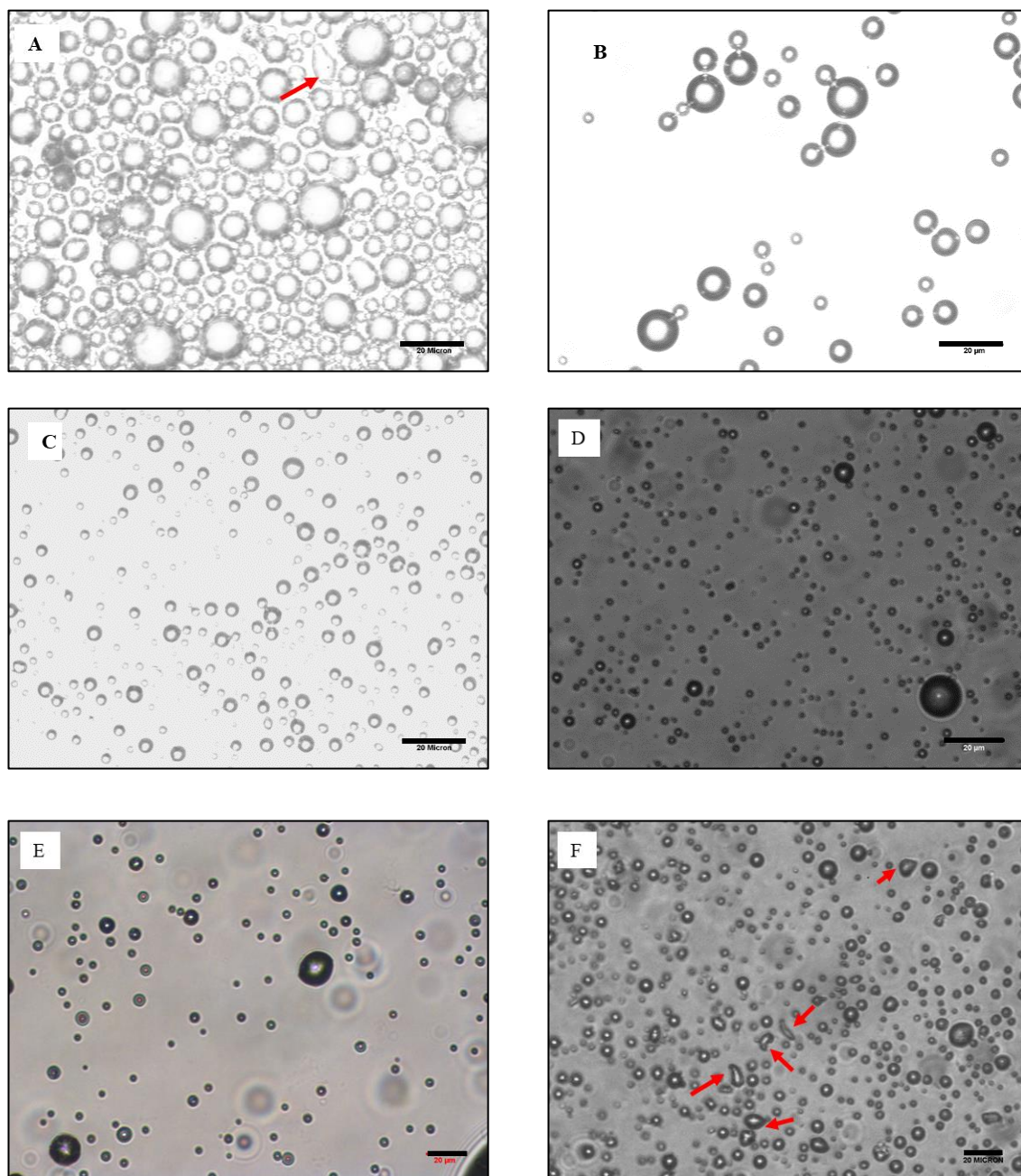


**Figure 3.3:** Representative micrographs of MBs stabilized by different NPs, 24 h after aeration. Scale bar = 20  $\mu\text{m}$ . (A): BCA, Tyloxapol, pH 4 (B): ECA, Tyloxapol, pH 4 (C): BCA, Triton X-100, pH 4, (D): OCA, Tyloxapol, pH 4 (E): BCA, Tyloxapol, pH 2.2 (F): BCA, Tyloxapol, pH 6. Red arrows pointed at the non-spherical MBs

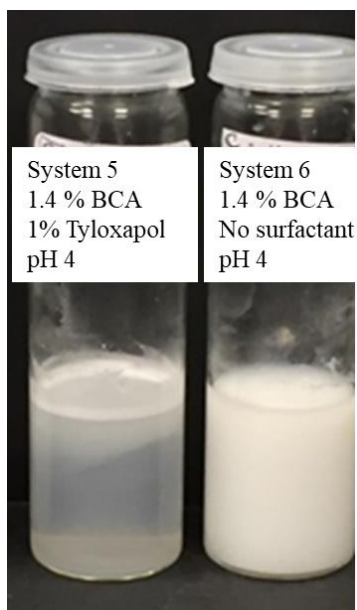


**Figure 3.4:** Shows system 5 and 6, 24 hours after aeration, the turbid layer at the surface of the system 5 represents the MBs creamed.

### 3.3.2 MBs stability

To follow any changes in the size distribution of the MBs and their stability, optical microscopy images of MBs were taken at regular time intervals, typically 1 h, 3 h, 1 day, 3 days, 1 week, 2 weeks, 3 weeks, 4 weeks, 8 weeks and 10 weeks (70 days). At least 5 images were taken and the diameters of at least 250 bubbles were highlighted by placing a circle around them and measuring their diameter via ImageJ for each time interval. Figure 3.5 shows typical micrographs used for such analysis.

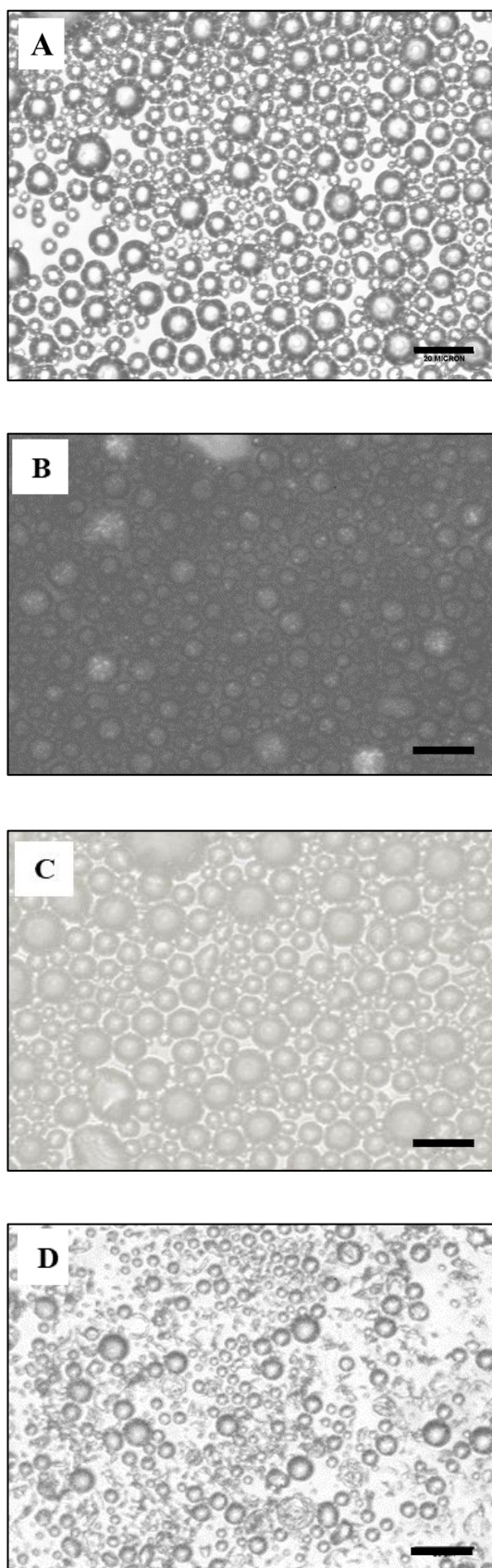


**Figure 3.5:** Micrographs of MBs stabilized by PBCA NPs (made at pH 4, 1wt.% Tyloxapol), (A): 1 hour, (B): 24 hours, (C): 1 week, (D) 70 days. Scale bar =20 $\mu$ m

The histograms of bubble size distributions obtained shown in figure 3.6. The MBs made with BCA in presence of Tyloxapol at pH 4 were stable for the period of this study (70 days), i.e., the size distribution did not change significantly over this time. The Sauter

mean diameter  $(d_{32} = \frac{\sum_{i=1}^n n_i d_i^3}{\sum_{i=1}^n n_i d_i^2})$  was calculated at each time intervals. The  $d_{32}$  at 1

hour was  $5.3 \pm 1.3 \mu\text{m}$  and at time 70 days it was equal to  $4.60 \pm 1.3 \mu\text{m}$ . In the case of MBs stabilized by PECA NPs the MBs were not so stable. The initial  $d_{32}$  was larger ( $8.35 \mu\text{m}$ ) but changed to  $1.25 \mu\text{m}$  in only 24 hours. After this time there were not enough visible bubbles to perform sizes. It is assumed the bubbles continued to shrink and dissolve completely.

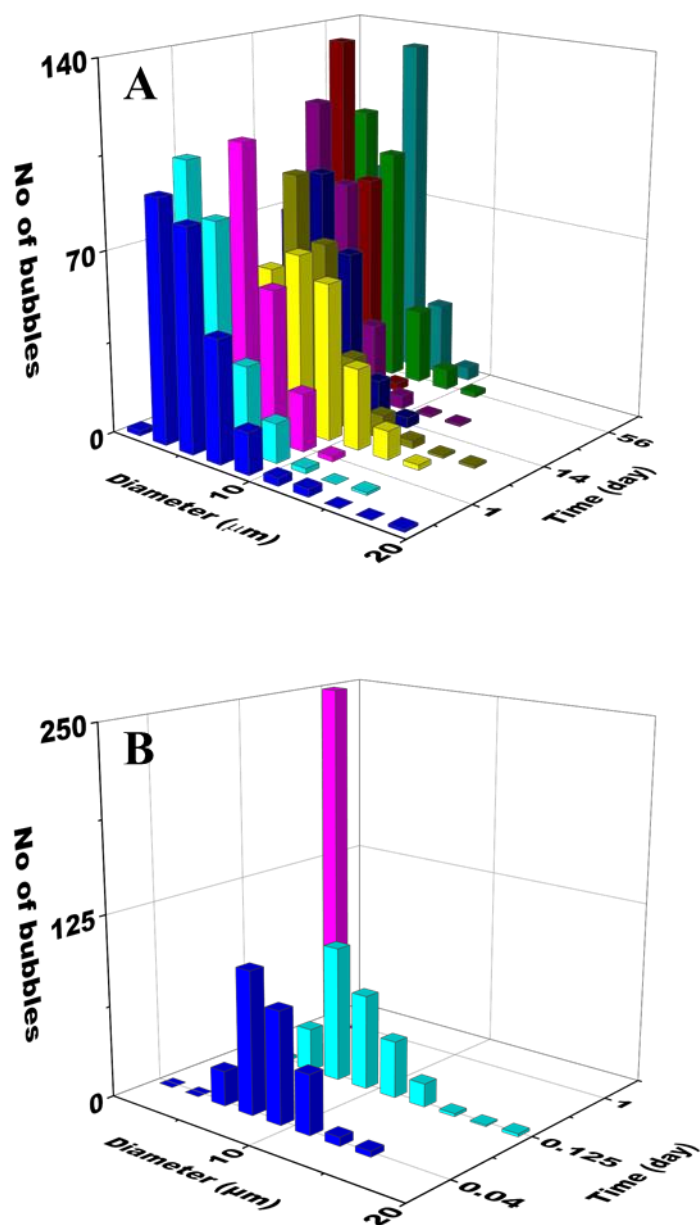


**Figure 3.6:** Histogram of MB size distributions at different storage times stabilized by PBCA (A) and PECA (B) NPs formed with 1wt.% Tyloxapol at pH 4

The volume fraction of MBs formed, stabilized the optimum systems were calculated from the density measurements of the aerated systems, as described in the Methods section. Densities were measured 15 min after each of 3 aerations on the same system, to see if repeated aeration increased the volume fraction of stable MBs, since the MBs formed after one aeration might be (a) stable to subsequent re-shearing or (b) coalesce on re-shearing, releasing NPs back into the aqueous phase to give essentially the same

dispersion as before the first aeration. Samples were also examined from each aerated system 48h after each aeration stage ceased, to examine longer term stability. Figure 3.7 shows the results of these multiple aerations.

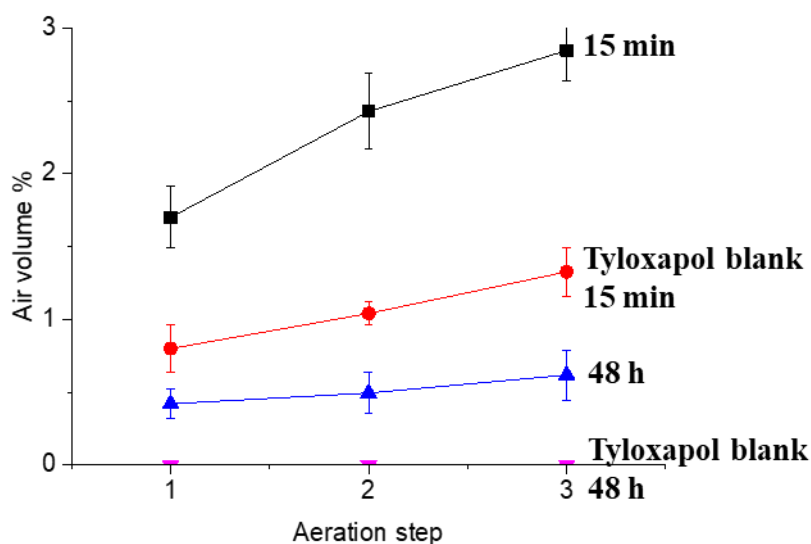
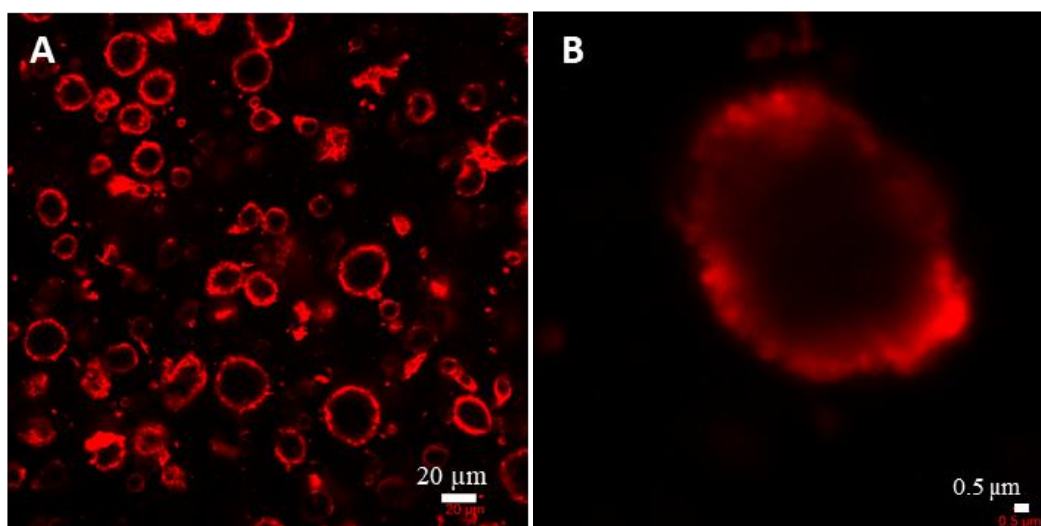


**Figure 3.7:** Volume% of MBs stabilized by PBCA NPs 15 min after aeration (■), and 48 h after aeration (▲), [Tyloxapol blank in 76% glycerol 15 minutes after aeration (●) and 48 hours after aeration (▼)]

The  $d_{32}$  was typically 4 - 5  $\mu\text{m}$ , which is so small that they must be NP-stabilized (i.e., Pickering stabilized) to exist for even a few seconds. The volume fraction of MBs formed was not high, e.g., 1.7 vol.% after the first aeration, but this probably reflects the difficulty (Ettelaie and Murray 2015) of coating bubbles fast enough to stop them shrinking and dissolving and/or coalescing, even under the very high shear rates of the UltraTurrax mixer. Repeating the aeration 15 min after the first aeration did increase the volume fraction further, and further still after the third aeration, reaching almost 3 vol.%. This suggests that a fair proportion of the MBs formed in one aeration can survive subsequent aerations, at least on examining the systems 15 min between aerations, opening up the possibility of producing higher and higher volume fractions of MBs from the same dispersion. We note that Schmidt and Roessling (2006) obtained 10 vol.% in a continuous

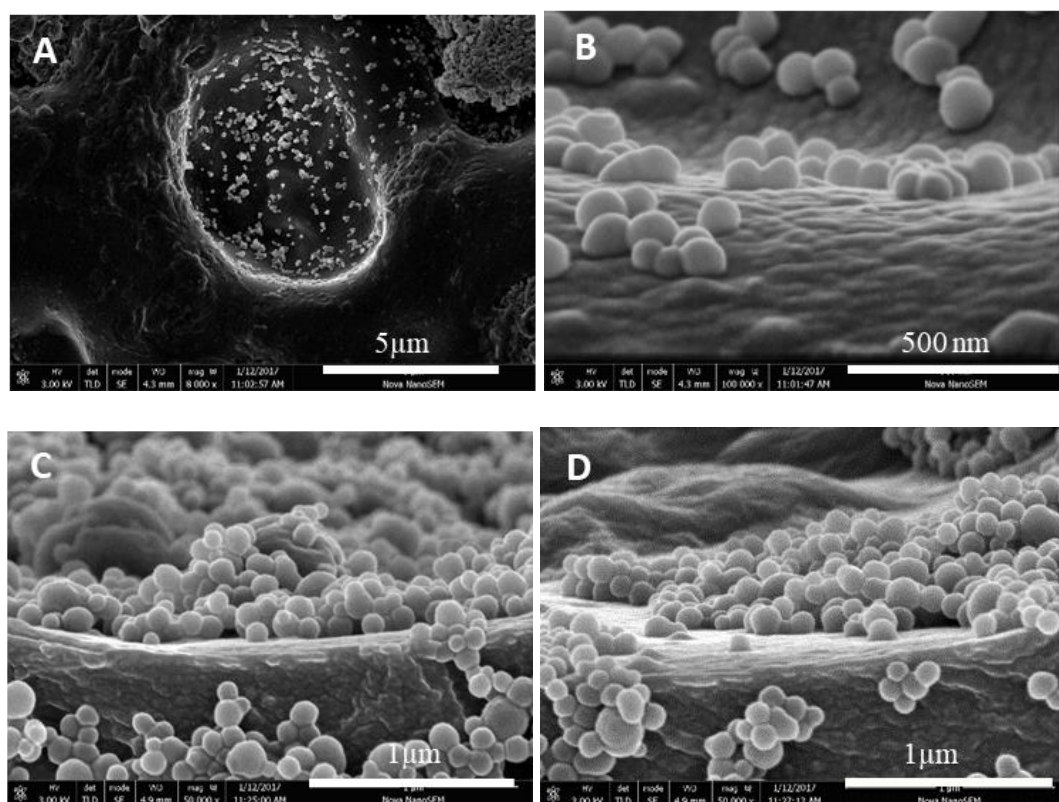
aeration system, but over 3 hours. However, the densities measured 48 h after each aeration all fell back to 0.4 vol.%, suggesting that there is still some shrinkage/dissolution and or coalescence and loss of bubbles over this time-scale. Nevertheless, considering the extreme instability to disproportionation of air bubbles of this size in water, the achievement of several vol.% in 3 steps (in less than 1 h) could be of technological significance and use, particularly if such MBs only need to be stable for a few hours or could be fairly quickly immobilized in a truly solid phase.

In the normal light microscopy images used to size the MBs, such as Figure 3.3, the resolution is obviously not good enough to visualize the NPs at the interface. CLSM was therefore used to confirm the presence of a layer of NPs at the air bubbles surfaces. As explained in the Methods section, the PBCA particles appeared to pick up the hydrophobic fluorescent stain Nile Red, which enabled their imaging. Representative images are shown in Figure 3.8, clearly indicating the presence of PBCA particles mainly at A/W interface, i.e., relatively few in the bulk aqueous phase, although it is still hard to discern whether some of the non-spherical objects are NP aggregates or shrunken air bubbles surrounded by particles. Non-spherical bubbles is a sure sign of Pickering stabilization, the strong driving force for bubble dissolution causing the adsorbed particle layer to crumple under the stress of shrinkage (Bala Subramaniam *et al.* 2005).



**Figure 3.8:** CLSM micrographs of PBCA stabilized MBs

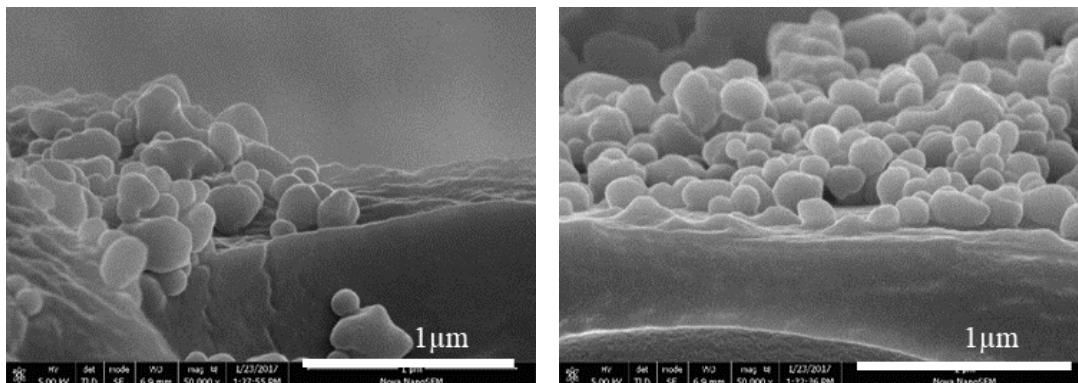
Although the CLSM images are good proof of Pickering stabilizations of the MBs, the resolution is still not high enough to discern individual NPs at the interface. Obtaining such images is difficult but important, because it can confirm the contact angles of particles at the interface and therefore confirm explanations of the different stabilizing properties of the different NP systems. Figure 3.9 shows some representative SEM images of PBCA NPs at the A/W interface of bubbles immobilized and embedded in the resin and imaged as described in the methods section. Not surprisingly, it only seemed possible to obtain images of MBs and NPs in those systems that had reasonably good stability – the preparation steps up to imaging presumably making these other systems less stable. Figure 3.9 shows representative images of PBCA-stabilized MBs at various magnifications and the presence of spherical NPs at the interface is clearly visible. High resolution images of selected regions where the coverage is not so crowded (such as Figure 3.9 (B)) even allowed estimation of the particle contact angle,  $\theta$ . Measurement of up to 20 such particles gave  $\theta = 77 \pm 10^\circ$ .



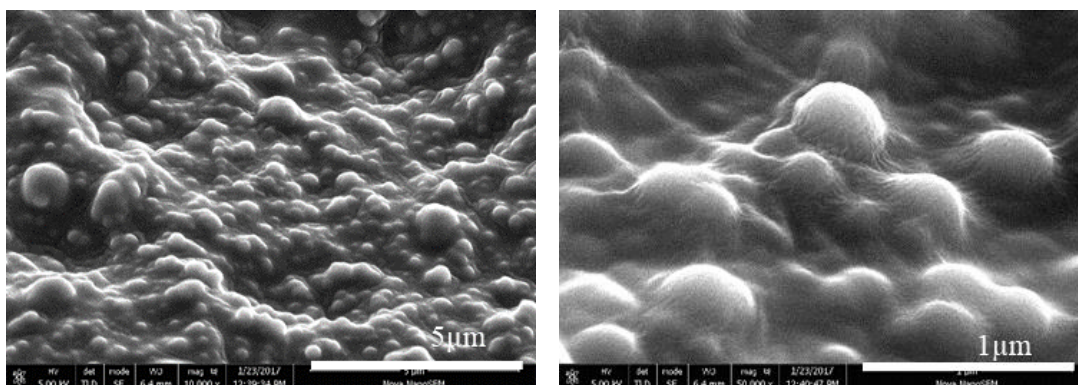
**Figure 3.9:** SEM micrographs of PBCA NPs at the A/W of MBs. In (B), the particle contact angle is measurable.

Figure 3.10 shows SEM micrographs obtained of PECA NPs, that were less effective at stabilizing MBs (see Table 3.1, system 10). The images show that these NPs were much less spherical than the PBCA NPs (Figure 3.9) and also that at the A/W interface they seemed to have aggregated or even merged together. Because of this, it was impossible to measure  $\theta$ . Some of these difference could be due electron beam damage, though care was taken to try and expose the sample to exactly the same imaging conditions. Finally, it was difficult but just possible to obtain some images (Figure 3.11) of the surface of larger bubbles formed on attempting to aerate the PBCA NP dispersion formed in the absence of surfactant. These NPs were very poor MB stabilizers (see Table 1, system 6). Figure 3.11 suggests that the NPs are located somewhat deeper in what was the aqueous phase compared to the PBCA NPs prepared with Tyloxapol (Figure 3.9). This supports

the idea put forward earlier that PBCA NPs formed without surfactant are too hydrophilic to be effective as MB-stabilizers.



**Figure 3.10:** Representative SEM micrograph of PECA NPs at the A/W interface



**Figure 3.11:** Representative SEM micrograph of PBCA NPs formed in absence of surfactant at the A/W interface

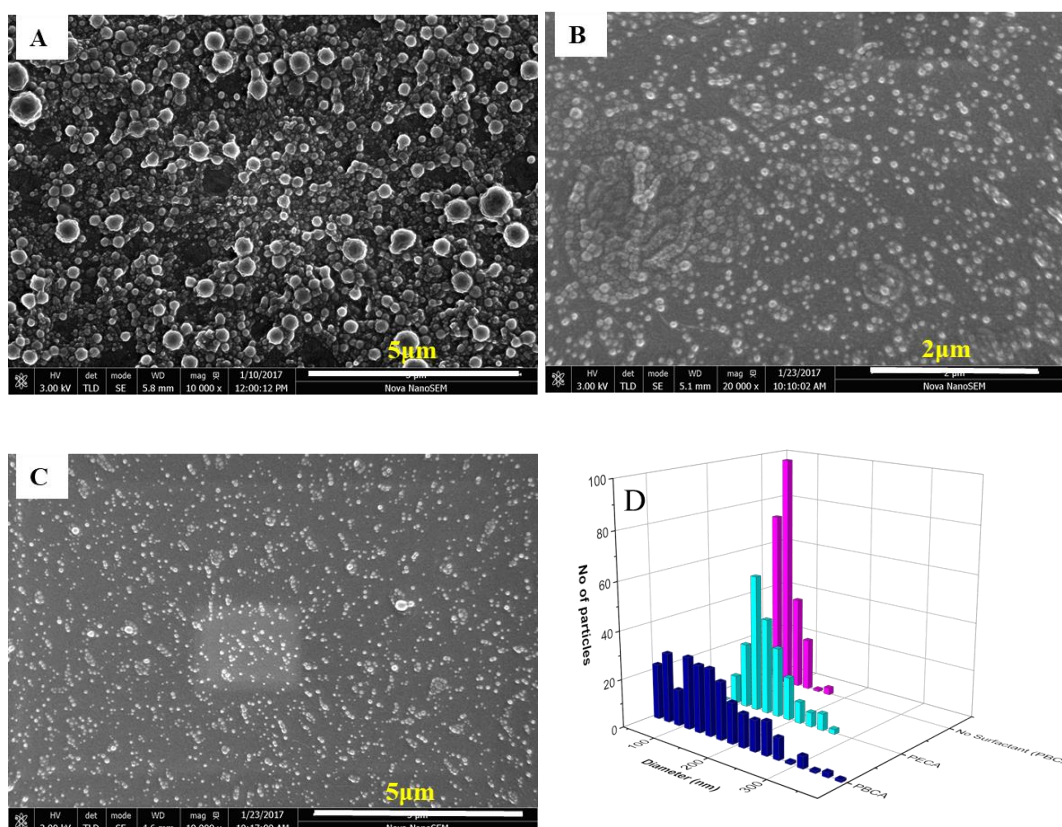


**Figure 3.12:** SEM micrographs of (A): PBCA NPs , (B): PACA NPs and (C): PBCA NPs made in absence of surfactant and (D): nanoparticle size distribution based on SEM images

The size distribution of PBCA , PECA and PBCA made in absence of surfactant were determined using SEM images. At least 250 NPs diameter were measured via ImageJ. figure 3.12 shows some of the SEM images that were used for analysis and the size distribution graph. The results are in excellent agreement with DLS measurement. The PBCA NPs made in presence of 1wt.% Tyloxapol formed, had a wide size distribution compared to the PECA and PBCA made in absence of surfactant. This can possibly explain why it was difficult to remove the particles by centrifuge as some of them are fairly small (e.g. smaller than 50 nm). The  $d_{32}$  of PBCA, PECA and PBCA NPs made in absence of surfactant calculated and was 149.2, 120.2 and 89.4 respectively.

### 3.3.3 Stability of MBs after freeze and thaw cycle

The stability of PBCA stabilized MBs under extreme conditions (freezing temperature) was studied. Three samples of system 5 were frozen in a domestic freezer at  $-18\text{ }^{\circ}\text{C}$  for 22 hours then thawed at room temperature. No visible foam loss observed after the freeze – thaw cycle. The  $d_{32}$  slightly increased from  $5.9 \pm 1.1\text{ }\mu\text{m}$  to  $8.5 \pm 3.3\text{ }\mu\text{m}$ . The increase in  $d_{32}$  value indicates some coalescence may have occurred. Also the microscopy images show that non-spherical microbubbles proportion was slightly increased, that may also contributed to the  $d_{32}$  increase (see Figure 3.13).

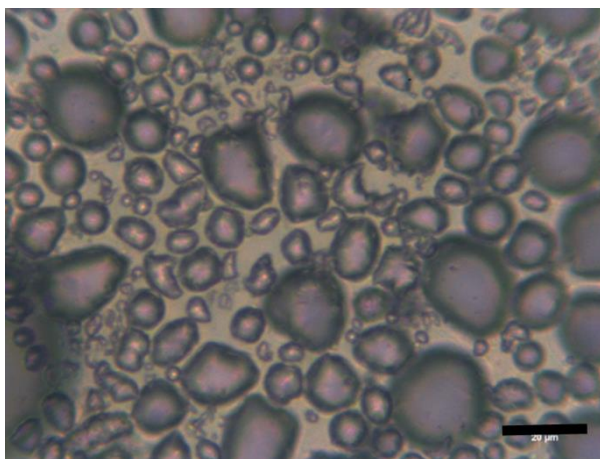


**Figure 3.13:** Micrograph of PBCA stabilized MBs (system 5) after 1 cycle of freeze – thaw

### 3.3.4 Determination of free Tyloxapol in the system

The concentration of free Tyloxapol in the PBCA NPs was measured via absorbance measurements. Tyloxapol has a phenol ring in its structure (Regev and Zana 1999). The highest absorbance of phenol ring is at 270nm (Nemethy and Ray 1973). In order to measure the free Tyloxapol it was necessary to remove all the PBCA NPs from the system since they also adsorb at 270nm. Removing the particles was very challenging. Different techniques including the high speed centrifuge (48000g for 1 hour) and depletion flocculation (chitosan, polyethylenimine and aluminium potassium sulphate) were unable to sediment and remove all the particles. Therefore the NPs were removed by carefully

filtering off the NP particles from the aqueous phase through the 30 kDa Ultracel membrane in the stirred cell, taking care to dilute solutions enough so that surfactant micelles were also not retained by the membrane. The result was that we calculated the free Tyloxapol concentration in the final dispersion to be 0.75 wt.%, i.e., 25% of the Tyloxapol in the system before polymerization either ended up adsorbed to the surface of the NPs and/or was incorporated into the particles on polymerization. Based on the total surface area of a typical NP dispersion of size 160 nm, this equates to a surface load of Tyloxapol of  $10.6 \text{ mg m}^{-2}$ . This is fairly high, considering typical monolayer coverage of surfactants is 2 - 3  $\text{mg m}^{-2}$ . Since addition of Tyloxapol after particle formation does not result in surface active NPs, we conclude that at least a significant amount of this 'lost' surfactant must be incorporated into the particles on polymerization, which somehow imparts the necessary surface hydrophobicity.

### **3.4 Conclusion**

A range of conditions of polymerization of alkyl cyanoacrylates leading to nanoparticles (NPs) potentially capable of stabilizing highly unstable microbubbles (MBs) of air in aqueous solutions were studied. From the results of our experiments, the optimum system seems to be butyl cyanoacrylate (BCA) polymerized into PBCA particles at pH 4 in the presence of 1 wt.% Tyloxapol surfactant. These PBCA particles are highly effective at stabilizing MBs of only a few microns in size for at least 2 months and microscopy over a range of length scales clearly indicates that these particles stabilized via a Pickering mechanism. However, only low volume fractions (ca. 1 vol.%) of MBs can be obtained in simple, single aeration steps in a high shear mixer, reflecting the difficulty of obtaining rapid enough particle coverage of bubbles and or its maintenance even under turbulent conditions.

One of the most significant findings is that only PBCA particles formed (polymerized from BCA) in the presence of Tyloxapol act as MB stabilizers. PBCA particles of similar size and charge but with the same surfactant added afterwards do not work. This leads to speculation that the surfactant itself may have to become incorporated into the surface of the PBCA particles in order to impart to it the correct contact angle/wetting properties at the A/W interface.

Such an effect may partly explain the conflicting results in some of the literature on the effects of different surfactants and polymerization conditions, but also suggests that more work needs to be done to understand the surface nature of such Pickering bubble stabilizers.

## Chapter 4 :

# Controlled Microbubble Production via Bubble Syringe

### 4.1 Introduction

Disproportionation is the main factor that affects the stability of microbubbles, where molecules move from high chemical potential to lower chemical potential regions in the system. In a closed system the movement of gas molecules from small bubbles to large bubbles results in foam coarsening. In an open system disproportionation leads to gas loss via the macroscopic product surface (Ettelaie and Murray 2014).

To stop disproportionation it is necessary to cover the surface of freshly formed bubbles with surface active material that can form an elastic film around the bubble (Meinders, Kloek and van Vliet 2001; Kloek, van Vliet and Meinders 2001). Solid particles are the best way to slow down or completely prevent disproportionation. Closely packed layers of particles at the air – water interface can effectively inhibit disproportionation process (Binks and Horozov 2006; Dickinson *et al.* 2004; Du *et al.* 2003; Binks and Horozov 2005).

Considering the relatively large size of nanoparticles compared to surfactants or even polymeric stabilizers (e.g., proteins) the adsorption of particles to the interface via diffusion is slow whilst disproportionation can be relatively quick when the bubbles are very small ( $< 1 \mu\text{m}$ ). So it is expected that system might undergo disproportionation before it is stabilized by nanoparticles (Ettelaie and Murray 2014).

The right balance between the surface activity of particles versus their tendency to aggregate in the bulk is required to form a stable bubble/ foam. However the presence of more hydrophobic particles in the system increases the likelihood of the particles to flocculate in the bulk and adsorb even more slowly or separate out. Therefore the particle is no longer available to adsorb to the air – water interface. Increasing the hydrophobicity of the particle can even cause phase inversion from air bubble in water to water droplets in air and so called “dry water” (Binks and Murakami 2006).

It is well established that nanoparticles are not good foaming agents even in presence of surface active molecules (Langevin 2008). A study by Hunter and co-workers found that almost 90 % of particles remained in the liquid phase after foam production, and did not participate in foam stabilization (Hunter, Wanless and Jameson 2009).

Pickering stabilized foams / bubbles cannot be made by simply adding air to the particle dispersion. The difficulty of foam stabilization by Pickering particles arises from high energy barrier that prevent particles from being adsorbed to the air water interface. The adsorption energy of a single particle is related to the contact angle  $\theta$  of the particle at the interface, the air – water surface tension  $\gamma_w$ , and the radius of particles  $r$  by

$$W_r = \gamma_w r^2 \pi (1 \pm \cos \theta)^2, \quad (4.1)$$

In which the sign within the brackets corresponds to particle centres above (+) or below (-) the interface. This adsorption barrier seems to be electrostatic in nature. Its existence also explains why generation of stable foams requires high energy techniques, such as

turbulent mixing. Producing stable foams also requires the right type of particles, with appropriate contact angles at the air – water interface (Stocco *et al.* 2011).

As previously mentioned one of the main applications of MBs is in the medical field where MBs are used for controlled drug delivery, ultrasound imaging and many more (Ferrara, Pollard and Borden 2007; Klibanov 2007; Lui, Miyoshi and Nakamura 2006). Therefore controlling the size of MBs as well as their size distribution is very critical. Furthermore creating a monodispersed MBs dispersion is important for fundamental studies, because it is easier to follow size changes and interpret the data. In addition the Laplace pressure is less important in a monodisperse system and Ostwald ripening can be significantly reduced in such a monodisperse system (Xu *et al.* 2006; Yasuno *et al.* 2004).

Sonication (Unger *et al.* 1998; Zhao *et al.* 2005) and mechanical agitation are the most widely used techniques to generate microbubbles (Fokong *et al.* 2011; Xu *et al.* 2008). However both techniques produce highly polydisperse bubble size distribution. Co-axial electro hydrodynamic atomisation is a relatively new technique for microbubble production (Farook *et al.* 2007) and has applications when multilayer coating of bubbles is required (Ahmad *et al.* 2008). Microfluidic devices can also be used to create a monodisperse microbubbles (Whitesides 2006). One major disadvantage of this technique is that the microfluidic devices operate under a narrow range of flow rate and pressure (Stride and Edirisinghe 2008).

In chapter 3 the impact of polymerization condition such as monomer type pH and surfactant type on PACA NP formation was investigated. In addition Ultraturrax was used to produce Pickering stabilized MBs. The size distribution and MB stability was also studied. PBCA monomer polymerized in presence of 1 wt. % Tyloxapol at pH 4, produced NPs with ability to stabilize fine MBs (radius  $\approx 5 \mu\text{m}$ ) for at least 10 weeks. Since the

results indicated that PBCA NPs are very promising in long term stability of MBs, the next step was to produce MBs in a more controlled way in order to be able to study the system more detailed.

In this work we have used a special needle to inject bubbles to the system in a more controlled conditions to allow comparison of experimental data with a mathematical model (Ettelaie and Murray 2014) to investigate how particle size versus initial bubble size, plus dynamics of particle adsorption versus bubble shrinkage, affect the final stable bubble size distribution.

## **4.2 Materials and methods**

### **4.2.1 Materials**

The same material was used in this chapter as already described in chapter 3. Potassium chloride (KCl) BioXtra,  $\geq 99.0\%$  purchased from Sigma – Aldrich.

### **4.2.2 Methods**

#### **4.2.2.1 PBCA NPs formation**

PBCA were made as described in chapter 2 (1.4 wt.% BCA monomer in aqueous solution of 1 wt.% Tyloxapol at pH 4). The yield of particles formation from monomer was equal to  $50 \pm 3\%$ . This PBCA NP dispersion is referred to as standard dispersion throughout this chapter. To be able to increase the concentration of PBCA NPs in a system the standard dispersion was centrifuged at 3000 g for 1 hour. Then the required amount of sedimented NPs were added to another standard dispersion to reach the desired concentration. This kept the concentration of Tyloxapol constant. The dispersion was then stirred well via a spatula followed by 1 minute sonication in a Kerry Ultrasonic Bath (Hitchin, UK) of 1 litre capacity at 60 Hz, to insure that the particles are well dispersed and not clogged together. To prepare a dilute system the standard dispersion was diluted with 1wt % Tyloxapol solution in water prior to aeration. To separate the larger particles from smaller ones a standard dispersion was centrifuged for 30 minutes at 500 g.

#### **4.2.2.2 MBs generation**

A special “bubble syringe” was used to inject the initial MBs into the PBCA NPs dispersion. The bubble syringe consists of a stainless steel capillary tube that has a stainless steel rod tightly fitted inside it. The rod diameter is just slightly smaller than the inner diameter of the tube (see Table 4.1). The bubble syringe was connected to a stainless steel piston. The piston was driven by a stepper motor and PDX13 stepper drive (Parker Hannifan Corp., CA) controlled via a PC. As the piston was moved the pressure increased

which led to formation of a stream of small bubbles at the tip of the bubble syringe. Two different bubble syringes were used to produce two different size of bubbles:  $553 \pm 3$  and  $386 \pm 5 \mu\text{m}$  for larger and smaller syringe respectively. It is not quite clear why the bubble syringe produces a monodisperse stream of bubbles of sizes smaller than the tube itself.

The initial size of the bubbles was measured by using bubble apparatus with a fitted Hitachi KP-MIE/K CCD camera connected to a microscope. The apparatus consists of an observation chamber with two optically polished glass windows fitted at both top and bottom. The upper window is used to fill the chamber with experimental sample and to clean the chamber. It is easily removed and can be quickly sealed at air pressure. The bottom window is connected to a Schott KL 1500 cold light source via a fibre optic cable which illuminates the system allowing clear images to be taken. The images were recorded via a Perception Digital Recorder (PVR) system and associated software (Digital Processing System INC., Faenham, UK) connected to the CCD camera. The images were captured at an appropriate time-lapse rate (typically 50 frame per minute). Bubble syringes, piston and bubble apparatus were designed and built by Mr P.V. Nelson in the workshop at the School of Food Science and Nutrition at the University of Leeds (Dickinson *et al.* 2002).

Figure 4.1 shows a schematic diagram of bubble syringe and the bubbles produced via the large bubble syringe. The bubbles were produced by inserting the syringe bubble into the solution of 1 wt.% Tyloxapol solution in deionized water.

Syringe	Length (mm)	External diameter (mm)	Internal diameter (mm)	Bubble size ( $\mu\text{m}$ )
Large	120	1.84	1.19	$553 \pm 3$
Small	114	0.79	0.43	$386 \pm 5$

**Table 4.1:** Shows the dimension and bubble size produced by each bubble syringe

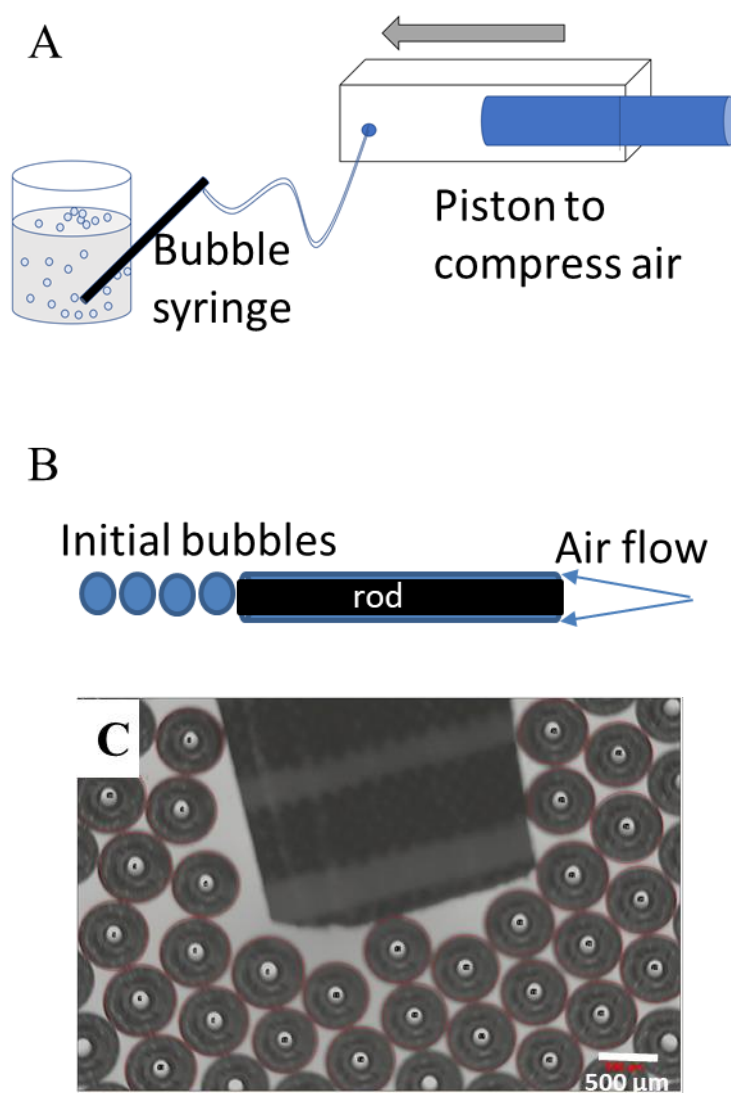


**Figure 4.1:** Schematic of (A): aeration by piston and bubble syringe and (B): bubble syringe, the air flows between wire and tube wall and comes out in a form of small monodispersed bubbles, (C): micrograph of initial bubbles

To aerate the system 100 ml of PBCA dispersion at the required concentration were transferred into a 500 ml beaker and aerated for 2 hours using the bubble syringe connected to the piston. During aeration the dispersion was under mild stirring (via a magnetic stirrer plate) to insure uniform distribution of bubbles and particles. After the aeration period was over, the aerated dispersion was covered by Parafilm and left for 24

hours. After 24 hours the dense creamy foam layer at the top was transferred into thin glass tubes (10 mm inner diameter, 100 mm height) and covered with a tightly fitting cap. The foam height was measured using a caliper. The remaining PBCA dispersion was aerated again as before and the foam generated after each cycle of aeration was kept in a new clean glass tube. The cycles of aeration were continued until no or very little foam (less than 1 mm height) was formed after the last cycle of aeration.

### **4.2.3 PBCA NPs size and $\zeta$ -potential**

Size and  $\zeta$ - potential of the particle dispersion were measured as described in 3.2.4.

### **4.2.4 Microscopy**

Microscopy images of microbubbles was carried out as described in 3.2.3.

### **4.2.5 Static light scattering**

Because the above system generated a much greater quantity of MBs it become possible to size them via light scattering. MBs sizes were measured using static light scattering technique via Malvern Mastersizer 3000 (Malvern Instruments, UK). Samples of MBs dispersions were added to distilled water in the instrument dispersion cell, Hydro EV, until laser obscuration of 1 – 3 % achieved. The size was measured using 1.33 as aqueous refractive index and 1 as the air refractive index. The absorbance value of air was set to 0.001. All the measurements were conducted at room temperature.

Static light scattering is an optical technique in physical chemistry that measures the intensity of the scattered light to obtain information on the scattering source. Typical application is to determine the molecular weight ( $M_w$ ) of a macromolecule such as proteins or polymers. Static light scattering is also widely used to determine the particle/ bubble/ droplet size. The mathematical relationship between the scattering pattern and the particle size is not simple and rather complex. Mie developed a theory that can be used to interpret the scattering patterns of dilute dispersions of any size (Wolfram and

Wriedt 2012). The Mie theory is relatively complicated, however using advanced computers makes it easy to use. The Mie theory gives excellent agreement with experimental measurements, and is used by most commercial particle sizing instruments. The Mie theory assumes that the light waves are only scattered by a single particle, and so it is only strictly applicable to dilute dispersions. In more concentrated dispersions, a light beam scattered by one droplet may subsequently interact with another droplet, and this alters the scattering pattern (McClements 2016).

The sample is diluted to avoid multiple scattering and placed in a transparent measurement cell. A light beam generated by a laser is directed to the measurement cell where it is scattered by droplets/ particles. The intensity of the scattered light is measured as a function of scattering angle using an array of photosensitive detectors located around the sample or by using a single photosensitive detector that can be moved around the sample. The scattering intensities of multiple angles are produced by a computer. Generally, the scattering angle is inversely related to the particle size, so that the scattering pattern of a sample contains information about the particle size distribution. This calculation requires knowledge of the (complex) refractive index of both the particles and dispersion medium at the wavelength of the laser used, which has to be entered by the user. Sometimes this information is not readily available in literature (McClements 2016).

## **4.3 Results and discussion**

### **4.3.1 Large bubble syringe**

#### **4.3.1.1 Multiple aeration**

The graph in Figure 4.2 shows that MBs produced with this technique were fairly stable from aeration to aeration and had a relatively narrow size distribution. Moreover it is clear that bubbles were very much smaller than these injected (553  $\mu\text{m}$ ) so that they had to

shrunk to around 10  $\mu\text{m}$  or less before being stabilized by PBCA NPs. In addition the foam height had a reverse relationship with cycle of aeration, and foam height decreasing after each aeration step. The foam height values are reported in Table 4.2. After four aeration cycles no stable foam was produced. To confirm no stable foam could be formed the remaining PBCA dispersion was aerated by the previous technique. The dispersion was aerated via the Ultraturrax T 25 (IKA Werke) as described earlier in previous chapter. After 24 hours no visible foam remained on top of the dispersion. The micrograph (Figure 4.3) shows the aerated dispersion after 24 hours. There were only few bubbles visible under light microscope.

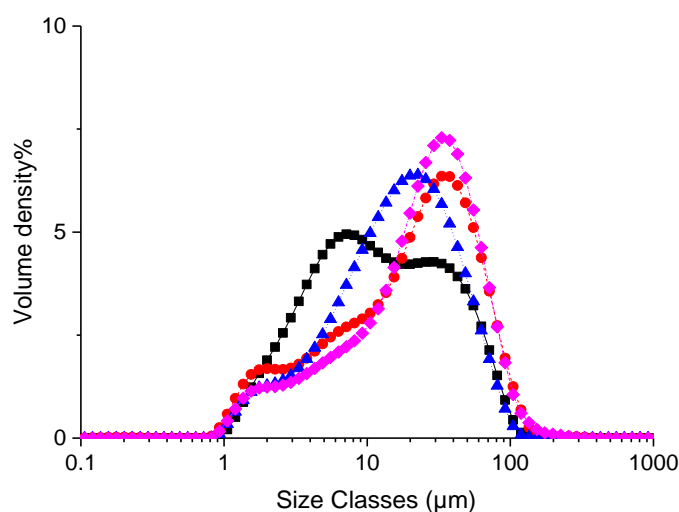


**Figure 4.2:** Size distribution of MBs produced from standard PBCA dispersion. 1<sup>st</sup> foam (■), 2<sup>nd</sup> foam (●), 3<sup>rd</sup> foam (▲), 4<sup>th</sup> foam (◆)

PBCA concentration / wt%	Foam height (mm)			
	1 <sup>st</sup> foam	2 <sup>nd</sup> foam	3 <sup>rd</sup> foam	4 <sup>th</sup> foam
0.7 (Standard)	10	8	3.5	$\leq 2$
0.15	3	2.5	$\leq 2$	No stable foam
1	25	11	5	$\leq 3$
2	42	30	21	10

**Table 4.2:** Foam heights of different PBCA concentration

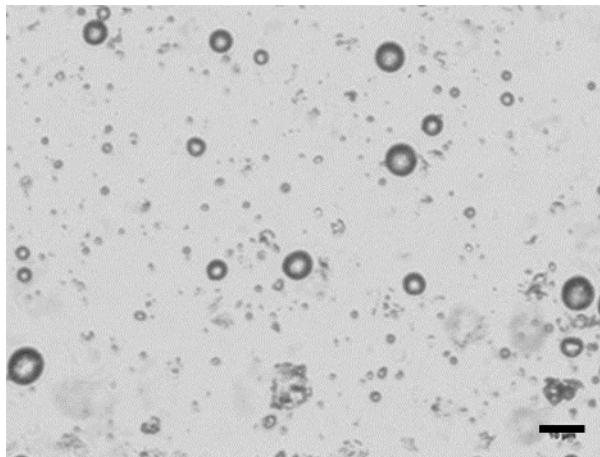


**Figure 4.3:** Micrograph of MBs aerated by Ultraturrax after 4 cycle aeration by cylinder, scale bar = 10  $\mu\text{m}$

The reason for the decreasing in MBs formed at repeated aeration could be that most of the stabilizing particles had been consumed in stabilizing the MBs already formed. However our calculations shows that less than 6 % of nanoparticles in the dispersion would have been adsorbed to the interface after 1st aeration. assuming a surface coverage,  $\alpha$ , of 50 %.

In order to calculate the particle adsorption one needs to know the following: The average

radius of the MBs is  $r_b$ . The volume of one MB,  $v_b$  equals  $\frac{4}{3}\pi r_b^3$  and the surface area

of one bubble,  $SA_b$ , equals  $4\pi r_b^2$ . The total number of MBs,  $N_b$ , in the 1<sup>st</sup> foam is  $\frac{v_{foam}}{v_b}$

.The area of one PBCA NP in contact with the bubble,  $A_p$ , is  $\pi r_p^2$  where  $r_p$  is the radius

of PBCA NP. The number of PBCA NPs in the dispersion,  $N_{p,total}$ , is  $\frac{v_{dispersion} c_p}{\rho \frac{4}{3}\pi r_p^3}$ . Where

$v_{dispersion}$  is the volume of dispersion,  $c_p$  denotes the concentration of NPs.  $\rho$  denotes the

density of particles. Number of particles required to cover the surface of all MBs in the

first foam,  $N_{p,1^{st} foam} = \frac{SA_b \alpha N_b}{A_p}$ . The number % of free particles,  $N_{p.free} \% =$

$$\frac{(N_{p,total} - N_{p,1^{st} foam}) \times 100}{N_{p,1^{st} foam}}. \text{ With } r_b = 3.6 \times 10^{-6} \text{ m, } r_p = 8 \times 10^{-8} \text{ m, } c_p = 0.7 \text{ kg m}^{-3},$$

$v_{dispersion} = 1 \times 10^{-6} \text{ m}^3$  and  $\rho = 1150 \text{ kg m}^{-3}$  then  $N_{p.free} \%$  equals 94 %.

CLSM was used to confirm that MBs were presented and stabilized by the PBCA NPs.

Figure 4.4 shows the structure of MBs with fluorescent dyed NPs at the air- water interface. Non- spherical shape of some of the MBs was a confirmation of Pickering stabilized bubbles (Bala Subramaniam *et al.* 2005).

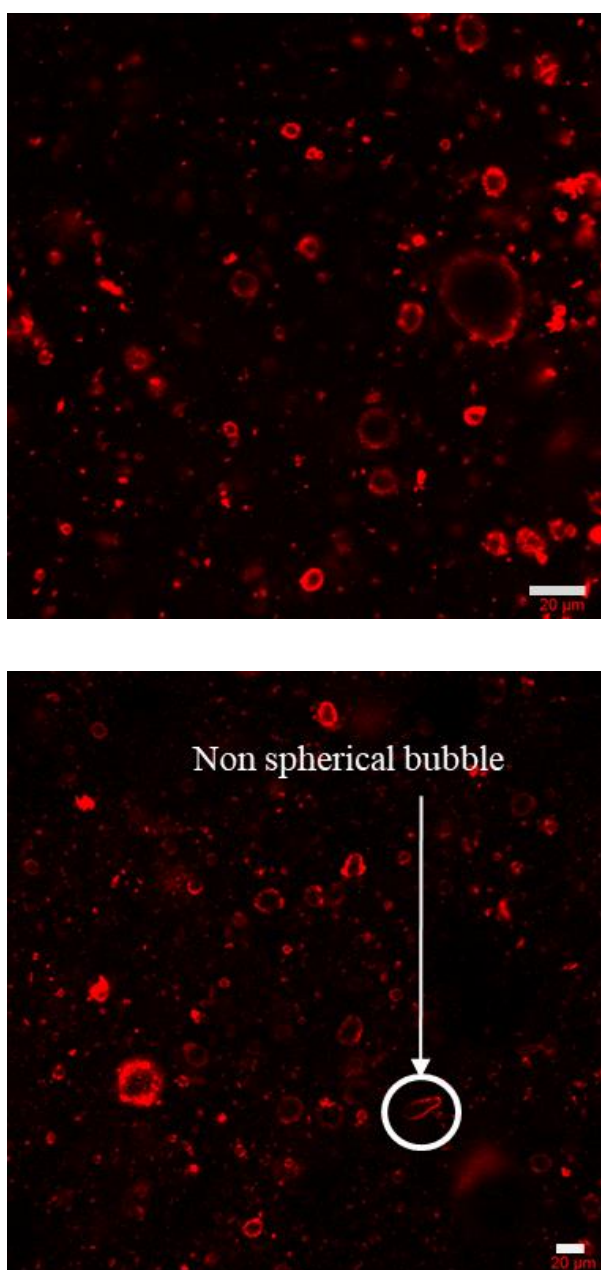


**Figure 4.4:** CLSM micrograph of PBCA stabilized MBs, taken from 3<sup>rd</sup> aeration, diluted in glycerol (ratio 1:20).scale bar = 20 μm

#### 4.3.1.2 Impact of particle concentration on MBs

The production of microbubbles via the cylinder and bubble syringe was very reproducible and therefore allowed us to study the effect of various factors such as NP concentration on MBs stabilization. under different conditions. This is important because potentially it allows us to test the theoretical model on bubble shrinkage versus particle

adsorption with time. Two higher concentrations of PBCA NPs were studied: 1 and 2 wt.% PBCA NPs while the concentration of the surfactant remained constant.

Increasing the concentration of PBCA NPs in the dispersion prior to aeration had a positive effect on foam production, increasing the foam height (see Table 4.2). The foam height increased from 10 mm for standard (0.7 wt.%) to 25 mm and 42 mm respectively. The MBs size distribution graph (Figure 4.5) shows that increasing the concentration of PBCA NPs had a direct effect on MBs size. The MBs produced at higher concentration of PBCA NPs had a relatively larger sizes ( $d_{32}$  were 7.4, 10.4 and 50.7 for standard, 1 and 2 wt% respectively).

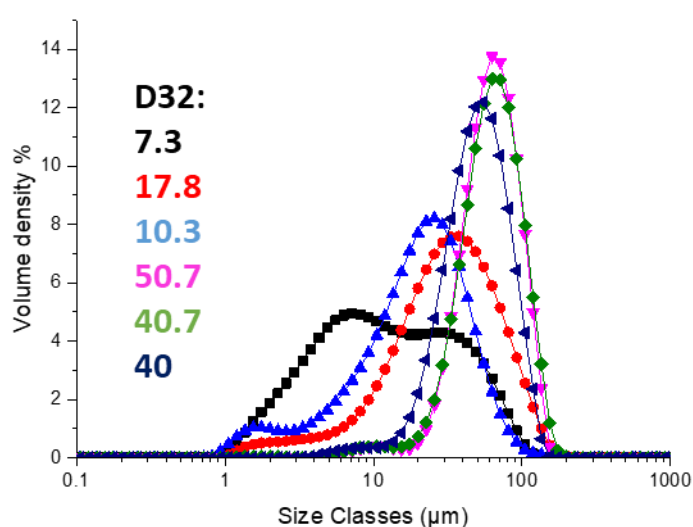


**Figure 4.5:** Comparison of size distribution of 1<sup>st</sup> foam produced at different concentration of PBCA NP. PBCA standard (■), 0.15 % PBCA (●), 1 % PBCA (▲), 2% PBCA (▼), Centrifuged and redispersed in its supernatant again (◆) and supernatant only (◄).

The significant increase in  $d_{32}$  when 2 wt.% NP was used is qualitatively explained by the greater availability of particles, providing sufficient surface coverage to stabilize the MBs at a larger size, i.e. before they had shrunk further. However a further consideration is that the centrifuged sediment added to create the higher concentration may have contained larger NPs that led to quicker stabilization so less time was required to stabilize

bubbles and therefore less shrinkage occurred. A third possibility is that large particles could only stabilize larger bubbles as illustrated in Figure 4.6.

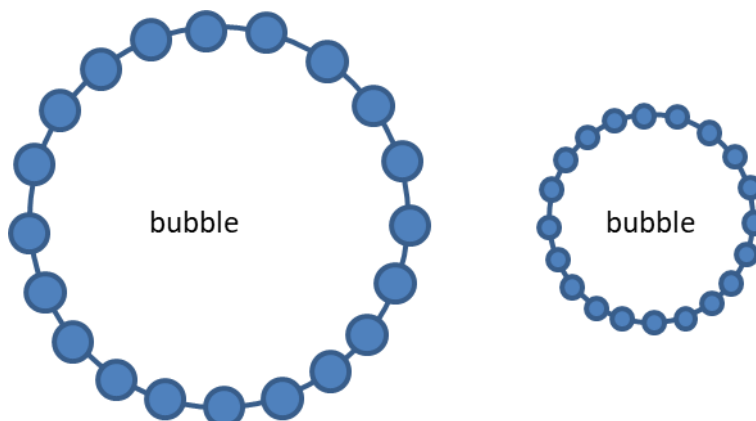


**Figure 4.6:** Schematic of impact of particle size on MB size, both bubbles have the same % particle coverage

Another way to increase the concentration of PBCA NPs in the dispersion was to slowly evaporate the water. This was done at room temperature or at 40° C. Interestingly no stable foam was produced via this technique, suggesting that the corresponding increase in Tyloxapol concentration was detrimental to NP adsorption and MB stabilization. As the ratio of surfactant to NPs increases the former will dominate the interface, i.e. frustrating Pickering stabilization.

Lowering the concentration of PBCA NPs prior to aeration had a negative impact on foam height (see Table 4.2). The foam height after first cycle of aeration was only 3 mm compared to the aerated standard PBCA which produced 10 mm. The  $d_{32}$  of the MBs were larger than expected ( $d_{32} = 17.5 \mu\text{m}$ ). The larger bubbles might have formed after inadequate initial stabilization of smaller bubbles, which then coalesced before sufficient NP coverage reached. Further investigation is required to confirm this.

#### 4.3.1.3 Effect of ionic strength

The effect of increasing the ionic strength on MBs production was studied to see how varying electrostatic repulsion between NPs and MBs might affect final MB. The ionic

strength of the standard PBCA dispersion was increased by adding KCl to give 0.01, 0.1 and 1 M KCl. The NP size and  $\zeta$ - potential of PBCA dispersion were measured before and after addition of KCl. Particle size did not change after addition of KCl and the average particle size was equal to  $120 \pm 5$  nm while polydispersity value was  $\leq 0.2$ . (Adding KCl also did not have any impact on the pH of the PBCA solution (pH 4).) However addition of KCl significantly changed the  $\zeta$ - potential of NPs. The  $\zeta$ - potential significantly reduced, potentially making the NPs more hydrophobic (The  $\zeta$ - potential shifted from  $-22$  mV to  $-4$  and  $-2$  mV after addition of 0.1 and 1 M KCl respectively, whereas addition of 0.01 M KCl had no effect on the  $\zeta$ - potential.).

After aeration MB size and foam height were measured (Figure 4.7 and Table 4.3). The 0.01 M KCl had no impact on the size distribution or foam height and the results were similar to aerated standard PBCA dispersion. Increasing the concentration of KCl to 0.1 M increased the foam height very significantly. The foam height after first aeration was almost doubled ( $19 \pm 2$  mm) compared to aerated standard PBCA (10 mm). The  $d_{32}$  was decreased from  $10 \mu\text{m}$  after first aeration to  $5.5 \mu\text{m}$  after last aeration. Addition of 1 M KCl to the PBCA dispersion prior to aeration led to extremely high foam production at least 9 times greater than the standard system. The MBs sizes were also considerably smaller than MBs produced from standard PBCA; the  $d_{32}$  of the first foam was  $5.1 \mu\text{m}$  and decreased to around  $3.8 \mu\text{m}$  after the fourth aeration.

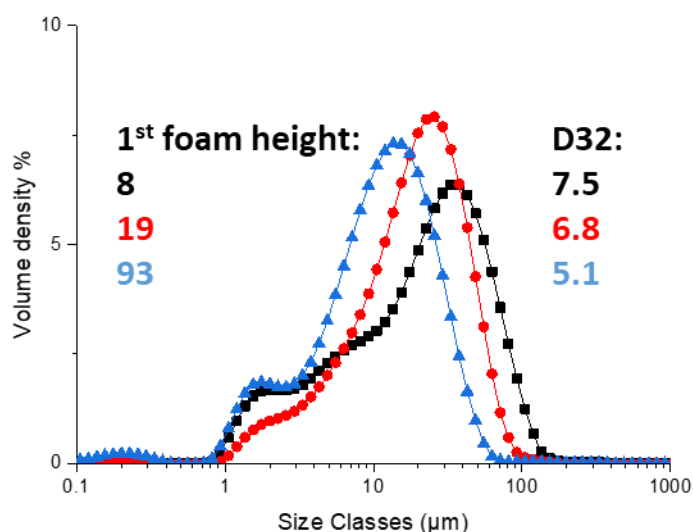


**Figure 4.7:** Shows the size distribution of aerated PBCA containing 0.01 M KCl (■), 0.1 M KCl (●) and 1 M KCl (▲). Foam height and  $d_{32}$  are also illustrated

KCl concentration (M)	Foam height (mm)			
	1 <sup>st</sup> foam	2 <sup>nd</sup> foam	3 <sup>rd</sup> foam	4 <sup>th</sup> foam
0.01	8 ± 1	7 ± 2	4 ± 1	≤ 2
0.1	19 ± 2	18 ± 0.5	10 ± 2	≤ 2
1	93 ± 3	27 ± 3	10 ± 2	≤ 3

**Table 4.3:** Shows the foam height of PBCA stabilized MBs in presence of different concentration of KCl

Binks and co-worker also reported addition of salt to a mixture of air, water and silica NPs led to formation of smaller bubbles (Binks, Duncumb and Murakami 2007). Increasing ionic strength has also been shown to have a positive effect on contact angle of adsorbed silica particles at the air – water interface via changing the surface chemistry of particles (increase the hydrophobicity) that increased the rate of absorption at the interface (Kostakis, Ettelaie and Murray 2006; Binks, Duncumb and Murakami 2007). Simovic and Prestidge also reported that adsorption of fumed silica particles was

increased when the ionic strength increased ( $10^{-1}$  M NaCl) and formed a more closed pack layer at the adsorption plateau (2003).

The interesting thing is that by 0.1 M there is hardly any repulsion left, so increasing it to 1 M should not make much difference, unless extremely strong range repulsions is important. This indeed might aid NPs packing at the surface.

So far no technique exists for measuring the contact angle at liquid interfaces. The only way to measure the contact angle of NPs was to solidify the air dispersion as described in chapter 3. SEM images (Figure **4.8**) of PBCA NP in 1 M KCl could not provide exclusive information on contact angle of the NPs at the air – water interface.

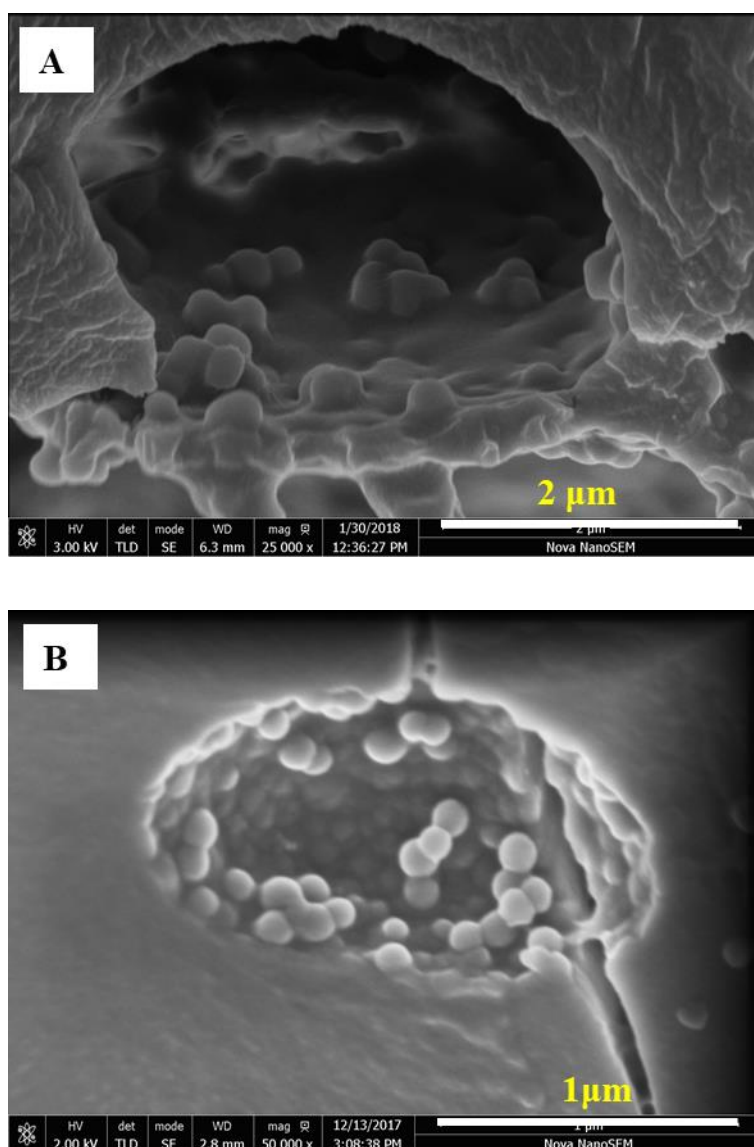


**Figure 4.8:** SEM micrographs of (A): PBCA stabilized microbubble produced during 4<sup>th</sup> cycle of aeration (B): PBCA stabilized microbubble in presence of 1M KCl produced during 1<sup>st</sup> cycle of aeration

#### 4.3.1.4 Effect of particle fractionation

The impact of low speed centrifugation of the PBCA NPs on microbubble formation was studied in detail to see if there were certain size fractions that were more important to the Pickering stabilization than others. Of the total NPs 67, wt %  $\pm$  2 was sedimented to the bottom of centrifuge tubes after 30 mins at 500 g. The supernatant (containing smaller NPs) and sediment (containing larger NPs) were then separated carefully. The sedimented NPs were re-dispersed in 1 wt.% Tyloxapol solution (or 0.2, 0.4, 0.6 and 0.8 wt.%)

Tyloxapol). After the NPs size measurement the dispersions were aerated for 2 hours with the bubble syringe, etc., as described above.

It was observed that the NP size of supernatant was only 24 nm smaller than the standard dispersion (136 and 160 nm respectively). However on average the sedimented particles were at least 3 times larger (471 nm) than the standard dispersion NPs. Table 4.4 gives the particle size and  $\zeta$ - potential of different fractions.

	Standard PBCA	Supernatant	Sediment
Size / nm	160	136	471
$\zeta$ - potential / mV	- 24.2 $\pm$ 1	- 22.8 $\pm$ 1	- 34.7 $\pm$ 2

**Table 4.4:** PBCA NPs size and  $\zeta$  – potential before and after centrifuge at 500 g

The  $\zeta$ - potential of NPs in the supernatant was very close to that of standard PBCA dispersion (– 22.8 and – 24.2 respectively). In contrast for the NPs in the sediment  $\zeta$ - potential was more negative at – 34.7 mV. Thus the degree of hydrophobicity of the sedimented NPs is expected to be lower, also suggesting hydrophobicity depends on particle size. It is not clear why this should be the case but what is obvious is that NPs with this sort of  $\zeta$ - potentials were unable to stabilize bubbles as seen in Table 4.5 where the foam height produced are shown.

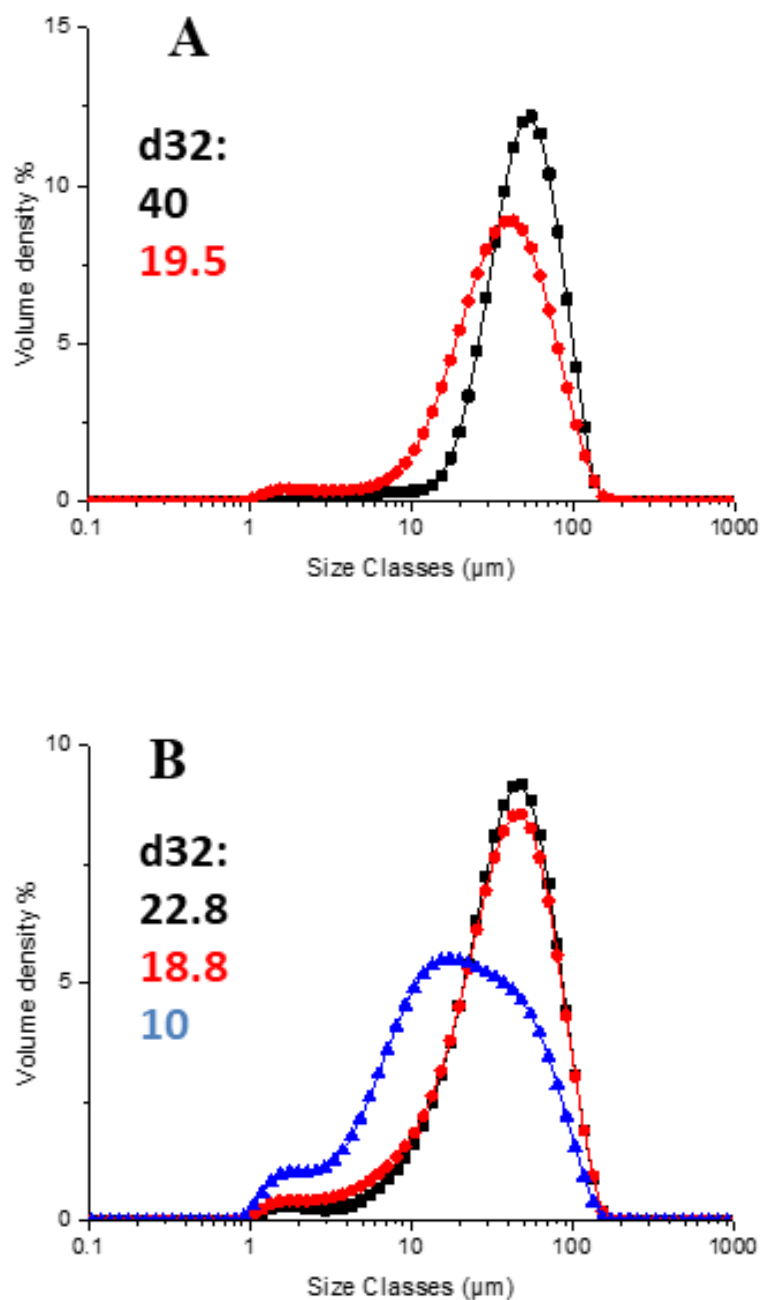
Aerating the sediment particles (at 3000 g, 1 hour) after re-dispersing in its own supernatant produced a stable foam, although the produced MBs were larger than the standard PBCA dispersion (see Figure 4.5). On the contrary if the sediment was re-dispersed in the aqueous solution of Tyloxapol at pH 4, containing different concentration of Tyloxapol (0.2 -1 wt.% Tyloxapol) no stable foam was produced. Aeration of supernatant i.e. smaller NPs with less negative  $\zeta$ - potential (Table 4.4) produced a 12 mm

stable foam after first aeration. The earlier results (section 4.3.1.2) on the evaporation of the standard dispersion clearly suggested that the ratio of surfactant concentration to NP concentration was important.

Centrifuge speed (g)	Dispersion used	Foam height (mm)			
		1 <sup>st</sup> foam	2 <sup>nd</sup> foam	3 <sup>rd</sup> foam	4 <sup>th</sup> foam
3000	Sediment re-dispersed in its own supernatant	7	Not measured	Not measured	Not measured
500	Sediment re-dispersed in water with different concentration of Tyloxapol (0.2 – 1 wt.% Tyloxapol)	No stable foam	No stable foam	No stable foam	No stable foam
500	Supernatant only	12	6	4	≤ 2

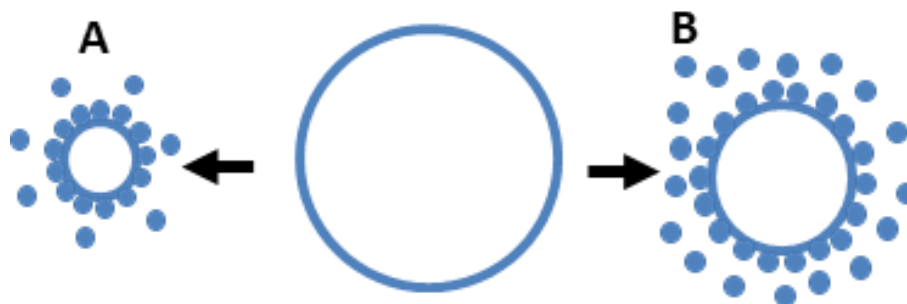
**Table 4.5:** Shows foam heights of centrifuged PBCA dispersions

Figure 4.8 shows the impact of NP fractionation on the final MB size distribution with or without added 1 M KCl. The PBCA dispersions were centrifuged at 500 g and the supernatant aerated in presence or absence of 1 M KCl. It was observed that with increasing the cycle of aeration the MB size distribution was shifted to the left corresponded to a lower sizes. Foam height and  $d_{32}$  had a direct positive correlation, a reduction in foam height corresponded to a reduction in  $d_{32}$  and vice versa. The  $d_{32}$  of the supernatant plus 1M KCl after 1<sup>st</sup>, 2<sup>nd</sup> and 3<sup>rd</sup> aeration was 22.2, 18.8 and 10  $\mu\text{m}$  respectively.



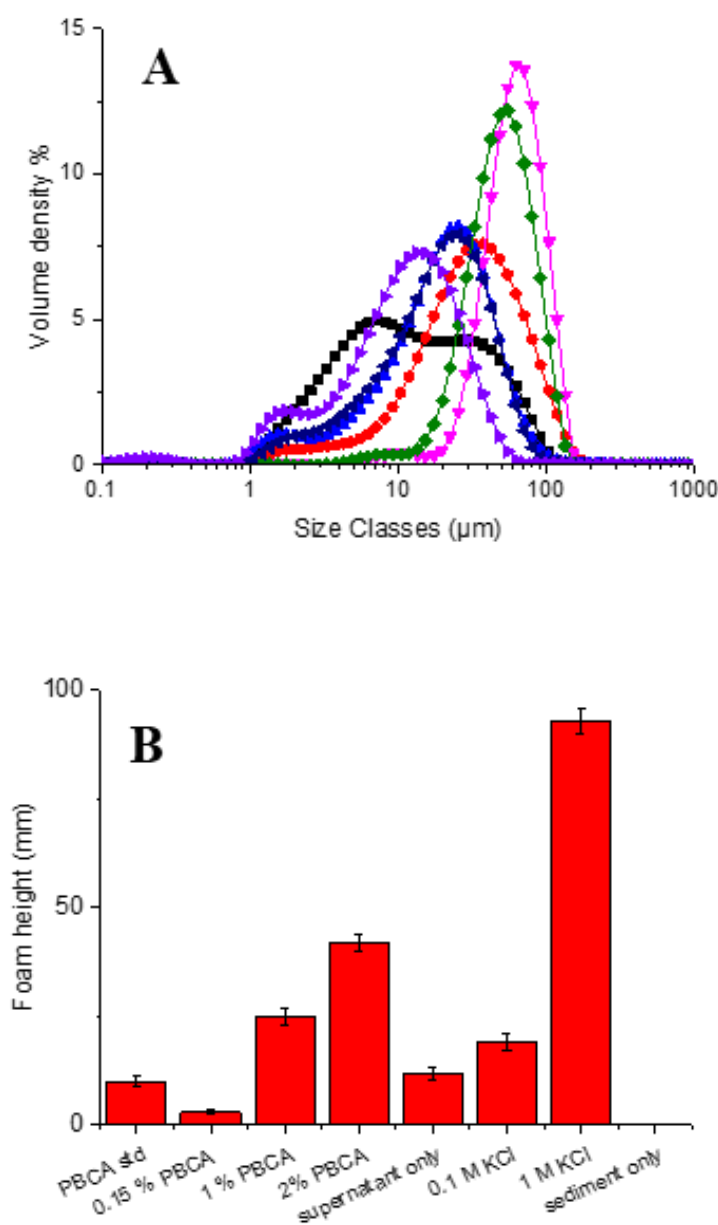
**Figure 4.9:** Impact of NP fractionation on MB size distribution (A): aerated supernatant, (B): aerated supernatant + 1 M KCl. 1<sup>st</sup> foam (■), 2<sup>nd</sup> foam (●), 3<sup>rd</sup> foam (▲).

Figure 4.10 shows schematically two different bubble shrinkage rates prepared in the two different systems, one rich in stabilizing NPs while the other system has a lower concentration of stabilizing NPs. A high concentration of NPs reduces the time of stabilization and therefore the bubbles shrink less.



**Figure 4.10:** Schematic of impact of low concentration (A) vs high concentration (B) of NPs on bubble stabilization

Figure 4.11 shows the size distribution and measured foam height after first aeration in most of the different systems described above. The results indicates that the standard (0.7 wt.% PBCA ) dispersion had the widest size distribution compared to all other ones. The 1 M KCl produced smallest MBs and highest foam height whilst 2 wt.% NPs and supernatant formed the most narrow size distribution but largest bubbles. Figure 4.11 (B), shows the foam heights (after 1<sup>st</sup> cycle of aeration) corresponded to the different systems. The system containing 1 M KCl produced the highest foam height while sedimented NPs produced no stable foam at all. The second lowest foam height belonged to the low concentration (0.15 wt.%) NPs dispersion. Increasing the PBCA NP concentration led to higher foam height compared to the standard system although larger bubbles were formed. Addition of 0.1 M KCl also significantly increased the foam production.



**Figure 4.11:** Comparison of 1st foam produced at different concentration of PBCA or different condition. (A) : size distribution PBCA standard ( $\blacksquare$ ), 0.15 % PBCA ( $\bullet$ ), 1 % PBCA ( $\blacktriangle$ ), 2% PBCA ( $\blacktriangledown$ ), supernatant only ( $\blacklozenge$ ), PBCA + 0.1 M KCl ( $\blacktriangleleft$ ), PBCA + 1 M KCl ( $\blacktriangleright$ ), (B): foam height

#### 4.3.1.5 Long term stability of MBs

All the MBs described in the above were clearly reasonably stable to be collected, sized, etc. however some longer term stability of MB stability was conducted. Samples of the first foam collected from the PBCA standard dispersion were kept at room temperature and the bubble size was measured after 6 months and 9 months (Figure 4.12). The size

distribution graph shows that the MBs grew slightly larger over time, but the process was very slow and after 9 months the very fine MBs were still present in the system. The  $d_{32}$  increased from 7.4 to 14.2 and to 18.4  $\mu\text{m}$  after 24 hours, 6 months and 9 months, respectively. Thus the rate of bubble growth / coarsening was very slow for these bubbles sizes, highlighting the effectiveness of Pickering stabilization of bubbles (Azmin *et al.* 2012).

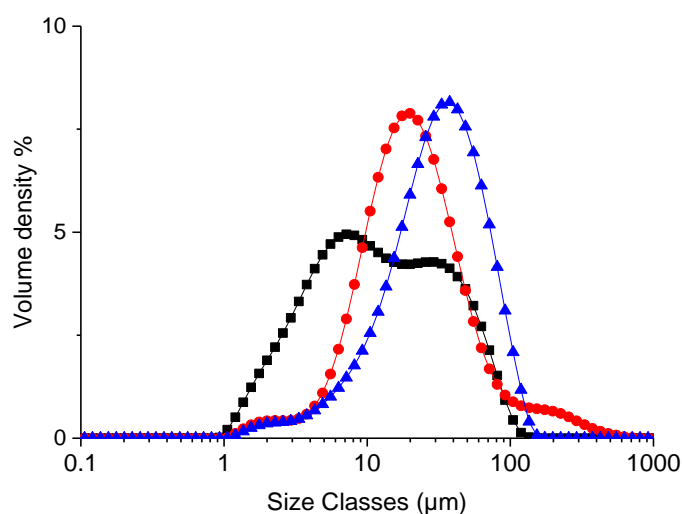


**Figure 4.12:** Long term stability of MBs (aerated PBCA standard), 24 h (■), 6 months (●), 9 months (▲)

The density of the standard PBCA foam layer was measured as  $275 - 320 \text{ kg/ m}^3$ . Hence the air volume fraction ( $\Phi$ ) of the foam was  $70 \pm 2 \%$ . This high volume fraction also shows the stability of the MBs to coalescence.

#### 4.3.2 Effect of initial bubble size on final bubble size and foam height

To be able to test the impact of initial bubble size on foam height and final bubble size, a smaller diameter bubble syringe was used to aerate the dispersion. The initial bubble size

was measured and was equal to 386  $\mu\text{m}$ . Aeration time was the same as previous experiment (i.e., 2 hours per each cycle).

The results (Figure 4.13 and Table 4.6) revealed that injecting the smaller initial bubbles affected not only the final bubble size, but also the foam height. Smaller initial bubble size led to larger final bubbles ( $d_{32} = 17 \mu\text{m}$ ) compared to the standard PBCA dispersion ( $d_{32} = 7.4 \mu\text{m}$ ). The average height of the first foam (where PBCA standard used) was  $6 \pm 1 \text{ mm}$ , at least 4 mm less than when larger needle was used for aeration. However the supernatant only (i.e., larger particles were removed by centrifugation at 500 g for 30 minutes) was aerated the foam height was very high and on average was equal to  $40 \pm 2 \text{ mm}$ . Thus foam height of aerated supernatant when small bubble syringe was used was at least 3 times larger than when large bubble syringe was used. In this system  $d_{32}$  of first foam when small bubble syringe was used was also much smaller ( $14 \mu\text{m}$ ) than that of when large syringe bubble used ( $40 \mu\text{m}$ ). The higher foam height and smaller  $d_{32}$  corresponds to formation of more bubbles of smaller size when smaller initial bubble size was used with the supernatant, i.e., the fraction enriched in smaller NPs.

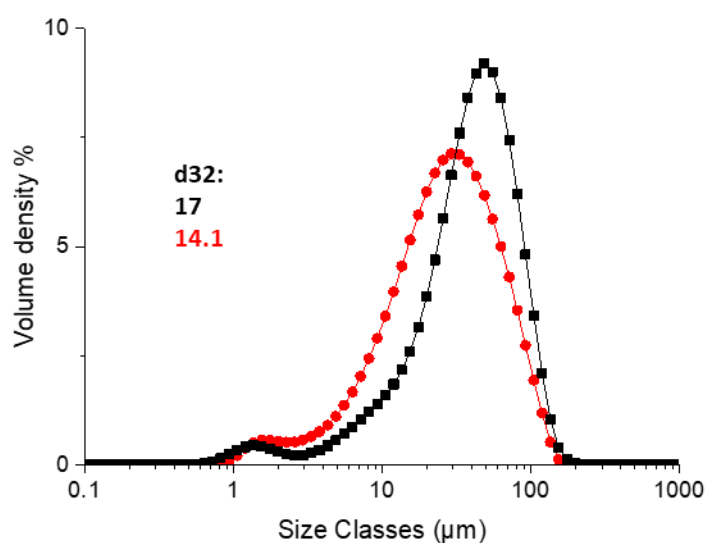


**Figure 4.13:** Size distribution after 24 hour when initial bubbles size were 386  $\mu\text{m}$ , PBCA standard (■), supernatant (●)

Dispersion	Foam height after each step of aeration (mm)		
	First	Second	Third
PBCA std	6	No stable foam	No stable foam
Supernatant	40	$\leq 2$	No stable foam

**Table 4.6:** Shows the foam heights when initial bubbles size were  $386 \mu\text{m}$

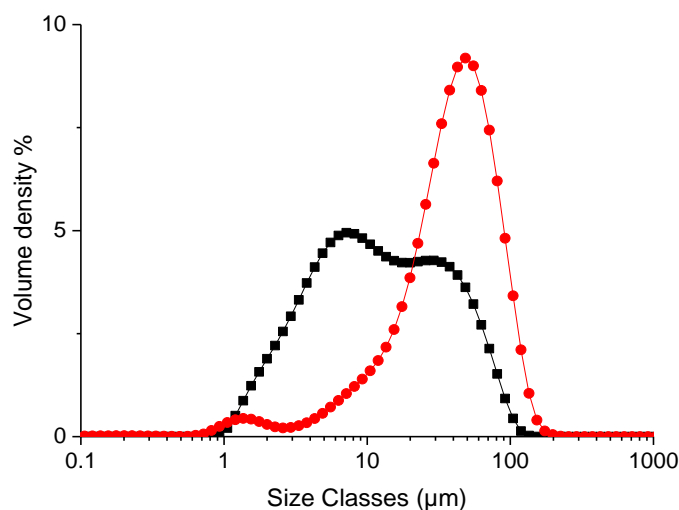


**Figure 4.14:** Represents the impact of initial bubble size on final bubble size distribution, large needle (■), small needle (●)

The size distribution of first foam where small bubble syringe was significantly narrower compared to where large bubble syringe used (Figure 4.14). A reverse correlation between initial and final bubble size was observed when standard PBCA dispersion aerated via different bubble syringes. This results suggests that smaller initial bubbles could produce less polydisperse final MBs. This can be due to less time for disproportionation before complete stabilization of the MBs.

## 4.4 Conclusion

In this study the impact of different factors on MBs stabilization was studied under controlled conditions.

Regardless of PBCA NP concentration, KCl concentration and initial bubble size, all bubbles shrank significantly before they stabilized. These could be either due to lack of enough free PBCA NPs in the system or difficulty in overcoming the adsorption energy barrier. During MB stabilization a major issue is the kinetics of adsorption of NPs to the freshly created interfaces. NPs are much larger than surfactant molecules thus they have a relatively small diffusion coefficient. MBs stabilized by NPs undergo a significant shrinkage during the period needed for the surface coverage by NPs.

When the standard NPs dispersion was aerated it was estimated that 6 % might be adsorbed to the interface after one cycle of aeration for both small and large needles. For 2 wt. % NPs the adsorption after the first cycle of aeration was estimated as only 1.4 %. It suggest that increasing (doubling) the NPs concentration decreases the efficiency of stabilization. Our results shows that larger particle had a more negative  $\zeta$ - potential that makes them less suitable for adsorption to the interface as discussed in chapter 3 another explanation might be that larger bubbles have smaller surface area therefore less NPs are required to stabilize them.

The highest adsorption was obtained on adding 1 M KCl before aeration giving an estimated 73 % of NPs adsorbed after only 1 cycle of aeration. This probably explains why the amount of foam produced in subsequent aerations dropped off rapidly (see Table 4.3). The second highest adsorption was obtained when supernatant was aerated using the smaller bubble syringe: 34 % of the NPs were estimated as adsorbed to the interface. In the fraction combination of supernatant plus 1 M KCl led to 30 % adsorption. Based on these results it can be concluded that degree of hydrophobicity (as measured by lower

magnitude of  $\zeta$ - potential) of NPs is more important than initial bubble size in terms of adsorption efficiency. Smaller NPs in the supernatant were more hydrophobic (less negative  $\zeta$ - potential) than larger ones and had a higher adsorption efficiency. Combining these more hydrophobic NPs with smaller initial bubble sizes helped to optimize the NP adsorption.

Another important factor for MB stabilization and NPs adsorption appears to be the ionic strength high concentration of KCl for some reason also reducing the  $\zeta$ - potential and making the NPs more hydrophobic. Presumably this increases the air – water the contact angle as already reported elsewhere or lower the energy barrier for particle adsorption (Paunov, Binks and Ashby 2002; Binks and Horozov 2005). On the other hand, higher ionic strength may aid particle close packing at the interface. Addition of very high concentrations of salt (KCl) to food is not feasible and requires careful consideration but lower concentrations in combination with more hydrophobic NP and smaller initial bubbles could be a better way to optimize NP adsorption and MBs stabilization in various real system.

The particle adsorption efficiency had a direct correlation with foam height and more importantly MB size. A given volume of foam with smaller MB sizes requires more NPs to cover the MB surfaces compared to foams with larger MB sizes.

Further investigation is required to find out why the larger PBCA NPs were less hydrophobic or how centrifugation process itself changed their hydrophobicity ( $\zeta$ - potential). It is as yet unclear why the sedimented NPs could not stabilize MBs. Even addition of surfactant back to the re-dispersed sedimented NPs could not help them to stabilize MBs, nor addition of KCl.

Nevertheless the main conclusion is that those MBs that could be formed in all the other system were highly stable and showed very little changes during their storage time of up

to 9 months. This is an advantage of stabilizing MBs via PBCA NPs, since they could be incorporated into products and remain intact during the shelf life of the product.

## Chapter 5 :

### Continuous Method for Microbubble Production

#### 5.1 Introduction

There is a need for producing highly stable microbubbles on large scale, as microbubbles have the potential to be used in commercial products. It is useful if such MBs could be produced, stored and be used as and when necessary. As already mentioned in chapter 1 and 4 there are many ways of producing monodispersed microbubbles such as using microfluidic devices. However these techniques are only effective in batch production of microbubbles and also have a very limited applications as they result in low yield of MBs (few nanolitres to few femtolitres). Another disadvantage of microfluidic devices is that they are susceptible to frequent channel blockage (Wielhorski *et al.* 2014).

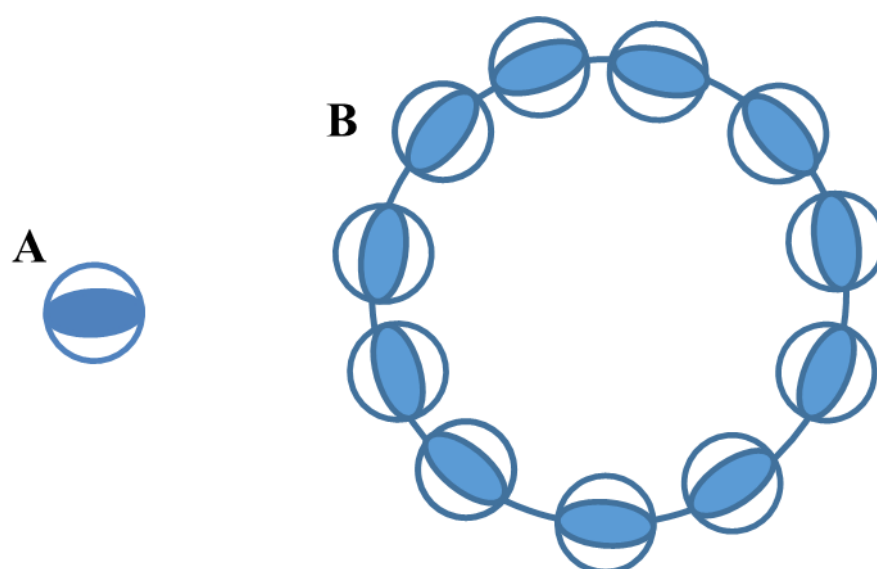
Currently spargers are used by many industries to generate and disperse microbubbles in a large variety of systems. Plate sparger, wheel-type sparger, pipe sparger and spider sparger are examples of most commonly sparger designs (Hanotu, Bandulasena and Zimmerman 2017). The spargers have a simple design and very efficient in terms of producing microbubbles. However they produce fairly coarse bubbles and therefore have

limited applications when the required size of bubbles is much smaller (Kulkarni and Joshi 2011).

The aim of this study was to develop a method for continuous production of MB which may in future be scaled up to industrial production level. Prior to design of any model process it is necessary to know what parameters influence the microbubble formation, size and stability. Among all the factors the number and size of NPs, the surface coverage of MB by NPs, the number and initial size of the bubbles introduced into the system and the number of MBs exit the system at any given time are the most important parameters that must be taken into account. This chapter consider the influence of these parameters in what may be a possible model for such continuous process of creating MBs, from a theoretical point of view.

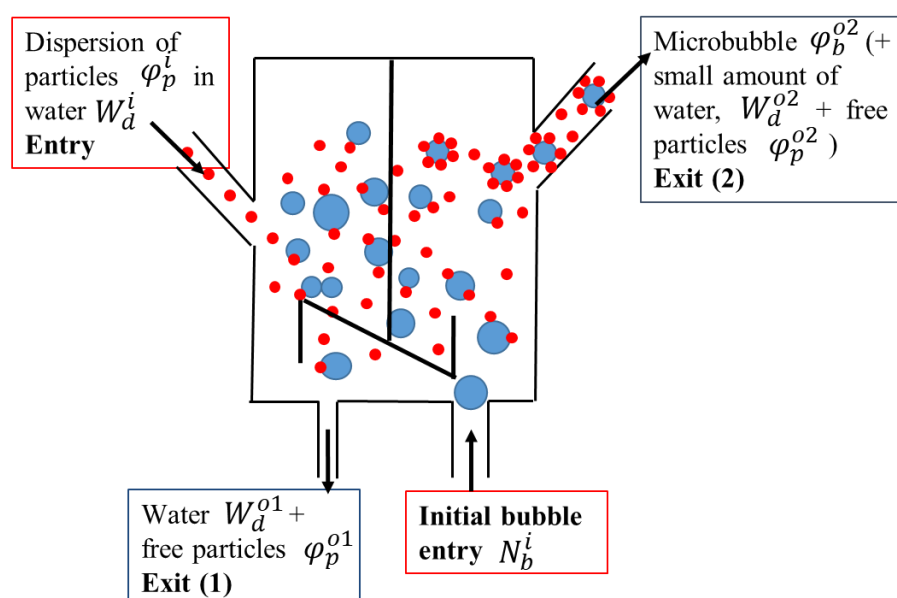
## 5.2 Numerical approach

Figure 5.1 (A) illustrates a single particle and 5.1 (B) a single bubble stabilized by particles, through a “Pickering-like” mechanism.



**Figure 5.1:** Schematic of (A) a single particle, (B) a single bubble covered and stabilized by nanoparticles

Figure 5.2 shows an outline of our proposed model chamber that may be used for continuous production of MBs. The chamber has an entrance for the dispersion of particles in the water to enter and a further separate entrance to introduce bubbles. The monodispersed size bubbles are injected to the chamber filled with particle dispersion. The chamber also has two exits, one for water and free (not adsorbed particle) particles (exit 1) and another for stabilized MBs (exit 2). It is assumed that only a small negligible amount of water and free particles can exit the system together with microbubbles from exit 2.



**Figure 5.2:** Schematic of continuous aeration chamber with 2 entries for water, particles ●, and bubbles ●, and two exits for water, particles and stabilized bubbles. The chamber is equipped with a stirrer

The blue area shown in the figure 5.1 (A) is the area occupied by a single particle residing at an air – water interface. This area equals  $\pi r_p^2$ . Where  $r_p$  is the radius of the particle (for PBCA NPs the  $r_p$  equals to  $\approx 80$  nm). Surface area of the bubble (figure 5.1 (B)) is  $4\pi r_b^2$ , where  $r_b$  denotes the radius of the bubble. The total number of bubbles in the system is determined by the equation 5.1:

$$N_b = \frac{v_t}{v_b} \quad (5.1)$$

Where  $v_t$  is the total volume of bubbles and  $v_b$  is the initial volume of a single bubble and equals  $\frac{4}{3}\pi r_b^3$ .

Next, equation 5.2 below is used to calculate the required number of particles to cover the surface of all microbubbles.

$$N_p = \frac{4\pi r_b^2 \times \alpha \times N_b}{\pi r_p^2} \quad (5.2)$$

In here we assume that the surface coverage ( $\alpha$ ) is 0.5.

This microbubble production system will reach a steady state after an initial transition period. When the system reaches such a state the following assumptions becomes valid:

- 1) The rate of the number of particles entering the system equals the rate of the number of particles exiting the system, either attached to MBs or as free particles. In other words the total mass of particles entering the system equals the mass of particles exiting the system.
- 2) Mass of water entering the system equals to mass of water exiting the system.

If it is assumed that bubbles do not completely dissolve or coalesce with each other, then the number of bubbles introduced to the system must also equal the number of MBs that exit the system. But the volume of initial bubbles is not equal to the volume of final bubbles, due to the considerable shrinkage that the bubbles undergo prior to them becoming stabilized.

The value of the water flow rate that enters ( $W_d^i$ ) the system can be adjusted by the system operator as one of the controlled parameters. Therefore:

$$W_d^i(1-\phi_p^i) = W_d^{o1}(1-\phi_p^{o1}) + W_d^{o2}(1-\phi_b^{o2}) \quad (5.3)$$

where  $\varphi_p^i$  is volume fraction of particles at the inlet of the system and  $\varphi_p^{o1}$  is the volume fractions of particles that exit the system via exit 1.  $\varphi_b^{o2}$  is the volume fraction of bubbles exit the system via exit 2. As  $\varphi_p^i \ll 1$  and  $\varphi_p^{o1} \ll 1$  and with  $W_d^{o2}(1-\varphi_b^{o2}) \ll W_d^{o1}$  approximately we have  $W_d^i \approx W_d^{o1}$ . In assuming that  $W_d^{o2}(1-\varphi_b^{o2})$  is small we are making the assumption that the foam coming out of the outlet 2 entirely consist of bubbles and not much liquid. This assumption is made to make the calculation tractable.

Based on the previous assumption (i.e., no full dissolution and coalescence)  $N_b^i = N_b^{o2}$ , where  $N_b^i$  is the rate of number of bubbles entering the system and  $N_b^{o2}$  is the rate of number of bubbles exiting the system. Therefore

$$\varphi_b^i = N_b^i \times \left( \frac{4\pi(r_b^i)^3}{3} \right) \quad (5.4)$$

$$W_d^{o2} \varphi_b^{o2} = N_b^{o2} \times \left( \frac{4\pi(r_b^{o2})^3}{3} \right) = N_b^i \times \left( \frac{4\pi(r_b^{o2})^3}{3} \right) \quad (5.5)$$

with  $r_b^i$  and  $r_b^{o2}$  denoting the initial and final size of introduced and leaving bubbles respectively.  $\varphi_b^i$  is the volume fraction of bubbles entering the system. Balancing the rate of total volume of particles entering the system with those leaving (from both exit 1 and 2), we have

$$W_d^i \varphi_p^i = W_d^{o1} \varphi_p^{o1} + W_d^{o2} (1 - \varphi_b^{o2}) \varphi_p^{o2} + W_d^{o2} \varphi_b^{o2} \frac{r_p}{r_b^{o2}} \quad (5.6)$$

Where  $\varphi_p^{o2}$  is the volume fractions of particles that exit the system via exit 2. The first term on the right hand side of equation 5.6 represents the volume of particles leaving via

exit 1. The second term is the free (non- adsorbed) particles exiting from exit 2. Finally, the last term gives the volume of particles leaving as particles adsorbed at the surface of bubbles (again from exit 2). This last term depends on the rate of the number of bubbles leaving, the surface area of such a bubbles and the degree of coverage of the surface by the particles. More specifically, rate of volume of bound particles leaving the system is:

$$\left(\frac{W_d^{o2} \phi_b^{o2}}{\frac{4}{3} \pi (r_b^{o2})^3}\right) \times \frac{4 \pi (r_b^{o2}) \alpha}{\pi r_p^2} \times \frac{4 \pi r_p^3}{3} = W_d^{o2} \phi_b^{o2} \frac{r_p}{r_b^{o2}} \quad (5.7)$$

which appears in equation **5.6**. The constant  $\alpha$  here indicates the efficiency of packing of the particles adsorbed at the surface of bubbles. For a perfect monodispersed size distribution of particles, averaged on a square lattice on the interface we have  $\alpha = 0.78$ .

The value of  $\alpha$  in practice will depends on polydispersity and shape of particles, as well as possible inter-particle forces between them. More practical values of the  $\alpha$  are likely to be closer to 0.5.

Now we may assume:

$$\phi_p^{o2} \approx 0$$

This means the number of free particles in water coming out without attachment to the bubbles is almost zero.

Since we also have:

$$W_d^{o1} \gg W_d^{o2} (1 - \phi_b^{o2})$$

we may ignore the last term in equation **5.6** and therefore approximate the equation as:

$$W_d^i \phi_p^i = W_d^{o1} \phi_p^{o1} + (\alpha \times W_d^{o2} \times \phi_b^{o2} \frac{r_p}{r_b^{o2}}) \quad (5.8)$$

Recalling that:

$$W_d^i \approx W_d^{o1}$$

equation 5.6 reduces to:

$$W_d^i (\varphi_p^i - \varphi_p^{o1}) = \alpha \times W_d^{o2} \times \varphi_b^{o2} \frac{r_p}{r_b^{o2}} \quad (5.9)$$

where we also assumed, the conservation of number of bubbles (though not their volume due to shrinkage); i.e.

$$N_b^i = N_b^{o2}$$

Hence:

$$N_b^{o2} = \frac{W_d^{o2} \times \varphi_b^{o2}}{\frac{4}{3} \pi (r_b^{o2})^3} = N_b^i \quad (5.10)$$

or alternatively:

$$\frac{4}{3} \pi (r_b^{o2})^3 \times N_b^i = W_d^{o2} \times \varphi_b^{o2} \quad (5.11)$$

Now the rate of shrinkage of bubbles (assuming that they do become eventually stabilized) depends on the time required for bubbles to gather sufficient particles on their surface. During this finite period bubbles shrinkage is driven by gas dissolution and disproportionation processes. The interplay between these two processes (particle adsorption versus disproportionation) dictates the amount of shrinkage suffered by bubbles of a given initial size before they are stabilized. The dynamics of such shrinkage was analysed by (Ettelaie and Murray 2014; Ettelaie and Murray 2015). For the cases where the transport of the particles to the surface is mainly due to diffusion, They provided an expression for the degree of shrinkage based on concentration of particles in the dispersion medium and the initial size of the bubbles.

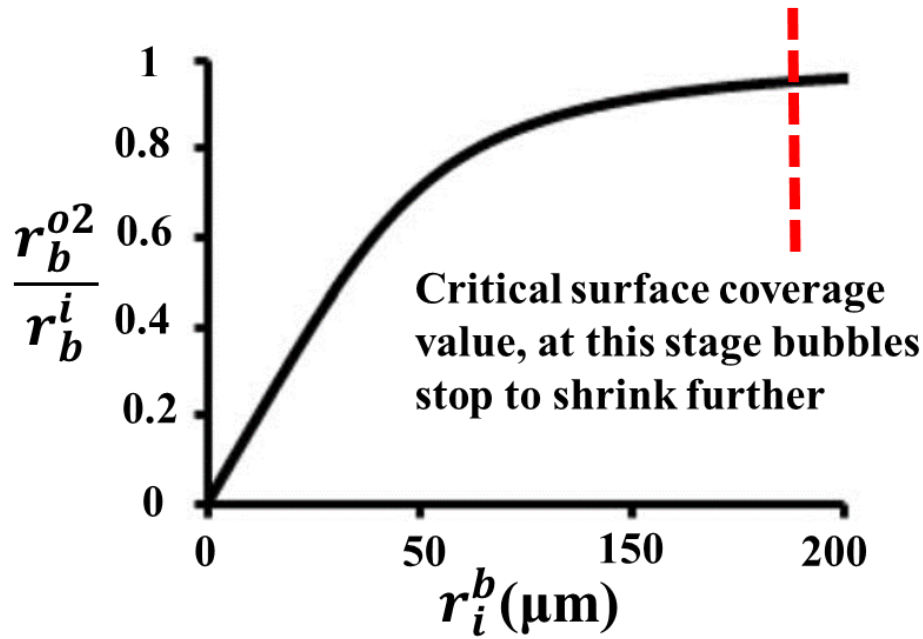


**Figure 5.3:** The shrinkage ratio defined as  $\frac{r_b^{o2}}{r_b^i}$  plotted versus initial size of bubbles,  $r_b^i$ , in a system with a large excess of stabilizing nanoparticles, taken from Ettelaie and Murray (2014). In such a system the shrinkage is determined by the rate of adsorption and not the number of available particles.

As a bubble shrinks the  $\alpha$  increases. The adsorption of particles on the surface of bubbles does not stop them from shrinking until the particle surface coverage reaches a critical value of  $\alpha$ , after achieving the critical surface coverage bubbles stop shrinking. The red line in figure 5.3 is roughly where the bubbles attain the required coverage,  $\alpha$ , before any significant shrinkage. For bubble size below this value, significant degree of shrinkage occurs prior to their stabilization (Ettelaie and Murray 2014).

Based on equation derived by Ettelaie and Murray (2014) :

$$\frac{r_b^{o2}}{r_b^i} = f(\varphi_p^{o1}, r_b^i) \quad (5.12)$$

Where function  $f(\varphi_p^i, r_b^i)$  found to have the following form:

$$f(\varphi_p^{ol}, r_b^i) = \frac{r_b^*}{r_b^i} \left[ \sqrt{1 + \left( \frac{r_b^i}{r_b^*} \right)^4} - 1 \right]^{\frac{1}{2}} \quad (5.13)$$

where we have defined a characteristic radius (in units of  $\langle r_b^i \rangle$ ) such that:

$$r_b^* = \sqrt{\frac{2c}{3}} \quad (5.14)$$

and  $c$  is the ratio of required time for the bubbles to achieve the necessary surface coverage by the particles in absence of shrinkage to the life time of the bubbles with no particle present:

$$c = \frac{t_c}{t_d} = \frac{\lambda^*}{\pi D_p n_0 r_b^2 r_p^2 \tau} = \frac{48\pi N_A \alpha \eta \gamma S D_g \left( \frac{r_p}{r_b} \right)^2}{P_0 \varphi_p^{ol}} \quad (5.15)$$

where  $N_A$  is the Avogadro's number, and the diffusion coefficient of the particles is expressed in terms of the viscosity of the solution,  $\eta$ , using the Stokes-Einstein equation  $D_p = (K_B T) / (6\pi\eta r_p)$ . Similarly, we have substituted for the number density of the particles in favour of their volume fraction,  $\varphi_p^{ol}$ , where  $n_0 = 3\varphi_p^{ol} (4\pi r_p^3)^{-1}$ . The gas – water surface tension is denoted by  $\gamma$  and  $P_0$  is the Henry's constant.  $S$  is the gas solubility and  $D_g$  is the diffusion coefficient of gas molecules in water (Ettelaie and Murray 2014). For a given set of operating conditions, the following parameters can be set by the operator  $N_b^i$ ,  $W_d^i$ ,  $\varphi_p^i$  (=0.7 for PBCA NPs),  $r_p$  (= 80 nm for PBCA NPs used),  $r_b^i$ . In addition we know that  $N_b^i = N_b^{ol}$  and  $W_d^i \approx W_d^{ol}$ . The parameter  $\alpha$  is determined by packing of particles at the surface, and as already mentioned here for the purpose of demonstration is taken as  $\alpha = 0.5$  not untypical of more realistic cases one may encounter in particles.

In order to determine  $\varphi_p^{o1}$ , it is necessary to know/ set the shrinkage rate,  $f(\varphi_p^{o1}, r_b^i)$ , first. Once we know it we can calculate the value of  $c$  by inverting equation **5.13** to express  $\varphi_p^{o1}$  in terms of  $f$ . The left side of equation **5.16** is obtained by inversion of **5.13**.

$$r_b^* = \frac{1}{f} \sqrt{\frac{1-f^4}{2}} = \sqrt{\frac{2c}{3}} \quad (5.16)$$

then:

$$c = \frac{3}{4f^2} (1-f^4) \quad (5.17)$$

The value of  $c$  could be determined by equation **5.17**. If the value of  $f$  assumed to be 0.1 then  $c$  equals 74.99.

Using the typical values for the quantities appearing in equation **5.15**,  $P_0 = 100$  kPa,  $\gamma = 0.07$  N m<sup>-1</sup>,  $D_g = 2 \times 10^{-9}$  m<sup>2</sup> s<sup>-1</sup>, and  $S = 7 \times 10^{-6}$  mol N<sup>-1</sup> m<sup>-1</sup> and  $\eta = 0.001$  kg m<sup>-1</sup> s<sup>-1</sup>, and assuming  $r_b^i = 100$   $\mu$ m ( $10^{-4}$  m) and  $r_p = 80$  nm ( $8 \times 10^{-8}$  m) the value of  $\varphi_p^{o1}$  calculated as 0.0004%.

One then needs of the following to be determined:  $W_d^{o2}$  and  $\varphi_b^{o2}$

Substituting equation **5.12** into **5.8** and **5.11** and rearranging these together with **5.10** we arrive at the following

$$\varphi_b^{o2} = \frac{\frac{4}{3} \pi N_b^{o2} (r_b^{o2})^3}{W_d^{o2}} = \frac{\frac{4}{3} \pi N_b^i (r_b^i)^3 [f]^3}{W_d^{o2}} \quad (5.18)$$

The foam coming out of outlet 2 consist predominantly of MBs, only containing very small amount of liquid. To first approximation then  $\varphi_b^{o2} \approx 1$ , which gives us the flow rate required from outlet 2, namely

$$W_d^{o2} = \frac{4}{3} \pi N_b^i (r_b^i)^3 [f]^3 \quad (5.19)$$

### 5.3 Results and discussion

Now that we have established all the required equations, it becomes possible to examine the numerical solutions to the above set of equation and discuss their implications.

#### 5.3.1 Impact of NPs volume fraction in the inlet of dispersion, $\varphi_p^i$ , on final bubble size

Initial particle concentration plays an important role on determining the final size of the MBs before they become stabilized. Figure 5.4 shows how  $\varphi_p^i$  affect the final size of MBs at different flow rates ( $W_d^i$ ), with other parameters (i.e.,  $\alpha$ ,  $W_d^{o2}$ ,  $\varphi_b^{o2}$  and  $r_p$ ) remaining constant. In the previous chapter (chapter 4) we already discussed that for a standard dispersion of PBCA NPs only 6 % of the total number of NPs adsorb to the freshly formed interfaces after first cycle of aeration. In here we are assuming that 100% of the NPs can be adsorbed to the interface.

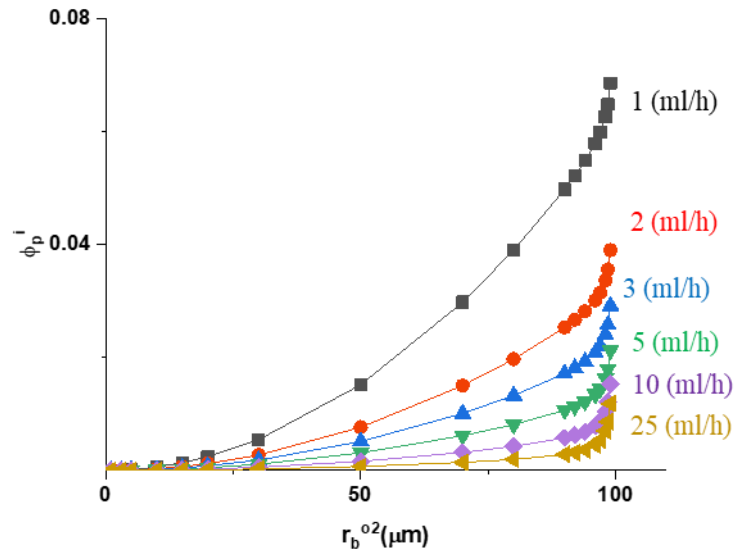


**Figure 5.4:**  $\phi_p^i$  plotted against  $r_b^{o2}$  for different  $W_d^i$ : 1 ml / h (■), 2 ml / h (●), 3 ml / h (▲), 5 ml / h (▼), 10 ml / h (◆) and 25 ml / h (◄). All results are calculated assuming that injected bubbles have a size of 100  $\mu m$ .

The model predicted that final bubble size increases if the volume fraction of the NPs in the dispersion entering the system increases. The graph (Figure 5.4) clearly indicates that if there are high number of NPs available in the system then more particles adsorb to the interface more quickly and therefore the bubbles stabilize against disproportionation much faster and with less shrinkage.

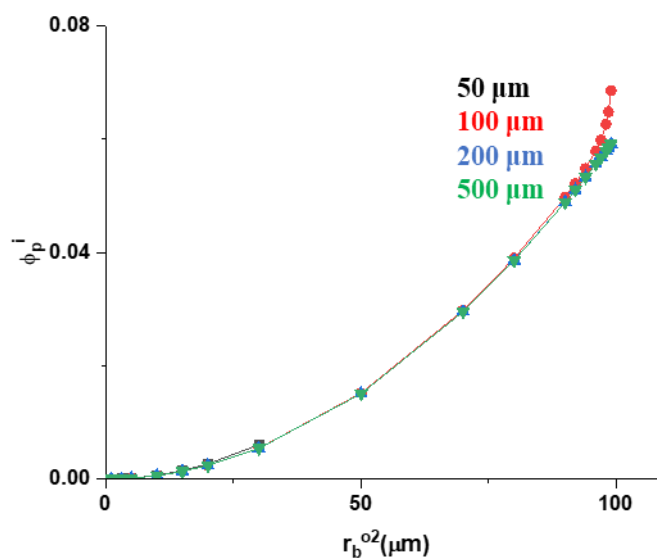


**Figure 5.5:** : The required volume fraction of particles ,  $\phi_p^i$  , needed to achieve the final size indicated on x – axis.  $\phi_p^i$  plotted against  $r_b^{o2}$  for different  $r_b^i$ , when  $W_d^i=1$  ml / h and the number of injected bubbles was 10000 bubbles per second.

The graph shown in figure 5.5 indicates that initial size of bubbles has no impact on the final size of MBs produced for any  $\phi_p^i$  . This implies when there are certain number/ volume fraction of NPs available in the system then bubbles have to shrink up to a degree that their particle surface coverage reaches a critical amount and therefore they become stabilized against disproportionation as a result of the sufficiently strong NP network formed at the interface. Therefore, in this example what determines the final size of bubbles is the number of particles not the initial size of bubbles (the shrinkage rate is altered as required to get the same final bubble size). It must be noted that the advantage of using larger initial bubbles is that they have larger life time so there will be more time for particles to adsorb to the interface before bubbles disappear.

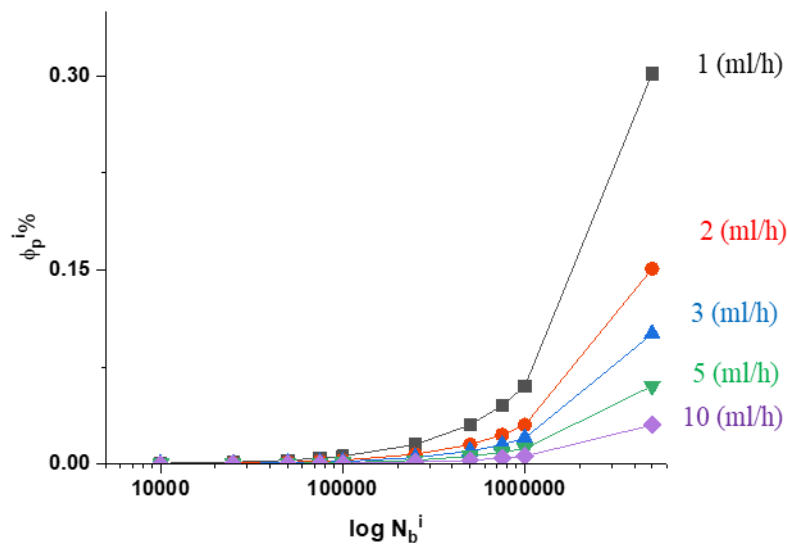


**Figure 5.6:**  $\phi_p^i$  plotted against  $N_b^i$  for different  $W_d^i$ , when  $r_b^{o2} = 10 \mu\text{m}$ . All the results are calculated assuming that initial bubble size is  $100 \mu\text{m}$ .

Figure 5.6 shows how the required  $\phi_p^i$  changes if the number of bubbles injected per second increases (with  $r_b^{o2} = 10 \mu\text{m}$ ). It clearly shows that a larger value of  $\phi_p^i$  is required if the number of bubbles per time generated increases. Increasing the number of bubbles per second generated corresponds to more interfaces creating and hence more NP are required to cover them. As a result more NPs are removed from the bulk. In order to keep the concentration of the NPs in the bulk constant (to ensure the same shrinkage factor), the  $\phi_p^i$  must be increased accordingly. The graph also indicates that there is a reverse correlation between  $W_d^i$  and  $\phi_p^i$  when other parameters are constant; this is also shown in figure 5.4. So for increasing the NP numbers entering the system in unit time, the system operator has a choice, either to increase the volume fraction of NPs at entry point or increase the flow rate of NPs, both of these will have the same result in providing more particles per unit time. However when the entry flow rate is increased, then the  $W_d^{o1}$  must be increased too, since the amount of water entering and leaving the system in a steady state operation conditions must be the same.

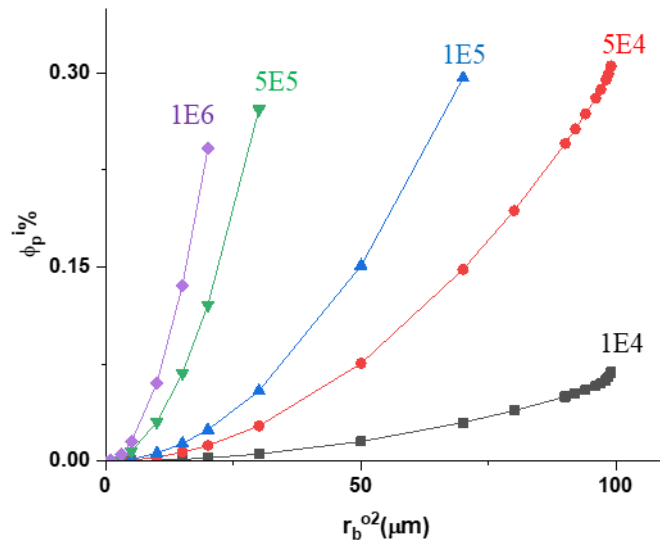


**Figure 5.7:**  $\phi_p^i$  plotted against  $r_b^{o2}$  for different  $N_b^i$  when  $W_d^i = 1$  ml / h. All the results are calculated assuming that initial bubble size is 100  $\mu\text{m}$ .

Figure 5.7 shows the relationship between  $\phi_p^i$  and  $r_b^{o2}$  when  $W_d^i$  is kept constant (i.e., 1 ml / h). The graph shows that  $\phi_p^i$  increases sharply when a large number of bubbles per second are required to be produced. The  $\phi_p^i$  is the highest if one wants to produce larger  $r_b^{o2}$  in large quantities per second (i.e.,  $\phi_p^i = 0.3$  if  $r_b^{o2} = 99$   $\mu\text{m}$  and  $N_b^i = 50000$ ). Clearly larger bubbles have larger surface areas, therefore  $\phi_p^i$  must be increased in order to stabilize these larger bubbles. In addition when the number of bubbles are increased, more NPs are required to stabilize them, hence  $\phi_p^i$  increases.

### 5.3.1 Impact of $W_d^i$ on $r_b^{o2}$

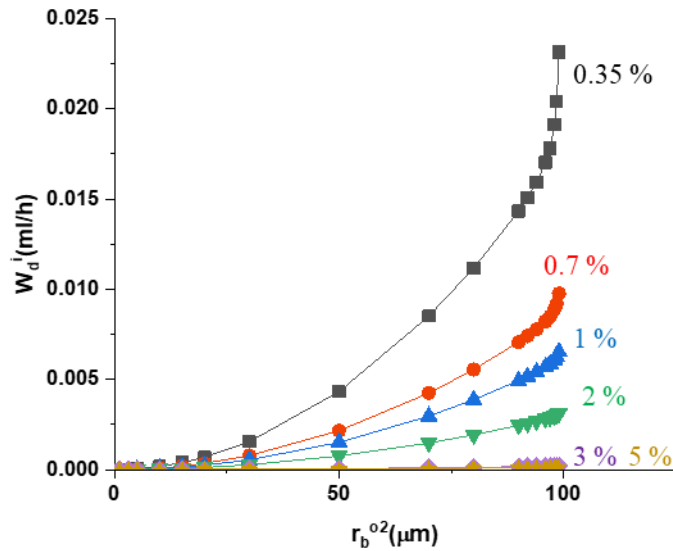


**Figure 5.8:**  $W_d^i$  plotted against  $r_b^{o2}$  for different  $\phi_p^i$  %. All the results are calculated assuming that initial bubble size is 100  $\mu\text{m}$  and injection rate is 10000 bubbles per second.

Figure 5.8 shows  $W_d^i$  plotted vs  $r_b^{o2}$  for different volume fraction of NPs ( $\phi_p^i$  %), range between 0.35 % and 5 %. As the  $W_d^i$  increases the final size of MBs increases when the  $\phi_p^i$  % remains constant. As already mentioned above when large concentration of NPs exist in the chamber, it is more likely that more NPs adsorb to the surface of the freshly formed bubbles more quickly. So in a shorter time the surface coverage reaches the needed critical surface coverage ( $\alpha$ ) so bubbles will tend to shrink less.

## 5.4 Conclusion

The impact of various parameters such as bubble size (initial), concentration and the flowrate of particles entering the system and also number of bubbles entering the system on final bubble size was theoretically studied. This model can help us to better understanding the continuous MB production system. The model anticipates the final size

of bubble under different operational conditions and will be a very useful tool when a continuous MB apparatus as explained in section 5.2 is finally devised.

The model shows that the main factors determine the final bubble size are  $\varphi_p^i$ ,  $W_d^i$  and  $N_b^i$ . The parameters  $\varphi_p^i$ ,  $W_d^i$  have a direct effect on final size ( $r_b^{o2}$ ) of MBs produced. Therefore, any increase in one of these two leads to an increase in  $r_b^{o2}$  as long as other parameters remains constant. In contrast increasing the  $N_b^i$  results into decrease of  $r_b^{o2}$  when all other parameters are constant.

## Chapter 6 :

### Summary

The aim of this project was to generate ultra-stable MBs for industrial applications in food and non-food products via Pickering particles. HFBII was used as an edible food grade nanoparticles and poly alkyl cyanoacrylates were used to stabilize MBs for non-food applications. The outcome of the experiments carried out in this study have suggested that Pickering stabilization is an effective way to stabilize MBs for a long period of times e.g., weeks or months. The finding of this study will help to decide the optimum conditions for producing highly stable MBs with high air volume fraction, using each of these NPs.

The results have suggested that HFBII can stabilize MBs against dissolution for a relatively long time when used with other surface active proteins or surfactants. HFBII is not a good foaming agent therefore produce a very low volume fraction of MBs. In contrast other proteins or small molecule surfactants can produce loads of not stables MBs. Therefore the combination of HFBII and other surface active materials is an effective way to produce higher volume fraction of stable MBs. The results also shows that surface activity of the second protein/ surfactant plays an important role on volume fraction of obtained MBs. By increasing the surface tension of the protein/ surfactant used in combination with HFBII up to a certain point the MBs volume fraction increases. If the surface tension is higher than this optimum value HFBII cannot displace protein/

surfactant adsorbed the air – water interface therefore less HFBII is involved in stabilizing MBs. As a consequence the volume fraction of MBs decreases.

The second part of this study focused on stabilization of MBs via synthesized poly alkyl cyanoacrylate (PACA) NPs under a range of various polymerization conditions (pH: 2.2, 4 & 6, surfactant type and concentration). The optimum system is butyl cyanoacrylate (BCA) polymerized into PBCA NPs at pH 4 in the presence of 1 wt.% Tyloxapol surfactant. CLSM and SEM micrograph indicate that MBs are stabilized by self-assembly of PBCA NPs around the MBs. SEM micrographs showed that these particles are spherical in shape and have a contact angle of  $77 \pm 10^\circ$  at the air water interface. These particular PBCA NPs are capable of stabilizing MBs for the period of at least 2 months. On the other hand SEM images suggested PECA NPs are not spherical and also the PECA NPs are merged together.

The air volume fraction measurement revealed that PBCA NPs can produce a low volume fraction of MBs in a simple, single step aeration via a high shear mixer. This suggests that the PBCA NPs adsorption at the interface is not a rapid process.

One of the most significant findings of this study suggests that the surfactant may have incorporated to the surface of the PBCA NPs made with 1wt.% Tyloxapol, and improved the contact angle/ wetting properties of the particles at the air – water interface. Because the PBCA NPs made in absence of surfactant failed to stabilize any bubbles even after addition of surfactant to the particle dispersion after NPs formed. These particles seems to be very hydrophilic and have preference to remain in the aqueous phase. Such an effect may partly explain the conflicting results in some of the literature on the effects of different surfactants and polymerization conditions, but also suggests that more work needs to be done to understand the surface nature of such Pickering bubble stabilizers.

By aerating the standard PBCA system by injecting bubbles of known size the air volume fraction increased - this technique was very useful to produce homogenous MBs. The bubbles have enough time to be covered by NPs before they dissolve. The results show that addition of salt (KCl) to the system improves the adsorption of NPs by optimising the  $\zeta$ - potential of the PBCA NPs. Larger PBCA NPs that are separated by centrifuge low speed seem not to be a suitable MBs stabilizer. These NPs were more hydrophilic compared to the standard PBCA NPs.

A simple apparatus design for continuous production of microbubbles was proposed. In addition main factors that governs the bubble formation, size and stability in this system were theoretically studied. The proposed model predicts that final size of microbubbles is strongly influenced by volume fraction of nanoparticles and the rate they enter the system, and also the number of bubbles injected to the system.

Overall HFBII and PBCA NPs are capable of stabilizing MBs for a long time however the dispersion conditions play an important role in foam stabilizing properties. Changes in the NP dispersion such as changing or removing the surfactant can decrease the foam stabilizing ability of the NPs by changing the surface chemistry of the NPs (e.g., for PBCA NPs) or any change in the ratio of surfactant to NPs can also change the foam stabilizing ability of the NPs used. This study has therefore provided in depth knowledge of Pickering stabilization and main factors to obtain the optimum result, particularly when HFBII or PBCA are used.

## References:

- ABASCAL, D. M. and J. GRACIA-FADRIQUE. 2009. Surface tension and foam stability of commercial calcium and sodium caseinates. *Food Hydrocolloids*, **23**(7), pp.1848-1852.
- ADAIR, J. H., E. SUVACI and J. SINDEL. 2001. Surface and Colloid Chemistry. In: K. H. J. BUSCHOW, R. W. CAHN, M. C. FLEMINGS, B. ILSCHNER, E. J. KRAMER, S. MAHAJAN and P. VEYSSIÈRE, eds. *Encyclopedia of Materials: Science and Technology*. Oxford: Elsevier, pp.1-10.
- AHMAD, Z., H. B. ZHANG, U. FAROOK, M. EDIRISINGHE, E. STRIDE and P. COLOMBO. 2008. Generation of multilayered structures for biomedical applications using a novel tri-needle coaxial device and electrohydrodynamic flow. *Journal of The Royal Society Interface*, **5**(27), pp.1255-1261.
- ALARGOVA, R. G., D. S. WARHADPANDE, V. N. PAUNOV and O. D. VELEV. 2004. *Langmuir*, **20**, p10371.
- ALLOUCHE, J. 2013. Synthesis of Organic and Bioorganic Nanoparticles: An Overview of the Preparation Methods. In: R. BRAYNER, F. FIÉVET and T. CORADIN, eds. *Nanomaterials: A Danger or a Promise? A Chemical and Biological Perspective*. London: Springer London, pp.27-74.
- ARDITTY, S., C. P. WHITBY, B. P. BINKS, V. SCHMITT and F. LEAL-CALDERON. 2003. Some general features of limited coalescence in solid-stabilized emulsions. *The European Physical Journal E*, **11**(3), pp.273-281.
- ASHBY, F. M., A. EVANS, N. FLECK, L. J GIBSON, J. W HUTCHINSON and H. N.G WADLEY. 2002. *Metal Foams: a Design Guide*.
- ASHOKKUMAR, M., J. LEE, S. KENTISH and F. GRIESER. 2007. Bubbles in an acoustic field: An overview. *Ultrasonics Sonochemistry*, **14**(4), pp.470-475.
- ASUA, J. M. 2002. Miniemulsion polymerization. *Progress in Polymer Science*, **27**(7), pp.1283-1346.
- ASUA, J. M. 2004. Emulsion polymerization: From fundamental mechanisms to process developments. *Journal of Polymer Science Part A: Polymer Chemistry*, **42**(5), pp.1025-1041.
- AVEYARD, R., J. H. CLINT, D. NEES and N. QUIRKE. 2000. Structure and Collapse of Particle Monolayers under Lateral Pressure at the Octane/Aqueous Surfactant Solution Interface. *Langmuir*, **16**(23), pp.8820-8828.

- AZMIN, M., G. MOHAMEDI, M. EDIRISINGHE and E. P. STRIDE. 2012. Dissolution of coated microbubbles: The effect of nanoparticles and surfactant concentration. *Materials Science and Engineering: C*, **32**(8), pp.2654-2658.
- BALA SUBRAMANIAM, A., M. ABKARIAN, L. MAHADEVAN and H. A. STONE. 2005. Non-spherical bubbles. *Nature*, **438**, p930.
- BAO, D. C., H. A. ZHANG, X. D. LIU, Y. J. ZHAO, X. J. MA and Q. YUAN. 2007. Preparation of Monodispersed Polymer Microspheres by SPG Membrane Emulsification-Solvent Evaporation Technology. *Journal of Dispersion Science and Technology*, **28**(3), pp.485-490.
- BEHAN, N., C. BIRKINSHAW and N. CLARKE. 2001. Poly n-butyl cyanoacrylate nanoparticles: a mechanistic study of polymerisation and particle formation. *Biomaterials*, **22**(11), pp.1335-1344.
- BERGERON, V. and P. WALSTRA. 2005. 7 - Foams. In: J. LYKLEMA, ed. *Fundamentals of Interface and Colloid Science*. Academic Press, pp.7.1-7.38.
- BEVERUNG, C. J., C. J. RADKE and H. W. BLANCH. 1999. Protein adsorption at the oil/water interface: characterization of adsorption kinetics by dynamic interfacial tension measurements. *Biophysical Chemistry*, **81**(1), pp.59-80.
- BINKS, B. P., B. DUNCUMB and R. MURAKAMI. 2007. Effect of pH and Salt Concentration on the Phase Inversion of Particle-Stabilized Foams. *Langmuir*, **23**(18), pp.9143-9146.
- BINKS, B. P. and T. HOROZOV. 2006. *Colloidal particles at liquid interfaces*. Cambridge: Cambridge University Press.
- BINKS, B. P. and T. S. HOROZOV. 2005. Aqueous Foams Stabilized Solely by Silica Nanoparticles. *Angewandte Chemie International Edition*, **44**(24), pp.3722-3725.
- BINKS, B. P. and R. MURAKAMI. 2006. Phase inversion of particle-stabilized materials from foams to dry water. *Nat Mater*, **5**(11), pp.865-869.
- BJERKNES, K., K. DYRSTAD, G. SMISTAD and I. AGERKVIST. 2000. Preparation of Polymeric Microcapsules: Formulation Studies. *Drug Development and Industrial Pharmacy*, **26**(8), pp.847-856.
- BÖKER, A., J. HE, T. EMRICK and T. P. RUSSELL. 2007. Self-assembly of nanoparticles at interfaces. *Soft Matter*, **3**(10), pp.1231-1248.
- BORDEN, M. A., G. V. MARTINEZ, J. RICKER, N. TSVETKOVA, M. LONGO, R. J. GILLIES, P. A. DAYTON and K. W. FERRARA. 2006. Lateral Phase Separation in Lipid-Coated Microbubbles. *Langmuir*, **22**(9), pp.4291-4297.

- BOS, M. A. and T. V. VLIET. 2001. Interfacial rheological properties of adsorbed protein layers and surfactants: a review. *Advances in Colloid and Interface Science*, **91**(3), pp.437-471.
- BROTCHIE, A., F. GRIESER and M. ASHOKKUMAR. 2010. Characterization of Acoustic Cavitation Bubbles in Different Sound Fields. *The Journal of Physical Chemistry B*, **114**(34), pp.11010-11016.
- BUDDE, U., A. BRIEL, G. ROSSLING, K. LOVIS, W. SCHMIDT, H. U. MORITZ, M. GOTTFRIED and J. P. INGWERSEN. 2003. *Multi-stage method for producing gas-filled microcapsules*. Google Patents.
- BURKE, J., A. COX, J. PETKOV and B. S. MURRAY. 2014. Interfacial rheology and stability of air bubbles stabilized by mixtures of hydrophobin and  $\beta$ -casein. *Food Hydrocolloids*, **34**, pp.119-127.
- BUTKO, P., J. P. BUFORD, J. S. GOODWIN, P. A. STROUD, C. L. MCCORMICK and G. C. CANNON. 2001. Spectroscopic Evidence for Amyloid-like Interfacial Self-Assembly of Hydrophobin Sc3. *Biochemical and Biophysical Research Communications*, **280**(1), pp.212-215.
- CHAN, D. Y. C., E. KLASEBOER and R. MANICA. 2011. Film drainage and coalescence between deformable drops and bubbles. *Soft Matter*, **7**(6), pp.2235-2264.
- CHERN, C. S. 2006. Emulsion polymerization mechanisms and kinetics. *Progress in Polymer Science*, **31**(5), pp.443-486.
- COUVREUR, P., B. KANTE, M. ROLAND, P. GUIOT, P. BAUDUIN and P. SPEISER. 1979. Polycyanoacrylate nanocapsules as potential lysosomotropic carriers: preparation, morphological and sorptive properties. *Journal of Pharmacy and Pharmacology*, **31**(1), pp.331-332.
- COX, A. R., D. L. ALDRED and A. B. RUSSELL. 2009. Exceptional stability of food foams using class II hydrophobin HFBII. *Food Hydrocolloids*, **23**(2), pp.366-376.
- COX, A. R., F. CAGNOL, A. B. RUSSELL and M. J. IZZARD. 2007. Surface properties of class II hydrophobins from *Trichoderma reesei* and influence on bubble stability. *Langmuir*, **23**(15), pp.7995-8002.
- CREAMER, L. K. and A. K. H. MACGIBBON. 1996. Some recent advances in the basic chemistry of milk proteins and lipids. *International Dairy Journal*, **6**(6), pp.539-568.
- CRESPY, D. and K. LANDFESTER. 2009. Synthesis of polyvinylpyrrolidone/silver nanoparticles hybrid latex in non-aqueous miniemulsion at high temperature. *Polymer*, **50**(7), pp.1616-1620.

- CRUCHO, C. I. C. and M. T. BARROS. 2017. Polymeric nanoparticles: A study on the preparation variables and characterization methods. *Materials Science and Engineering: C*, **80**, pp.771-784.
- DAMODARAN, S. 2005. Protein stabilization of emulsions and foams. *Journal of Food Science*, **70**(3), pp.R54-R66.
- DE CORATO, M. and V. GARBIN. 2018. Capillary interactions between dynamically forced particles adsorbed at a planar interface and on a bubble. *Journal of Fluid Mechanics*, **847**, pp.71-92.
- DELGADO, J. and M. S. EL-AASSER. 1990. Kinetic and thermodynamic aspects of miniemulsion copolymerization. *Makromolekulare Chemie. Macromolecular Symposia*, **31**(1), pp.63-87.
- DENKOV, N. D., K. G. MARINOVA, C. CHRISTOVA, A. HADJIISKI and P. COOPER. 2000. Mechanisms of Action of Mixed Solid-Liquid Antifoams: 3. Exhaustion and Reactivation. *Langmuir*, **16**(6), pp.2515-2528.
- DESFOUGERES, Y., V. LECHEVALIER, S. PEZENNEC, F. ARTZNER and F. NAU. 2008. Dry-heating makes hen egg white lysozyme an efficient foaming agent and enables its bulk aggregation. *Journal of Agricultural and Food Chemistry*, **56**(13), pp.5120-5128.
- DHARAIYA, N., V. K. ASWAL and P. BAHADUR. 2015. Characterization of Triton X-100 and its oligomer (Tyloxapol) micelles vis-à-vis solubilization of bisphenol A by spectral and scattering techniques. *Colloids and Surfaces A: Physicochemical and Engineering Aspects*, **470**, pp.230-239.
- DICKINSON, E. 1989. Protein Adsorption at Liquid Interfaces and the Relationship to Foam Stability. In: *Foams: Physics, Chemistry and Structure*, 1989//, London. Springer London, pp.39-53.
- DICKINSON, E. 1992. *An introduction to food colloids*. New York;Oxford;: Oxford University Press.
- DICKINSON, E. 1999. Adsorbed protein layers at fluid interfaces: interactions, structure and surface rheology. *Colloids and Surfaces B: Biointerfaces*, **15**(2), pp.161-176.
- DICKINSON, E. 2003. Hydrocolloids at interfaces and the influence on the properties of dispersed systems. *Food Hydrocolloids*, **17**(1), pp.25-39.
- DICKINSON, E. 2006. *Interfacial Particles in Food Emulsions and Foams Colloidal Particles at Liquid Interfaces*. Cambridge University Press.
- DICKINSON, E. 2010a. Flocculation of protein-stabilized oil-in-water emulsions. *Colloids and Surfaces B: Biointerfaces*, **81**(1), pp.130-140.

- DICKINSON, E. 2010b. Food emulsions and foams: Stabilization by particles. *Current Opinion in Colloid & Interface Science*, **15**(1), pp.40-49.
- DICKINSON, E. 2013. Structure and rheology of colloidal particle gels: Insight from computer simulation. *Advances in Colloid and Interface Science*, **199-200**, pp.114-127.
- DICKINSON, E., R. ETTELAIE, T. KOSTAKIS and B. S. MURRAY. 2004. Factors controlling the formation and stability of air bubbles stabilized by partially hydrophobic silica nanoparticles. *Langmuir*, **20**(20), pp.8517-8525.
- DICKINSON, E., R. ETTELAIE, B. S. MURRAY and Z. DU. 2002. Kinetics of Disproportionation of Air Bubbles beneath a Planar Air–Water Interface Stabilized by Food Proteins. *Journal of Colloid and Interface Science*, **252**(1), pp.202-213.
- DICKINSON, E., E. W. ROBSON and G. STAINSBY. 1983. Colloid stability of casein-coated polystyrene particles. *Journal of the Chemical Society, Faraday Transactions 1: Physical Chemistry in Condensed Phases*, **79**(12), pp.2937-2952.
- DIMITROVA, L. M., P. V. PETKOV, P. A. KRALCHEVSKY, S. D. STOYANOV and E. G. PELAN. 2017. Production and characterization of stable foams with fine bubbles from solutions of hydrophobin HFBII and its mixtures with other proteins. *Colloids and Surfaces A: Physicochemical and Engineering Aspects*, **521**, pp.92-104.
- DISALVO, E. A. 1988. Permeability of water and polar solutes in lipid bilayers. *Advances in Colloid and Interface Science*, **29**(1), pp.141-170.
- DOUGLAS, S. J., L. ILLUM, S. S. DAVIS and J. KRUETER. 1984. Particle size and size distribution of poly(butyl-2-cyanoacrylate) nanoparticles: I. Influence of physicochemical factors. *Journal of Colloid and Interface Science*, **101**(1), pp.149-158.
- DU, Z., M. P. BILBAO-MONTOYA, B. P. BINKS, E. DICKINSON, R. ETTELAIE and B. S. MURRAY. 2003. Outstanding Stability of Particle-Stabilized Bubbles. *Langmuir*, **19**(8), p3106.
- ETTELAIE, R., E. DICKINSON, Z. DU and B. S. MURRAY. 2003. Disproportionation of clustered protein-stabilized bubbles at planar air–water interfaces. *Journal of Colloid and Interface Science*, **263**(1), pp.47-58.
- ETTELAIE, R. and B. MURRAY. 2014. Effect of particle adsorption rates on the disproportionation process in pickering stabilised bubbles. *The Journal of Chemical Physics*, **140**(20), p204713.
- ETTELAIE, R. and B. S. MURRAY. 2015. Evolution of bubble size distribution in particle stabilised bubble dispersions: Competition between particle adsorption

and dissolution kinetics. *Colloids and Surfaces A: Physicochemical and Engineering Aspects*, **475**, pp.27-36.

EVANS, D. F. and H. WENNERSTRÖM. 1994. *The colloidal domain: where physics, chemistry, biology, and technology meet*. New York, NY: VCH Publishers.

EVANS, D. F. and H. WENNERSTRÖM. 1999. *The colloidal domain: where physics, chemistry, biology, and technology meet*. 2nd ed. New York: Wiley-VCH.

FAIRLEY, P. 1992. Ultrasonic Studies of Foods Containing Air. *PhD thesis, University of Leeds*.

FAROOK, U., E. STRIDE, M. J. EDIRISINGHE and R. MOALEJI. 2007. Microbubbling by co-axial electrohydrodynamic atomization. *Medical & Biological Engineering & Computing*, **45**(8), pp.781-789.

FERRARA, K., R. POLLARD and M. BORDEN. 2007. Ultrasound Microbubble Contrast Agents: Fundamentals and Application to Gene and Drug Delivery. *Annual Review of Biomedical Engineering*, **9**(1), pp.415-447.

FOKONG, S., M. SIEPMANN, Z. LIU, G. SCHMITZ, F. KIESSLING and J. GÄTJENS. 2011. Advanced Characterization and Refinement of Poly N-Butyl Cyanoacrylate Microbubbles for Ultrasound Imaging. *Ultrasound in Medicine & Biology*, **37**(10), pp.1622-1634.

FRELICHOWSKA, J., M.-A. BOLZINGER, J. PELLETIER, J.-P. VALOUR and Y. CHEVALIER. 2009. Topical delivery of lipophilic drugs from o/w Pickering emulsions. *International Journal of Pharmaceutics*, **371**(1), pp.56-63.

GARSTECKI, P., I. GITLIN, W. DILUZIO, G. M. WHITESIDES, E. KUMACHEVA and H. A. STONE. 2004. *Formation of monodisperse bubbles in a microfluidic flow-focusing device*.

GONZENBACH, U. T., A. R. STUDART, E. TERVOORT and L. J. GAUCKLER. 2006. Ultrastable particle-stabilized foams. *Angewandte Chemie International Edition*, **45**(21), pp.3526-3530.

HAEDEL, J., S. T. BECKETT and K. NIRANJAN. 2007. Bubble-Included Chocolate: Relating Structure with Sensory Response. *Journal of Food Science*, **72**(3), pp.E138-E142.

HAKANPAA, J., M. LINDER, A. POPOV, A. SCHMIDT and J. ROUVINEN. 2006. Hydrophobin HFBII in detail: ultrahigh-resolution structure at 0.75 angstrom. *Acta Crystallographica Section D-Biological Crystallography*, **62**, pp.356-367.

HANOTU, J. O., H. BANDULASENA and W. B. ZIMMERMAN. 2017. Aerator design for microbubble generation. *Chemical Engineering Research and Design*, **123**, pp.367-376.

- HARRIS, J. R., F. DEPOIX and K. URICH. 1995. The structure of gas-filled n-butyl-2-cyanoacrylate (BCA) polymer particles. *Micron*, **26**(2), pp.103-111.
- HARTLAND, S., B. YANG and S. A. K. JEELANI. 1994. Dimple formation in the thin film beneath a drop or bubble approaching a plane surface. *Chemical Engineering Science*, **49**(9), pp.1313-1322.
- HENCH, L. L. and J. M. POLAK. 2002. Third-Generation Biomedical Materials. *Science*, **295**(5557), pp.1014-1017.
- HETH, A. A. and H. E. SWAISGOOD. 1982. Examination of Casein Micelle Structure by a Method for Reversible Covalent Immobilization<sup>1</sup>. *Journal of Dairy Science*, **65**(11), pp.2047-2054.
- HETTIARACHCHI, K., E. TALU, M. L. LONGO, P. A. DAYTON and A. P. LEE. 2007. On-chip generation of microbubbles as a practical technology for manufacturing contrast agents for ultrasonic imaging. *Lab on a Chip*, **7**(4), pp.463-468.
- HOTRUM, N. E., T. VAN VLIET, M. A. COHEN STUART and G. A. VAN AKEN. 2002. Monitoring Entering and Spreading of Emulsion Droplets at an Expanding Air/Water Interface: A Novel Technique. *Journal of Colloid and Interface Science*, **247**(1), pp.125-131.
- HUNTER, R. J. 2001. *Foundations of colloid science*. Second ed. New York;Oxford;: Oxford University Press.
- HUNTER, T. N., E. J. WANLESS and G. J. JAMESON. 2009. Effect of esterically bonded agents on the monolayer structure and foamability of nano-silica. *Colloids and Surfaces A: Physicochemical and Engineering Aspects*, **334**(1-3), pp.181-190.
- ISRAELACHVILI, J. N. 2011. *Intermolecular and surface forces*. Burlington, MA: Academic Press.
- JOHNSON, B. D. and P. J. WANGERSKY. 1987. Microbubbles: Stabilization by monolayers of adsorbed particles. *Journal of Geophysical Research: Oceans*, **92**(C13), pp.14641-14647.
- JOSCELYNE, S. M. and G. TRÄGÅRDH. 2000. Membrane emulsification — a literature review. *Journal of Membrane Science*, **169**(1), pp.107-117.
- KING, M. E. and A. Y. KINNEY. 1999. Tissue Adhesives: A New Method of Wound Repair. *The Nurse Practitioner*, **24**(10), pp.66-75.
- KLIBANOV, A. L. 2007. Ultrasound molecular imaging with targeted microbubble contrast agents. *J. Nucl. Cardiol.*, **14**(6), p876.

- KLOEK, W., T. VAN VLIET and M. MEINDERS. 2001. Effect of Bulk and Interfacial Rheological Properties on Bubble Dissolution. *Journal of Colloid and Interface Science*, **237**(2), pp.158-166.
- KOSTAKIS, T., R. ETTALAIE and B. S. MURRAY. 2006. Effect of High Salt Concentrations on the Stabilization of Bubbles by Silica Particles. *Langmuir*, **22**(3), pp.1273-1280.
- KOSTAKIS, T., R. ETTALAIE and S. B. MURRAY. 2007. Enhancement of Stability of Bubbles to Disproportionation Using Hydrophilic Silica Particles Mixed with Surfactants or Proteins. *Food Colloids: Self-Assembly and Material Science*. Royal Society of Chemistry, pp.357-368.
- KOTHEKAR, S. C., A. M. WARE, J. T. WAGHMARE and S. A. MOMIN. 2007. Comparative Analysis of the Properties of Tween-20, Tween-60, Tween-80, Arlacel-60, and Arlacel-80. *Journal of Dispersion Science and Technology*, **28**(3), pp.477-484.
- KRÄGEL, J., R. WÜSTNECK, F. HUSBAND, P. J. WILDE, A. V. MAKIEVSKI, D. O. GRIGORIEV and J. B. LI. 1999. Properties of mixed protein/surfactant adsorption layers. *Colloids and Surfaces B: Biointerfaces*, **12**(3), pp.399-407.
- KRALCHEVSKY, P. A. and N. D. DENKOV. 2001. Capillary forces and structuring in layers of colloid particles. *Current Opinion in Colloid & Interface Science*, **6**(4), pp.383-401.
- KRAUSE, W. 2002. *Contrast Agents II: Optical, Ultrasound, X-Ray Imaging and Radiopharmaceutical Imaging*. Springer Science & Business Media.
- KREMKAU, F., R. GRAMIAK, E. CARSTENSEN, P. SHAH and D. KRAMER. 1970. Ultrasonic detection of cavitation at catheter tips. *American Journal of Roentgenology*, **110**(1), pp.177-183.
- KREUTER, J. 1982. On the mechanism of termination in heterogeneous polymerization. *Journal of Polymer Science: Polymer Letters Edition*, **20**(10), pp.543-545.
- KUKIZAKI, M. and M. GOTO. 2006. Size control of nanobubbles generated from Shirasu-porous-glass (SPG) membranes. *Journal of Membrane Science*, **281**(1), pp.386-396.
- KULKARNI, A. V. and J. B. JOSHI. 2011. Design and selection of sparger for bubble column reactor. Part II: Optimum sparger type and design. *Chemical Engineering Research and Design*, **89**(10), pp.1986-1995.
- LAM, S., K. P. VELIKOV and O. D. VELEV. 2014. Pickering stabilization of foams and emulsions with particles of biological origin. *Current Opinion in Colloid & Interface Science*, **19**(5), pp.490-500.

- LANGEVIN, D. 2000. Influence of interfacial rheology on foam and emulsion properties. *Advances in Colloid and Interface Science*, **88**(1), pp.209-222.
- LANGEVIN, D. 2008. Aqueous Foams: A Field of Investigation at the Frontier Between Chemistry and Physics. *ChemPhysChem*, **9**(4), pp.510-522.
- LANGEVIN, D. 2015. Bubble coalescence in pure liquids and in surfactant solutions. *Current Opinion in Colloid & Interface Science*, **20**(2), pp.92-97.
- LANGEVIN, D. 2017. Aqueous foams and foam films stabilised by surfactants. Gravity-free studies. *Comptes Rendus Mécanique*, **345**(1), pp.47-55.
- LEVICH, V. G. 1962. *Physicochemical hydrodynamics*. London Prentice-Hall.
- LI, J. B., Y. ZHANG and L. L. YAN. 2001. Multilayer Formation on a Curved Drop Surface. *Angewandte Chemie International Edition*, **40**(5), pp.891-894.
- LINDER, M., G. R. SZILVAY, T. NAKARI-SETÄLÄ, H. SÖDERLUND and M. PENTTILÄ. 2002. Surface adhesion of fusion proteins containing the hydrophobins HFBI and HFBII from *Trichoderma reesei*. *Protein Science : A Publication of the Protein Society*, **11**(9), pp.2257-2266.
- LINDER, M. B., G. R. SZILVAY, T. NAKARI-SETÄLÄ and M. E. PENTTILÄ. 2005. Hydrophobins: the protein-amphiphiles of filamentous fungi. *FEMS Microbiology Reviews*, **29**(5), pp.877-896.
- LIU, Z., T. LAMMERS, J. EHLING, S. FOKONG, J. BORNEMANN, F. KIESSLING and J. GÄTJENS. 2011. Iron oxide nanoparticle-containing microbubble composites as contrast agents for MR and ultrasound dual-modality imaging. *Biomaterials*, **32**(26), pp.6155-6163.
- LUCASSEN, J. 1992. Capillary forces between solid particles in fluid interfaces. *Colloids and Surfaces*, **65**(2), pp.131-137.
- LUI, Y., H. MIYOSHI and M. NAKAMURA. 2006. Encapsulated Ultrasound Microbubbles: Therapeutic Application in Drug/Gene Delivery. *J. Controlled Release*, **114**(1), p89.
- LUMSDON, S. O., J. GREEN and B. STIEGLITZ. 2005. Adsorption of hydrophobin proteins at hydrophobic and hydrophilic interfaces. *Colloids and Surfaces B: Biointerfaces*, **44**(4), pp.172-178.
- MACKIE, A. R., A. P. GUNNING, M. J. RIDOUT, P. J. WILDE and J. RODRIGUEZ PATINO. 2001. In Situ Measurement of the Displacement of Protein Films from the Air/Water Interface by Surfactant. *Biomacromolecules*, **2**(3), pp.1001-1006.
- MARINOVA, K. G., E. S. BASHEVA, B. NENOVA, M. TEMELSKA, A. Y. MIRAREFI, B. CAMPBELL and I. B. IVANOV. 2009. Physico-chemical factors

controlling the foamability and foam stability of milk proteins: Sodium caseinate and whey protein concentrates. *Food Hydrocolloids*, **23**(7), pp.1864-1876.

MARTINEZ, C. A., E. RIO, G. DELON, A. SAINT-JALMES, D. LANGEVIN and B. P. BINKS. 2008. On the origin of the remarkable stability of aqueous foams stabilised by nanoparticles: link with microscopic surface properties. *Soft Matter*, **4**(7), pp.1531-1535.

MCCLEMENTS, D. J. 2016. *Food emulsions: principles, practices, and techniques*. Boca Raton, FL: CRC Press LLC.

MEINDERS, M. B. J., W. KLOEK and T. VAN VLIET. 2001. Effect of Surface Elasticity on Ostwald Ripening in Emulsions. *Langmuir*, **17**(13), pp.3923-3929.

MEWIS, J. and N. J. WAGNER. 2011. *Introduction to colloid science and rheology*. Cambridge: Cambridge University Press, pp.1-35.

MOHAMEDI, G., M. AZMIN, I. PASTORIZA-SANTOS, V. HUANG, J. PÉREZ-JUSTE, L. M. LIZ-MARZÁN, M. EDIRISINGHE and E. STRIDE. 2012. Effects of Gold Nanoparticles on the Stability of Microbubbles. *Langmuir*, **28**(39), pp.13808-13815.

MØRCH, Ý., R. HANSEN, S. BERG, A. K. O. ÅSLUND, W. R. GLOMM, S. EGGEN, R. SCHMID, H. JOHNSEN, S. KUBOWICZ, S. SNIPSTAD, E. SULHEIM, S. HAK, G. SINGH, B. H. MCDONAGH, H. BLOM, C. DE LANGE DAVIES and P. M. STENSTAD. 2015. Nanoparticle-stabilized microbubbles for multimodal imaging and drug delivery: NP-Stabilized Microbubbles for Multimodal Imaging and Drug Delivery. *Contrast Media & Molecular Imaging*, **10**(5), pp.356-366.

MÜLLER, R. H., C. LHERM, J. HERBORT, T. BLUNK and P. COUVREUR. 1992. Alkylcyanoacrylate drug carriers: I. Physicochemical characterization of nanoparticles with different alkyl chain length. *International Journal of Pharmaceutics*, **84**(1), pp.1-11.

MURRAY, B. S. 2011. Rheological properties of protein films. *Current Opinion in Colloid & Interface Science*, **16**(1), pp.27-35.

MURRAY, B. S., E. DICKINSON, C. K. LAU, P. V. NELSON and E. SCHMIDT. 2005. Coalescence of Protein-Stabilized Bubbles Undergoing Expansion at a Simultaneously Expanding Planar Air–Water Interface. *Langmuir*, **21**(10), pp.4622-4630.

MURRAY, B. S. and R. ETTELAIE. 2004. Foam stability: proteins and nanoparticles. *Current Opinion in Colloid & Interface Science*, **9**(5), pp.314-320.

NAPPER, D. H. 1977. Steric stabilization. *Journal of Colloid and Interface Science*, **58**(2), pp.390-407.

- NASIR, A., A. KAUSAR and A. YOUNUS. 2015. A Review on Preparation, Properties and Applications of Polymeric Nanoparticle-Based Materials. *Polymer-Plastics Technology and Engineering*, **54**(4), pp.325-341.
- NEMETHY, G. and A. RAY. 1973. *Solvent effects on the near-ultraviolet spectrum of phenol and its distribution in micellar solutions.*
- NICOLAS, J. and P. COUVREUR. 2009. Synthesis of poly (alkyl cyanoacrylate)-based colloidal nanomedicines. *Wiley Interdisciplinary Reviews: Nanomedicine and Nanobiotechnology*, **1**(1), pp.111-127.
- OLBRICH, C., P. HAUFF, F. SCHOLLE, W. SCHMIDT, U. BAKOWSKY, A. BRIEL and M. SCHIRNER. 2006. The in vitro stability of air-filled polybutylcyanoacrylate microparticles. *Biomaterials*, **27**(19), pp.3549-3559.
- PALMOWSKI, M., B. MORGENSTERN, P. HAUFF, M. REINHARDT, J. HUPPERT, M. MAURER, E. C. WOENNE, S. DOERK, G. LADEWIG, J. W. JENNE, S. DELORME, L. GRENACHER, P. HALLSCHEIDT, G. W. KAUFFMANN, W. SEMMLER and F. KIESSLING. 2008. Pharmacodynamics of Streptavidin-Coated Cyanoacrylate Microbubbles Designed for Molecular Ultrasound Imaging. *Investigative Radiology*, **43**(3), pp.162-169.
- PANCHOLI, K. P., U. FAROOK, R. MOALEJI, E. STRIDE and M. J. EDIRISINGHE. 2008. Novel methods for preparing phospholipid coated microbubbles. *European Biophysics Journal*, **37**(4), pp.515-520.
- PAUNOV, V. N., B. P. BINKS and N. P. ASHBY. 2002. Adsorption of Charged Colloid Particles to Charged Liquid Surfaces. *Langmuir*, **18**(18), pp.6946-6955.
- PAVEL, F. M. 2004. Microemulsion Polymerization. *Journal of Dispersion Science and Technology*, **25**(1), pp.1-16.
- PICKERING, S. 1907. Emulsions. *J. Chem. Soc. Trans.*, **91**, p2001.
- PIRKER, S., J. KRUSE, C. NOE, K. LANGER, A. ZIMMER and J. KREUTER. 1996. Characterization of polybutylecyanoacrylate nanoparticles. Part II: Determination of polymer content by NMR-analysis. *International Journal of Pharmaceutics*, **128**(1), pp.189-195.
- PRINS, A. 1999. Stagnant surface behaviour and its effect on foam and film stability. *Colloids and Surfaces A: Physicochemical and Engineering Aspects*, **149**(1), pp.467-473.
- PUGH, R. J. 1996. Foaming, foam films, antifoaming and defoaming. *Advances in Colloid and Interface Science*, **64**, pp.67-142.
- RADULOVA, G. M., K. GOLEMANOV, K. D. DANOV, P. A. KRALCHEVSKY, S. D. STOYANOV, L. N. ARNAUDOV, T. B. J. BLIJDENSTEIN, E. G. PELAN

- and A. LIPS. 2012. Surface Shear Rheology of Adsorption Layers from the Protein HFBII Hydrophobin: Effect of Added  $\beta$ -Casein. *Langmuir*, **28**(9), pp.4168-4177.
- RAMSDEN, W. 1904. Separation of solids in the surface-layers of solutions and 'suspensions' (observations on surface-membranes, bubbles, emulsions, and mechanical coagulation).—Preliminary account. *Proceedings of the Royal Society of London*, **72**(477-486), pp.156-164.
- RAO, J. P. and K. E. GECKELER. 2011. Polymer nanoparticles: Preparation techniques and size-control parameters. *Progress in Polymer Science*, **36**(7), pp.887-913.
- RAVERA, F., E. SANTINI, G. LOGLIO, M. FERRARI and L. LIGGIERI. 2006. Effect of Nanoparticles on the Interfacial Properties of Liquid/Liquid and Liquid/Air Surface Layers. *The Journal of Physical Chemistry B*, **110**(39), pp.19543-19551.
- REGEV, O. and R. ZANA. 1999. Aggregation Behavior of Tyloxapol, a Nonionic Surfactant Oligomer, in Aqueous Solution. *Journal of Colloid and Interface Science*, **210**(1), pp.8-17.
- ROBINSON, J. E., C. M. SUTTON and G. F. REID. 2014. Dilute Triton X-100 in water as a reference liquid for hydrometer calibration using Cuckow's method. *Measurement*, **57**, pp.132-137.
- ROVERS, T. A. M., G. SALA, E. VAN DER LINDEN and M. B. J. MEINDERS. 2016. Temperature is key to yield and stability of BSA stabilized microbubbles. *Food Hydrocolloids*, **52**, pp.106-115.
- ROY, K., S. KAR and R. N. DAS. 2015. Chapter 1 - Background of QSAR and Historical Developments. In: K. ROY, S. KAR and R. N. DAS, eds. *Understanding the Basics of QSAR for Applications in Pharmaceutical Sciences and Risk Assessment*. Boston: Academic Press, pp.1-46.
- RULLIER, B., B. NOVALES and M. A. V. AXELOS. 2008. Effect of protein aggregates on foaming properties of  $\beta$ -lactoglobulin. *Colloids and Surfaces A: Physicochemical and Engineering Aspects*, **330**(2), pp.96-102.
- SAFOUANE, M., D. LANGEVIN and B. P. BINKS. 2007. Effect of Particle Hydrophobicity on the Properties of Silica Particle Layers at the Air–Water Interface. *Langmuir*, **23**(23), pp.11546-11553.
- SCHMIDT, W. and G. ROESSLING. 2006. Novel manufacturing process of hollow polymer microspheres. *Chemical Engineering Science*, **61**(15), pp.4973-4981.
- SHELUDKO, A. 1967. Thin liquid films. *Advances in Colloid and Interface Science*, **1**(4), pp.391-464.

- SHEPPARD, E. and N. TCHEUREKDJIAN. 1968. Monolayer studies: IV. Surface films of emulsion latex particles. *Journal of Colloid and Interface Science*, **28**(3), pp.481-486.
- SIMOVIC, S. and C. A. PRESTIDGE. 2003. Hydrophilic Silica Nanoparticles at the PDMS Droplet–Water Interface. *Langmuir*, **19**(9), pp.3785-3792.
- SIRSI, S. and M. BORDEN. 2009. Microbubble Compositions, Properties and Biomedical Applications. *Bubble science engineering and technology*, **1**(1-2), pp.3-17.
- STOCCO, A., E. RIO, B. P. BINKS and D. LANGEVIN. 2011. Aqueous Foams Stabilized Solely by Particles. *Soft Matter*, **7**, p1260.
- STRIDE, E. and M. EDIRISINGHE. 2008. Novel microbubble preparation technologies. *SOFT MATTER*, **4**(12), pp.2350-2359.
- SUBRAMANIAM, A. B., M. ABKARIAN, L. MAHADEVAN and H. A. STONE. 2006. Mechanics of Interfacial Composite Materials. *Langmuir*, **22**(24), pp.10204-10208.
- SULHEIM, E., H. BAGHIROV, E. VON HAARTMAN, A. BØE, A. K. O. ÅSLUND, Y. MØRCH and C. D. L. DAVIES. 2016. Cellular uptake and intracellular degradation of poly(alkyl cyanoacrylate) nanoparticles. *Journal of Nanobiotechnology*, **14**(1), p1.
- SUSLICK, K. S. and M. W. GRINSTAFF. 1990. Protein microencapsulation of nonaqueous liquids. *Journal of the American Chemical Society*, **112**(21), pp.7807-7809.
- SUSLICK, S., Y. DIDENKO, M. M. FANG, T. HYEON, K. J. KOLBECK, W. B. MCNAMARA III, M. M. MDLELENI and M. WONG. 2000. *Acoustic Cavitation and Its Chemical Consequences*.
- TCHUENBOU-MAGAIA, F., I. NORTON and P. COX. 2009. Hydrophobins Stabilised Air-Filled Emulsions for the Food Industry. *Food Hydrocolloids*, **23**(7), p1877.
- TCHUENBOU-MAGAIA, F. L., N. AL-RIFAI, N. E. M. ISHAK, I. T. NORTON and P. W. COX. 2011. Suspensions of air cells with cysteine-rich protein coats: Air-filled emulsions. *Journal of Cellular Plastics*, **47**(3), pp.217-232.
- TUCKER, I. M., J. T. PETKOV, J. PENFOLD, R. K. THOMAS, A. R. COX and N. HEDGES. 2015. Adsorption of Hydrophobin-Protein Mixtures at the Air-Water Interface: The Impact of pH and Electrolyte. *LANGMUIR*, **31**(36), pp.10008-10016.

- TYOWUA, A. T., S. G. YIASE and B. P. BINKS. 2017. Double oil-in-oil-in-oil emulsions stabilised solely by particles. *Journal of Colloid and Interface Science*, **488**, pp.127-134.
- UNGER, E. C., T. O. MATSUNAGA, T. MCCREERY, P. SCHUMANN, R. SWEITZER and R. QUIGLEY. 2002. Therapeutic applications of microbubbles. *European Journal of Radiology*, **42**(2), pp.160-168.
- UNGER, E. C., T. P. MCCREERY, R. H. SWEITZER, V. E. CALDWELL and Y. WU. 1998. Acoustically Active Lipospheres Containing Paclitaxel: A New Therapeutic Ultrasound Contrast Agent. *Investigative Radiology*, **33**(12), pp.886-892.
- VRIJ, A. 1966. Possible mechanism for the spontaneous rupture of thin, free liquid films. *Discussions of the Faraday Society*, **42**(0), pp.23-33.
- WALSTRA, P. 1989. Principles of Foam Formation and Stability. In: London. Springer London, pp.1-15.
- WALSTRA, P. 2003. *Physical chemistry of foods*. New York: Marcel Dekker.
- WANG, W., C. C. MOSER and M. A. WHEATLEY. 1996. Langmuir Trough Study of Surfactant Mixtures Used in the Production of a New Ultrasound Contrast Agent Consisting of Stabilized Microbubbles. *The Journal of Physical Chemistry*, **100**(32), pp.13815-13821.
- WANG, Y., C. BOUILLON, A. COX, E. DICKINSON, K. DURGA, B. S. MURRAY and R. XU. 2013. Interfacial Study of Class II Hydrophobin and Its Mixtures with Milk Proteins: Relationship to Bubble Stability. *Journal of Agricultural and Food Chemistry*, **61**(7), pp.1554-1562.
- WASAN, D. T., A. D. NIKOLOV and F. AIMETTI. 2004. Texture and stability of emulsions and suspensions: role of oscillatory structural forces. *Advances in Colloid and Interface Science*, **108-109**, pp.187-195.
- WEAIRE, D. L. and S. HUTZLER. 1999. *The physics of foams*. Oxford: Clarendon Press.
- WESSELS, J. G. H. 1996. Hydrophobins: Proteins that Change the Nature of the Fungal Surface. In: R. K. POOLE, ed. *Advances in Microbial Physiology*. Academic Press, pp.1-45.
- WHITESIDES, G. M. 2006. The origins and the future of microfluidics. *Nature*, **442**, p368.
- WIELHORSKI, Y., A. B. ABDELWAHED, E. ARQUIS, S. GLOCKNER and J. BRÉARD. 2014. Numerical Simulation of Bubble Formation and Transport in Cross-Flowing Streams. *The Journal of Computational Multiphase Flows*, **6**(3), pp.299-312.

- WIERENGA, P. A. and H. GRUPPEN. 2010. New views on foams from protein solutions. *Current Opinion in Colloid & Interface Science*, **15**(5), pp.365-373.
- WILSON, A. J. 1989. *Foams: physics, chemistry and structure*. London: Springer-Verlag.
- WOLFRAM, H. and T. WRIEDT. 2012. *The Mie Theory Basics and Applications*.
- WONG, J. C. H., E. TERVOORT, S. BUSATO, L. J. GAUCKLER and P. ERMANNI. 2011. Controlling Phase Distributions in Macroporous Composite Materials through Particle-Stabilized Foams. *LANGMUIR*, **27**(7), pp.3254-3260.
- WOOD, R. J., J. LEE and M. J. BUSSEMAKER. 2017. A parametric review of sonochemistry: Control and augmentation of sonochemical activity in aqueous solutions. *Ultrasonics Sonochemistry*, **38**, pp.351-370.
- WOODWARD, N. C., P. J. WILDE, A. R. MACKIE, A. P. GUNNING, P. A. GUNNING and V. J. MORRIS. 2004. Effect of Processing on the Displacement of Whey Proteins: Applying the Orogenic Model to a Real System. *Journal of Agricultural and Food Chemistry*, **52**(5), pp.1287-1292.
- WÖSTEN, H. A. B. 2001. Hydrophobins: Multipurpose Proteins. *Annual Review of Microbiology*, **55**(1), pp.625-646.
- XIONG, X., F. ZHAO, M. SHI, H. YANG and Y. LIU. 2011. Polymeric Microbubbles for Ultrasonic Molecular Imaging and Targeted Therapeutics. *Journal of Biomaterials Science, Polymer Edition*, **22**(4-6), pp.417-428.
- XU, J. H., S. W. LI, G. G. CHEN and G. S. LUO. 2006. Formation of monodisperse microbubbles in a microfluidic device. *AIChE Journal*, **52**(6), pp.2254-2259.
- XU, Q., M. NAKAJIMA, S. ICHIKAWA, N. NAKAMURA and T. SHIINA. 2008. A comparative study of microbubble generation by mechanical agitation and sonication. *Innovative Food Science & Emerging Technologies*, **9**(4), pp.489-494.
- YASUNO, M., S. SUGIURA, S. IWAMOTO, M. NAKAJIMA, A. SHONO and K. SATOH. 2004. Monodispersed microbubble formation using microchannel technique. *AIChE Journal*, **50**(12), pp.3227-3233.
- YBERT, C. and J.-M. D. MEGLIO. 2000. Ascending air bubbles in solutions of surface-active molecules: Influence of desorption kinetics. *The European Physical Journal E*, **3**(2), pp.143-148.
- YILDIZ, U. and K. LANDFESTER. 2008. Miniemulsion polymerization of styrene in the presence of macromonomeric initiators. *Polymer*, **49**(23), pp.4930-4934.
- YORDANOV, G., N. ABRASHEV and C. DUSHKIN. 2010. Poly(n-butylcyanoacrylate) Submicron Particles Loaded with Ciprofloxacin for Potential Treatment of

Bacterial Infections. *In*: Berlin, Heidelberg. Springer Berlin Heidelberg, pp.53-59.

ZANG, D. Y., E. RIO, D. LANGEVIN, B. WEI and B. P. BINKS. 2010. Viscoelastic properties of silica nanoparticle monolayers at the air-water interface. *The European Physical Journal E*, **31**(2), pp.125-134.

ZHANG, G., A. NIU, S. PENG, M. JIANG, Y. TU, M. LI and C. WU. 2001. Formation of Novel Polymeric Nanoparticles. *Accounts of Chemical Research*, **34**(3), pp.249-256.

ZHAO, Y.-Z., H.-D. LIANG, X.-G. MEI and M. HALLIWELL. 2005. Preparation, characterization and in vivo observation of phospholipid-based gas-filled microbubbles containing hirudin. *Ultrasound in Medicine & Biology*, **31**(9), pp.1237-1243.

ZÚÑIGA, R. N. and J. M. AGUILERA. 2008. Aerated food gels: fabrication and potential applications. *Trends in Food Science & Technology*, **19**(4), pp.176-187.